

General Relativity and Gravitation: A Centennial Perspective*

Chapter 6: Sources of Gravitational Waves: Theory and Observations

Alessandra Buonanno¹ and B.S. Sathyaprakash²

¹*Maryland Center for Fundamental Physics & Joint Space-Science Institute, Department of Physics, University of Maryland, College Park, MD 20742, USA*

²*School of Physics and Astronomy, Cardiff University, 5, The Parade, Cardiff, UK, CF24 3YB*

* Please note that the references are updated through Spring 2014, which is when the article was finalized for the Centenary volume.

Contents

6	Sources of Gravitational Waves: Theory and Observations	<i>page</i>	4
6.1	Historical perspective		4
6.2	Analytical approximation methods		7
6.2.1	Post-Newtonian formalism		10
6.2.2	Perturbation theory and gravitational self force		21
6.2.3	The effective-one-body formalism		26
6.3	Compact-object binaries		33
6.3.1	Characteristic evolution time scales and strain amplitude		33
6.3.2	Frequency-mass diagram		34
6.3.3	Zoo of compact-object binaries		36
6.3.4	Interface between theory and observations		40
6.3.5	Results from LIGO and Virgo		44
6.3.6	Science targets and challenges		45
6.4	Isolated compact objects		52
6.4.1	A menagerie of neutron-star sources		52
6.4.2	Results from LIGO and Virgo		55
6.4.3	Science targets and challenges		58
6.5	Gravitational radiation from the early Universe		60
6.5.1	Primordial sources and expected strengths		60
6.5.2	Results from LIGO and Virgo		62
6.5.3	Science targets and challenges		63
	<i>References</i>		66

6

Sources of Gravitational Waves: Theory and Observations

Abstract

Gravitational-wave astronomy will soon become a new tool for observing the Universe. Detecting and interpreting gravitational waves will require deep theoretical insights into astronomical sources. The past three decades have seen remarkable progress in analytical and numerical computations of the source dynamics, development of search algorithms and analysis of data from detectors with unprecedented sensitivity. This Chapter is devoted to examine the advances and future challenges in understanding the dynamics of binary and isolated compact-object systems, expected cosmological sources, their amplitudes and rates, and highlights of results from gravitational-wave observations. All of this is a testament to the readiness of the community to open a new window for observing the cosmos, a century after gravitational waves were first predicted by Albert Einstein.

6.1 Historical perspective

James Clerk Maxwell discovered in 1865 that electromagnetic phenomena satisfied wave equations and found that the velocity of these waves in vacuum was numerically the same as the speed of light [1]. Maxwell was puzzled at this coincidence between the speed of light and his theoretical prediction for the speed of electromagnetic phenomena and proposed that “light is electromagnetic disturbance propagated through the field according to electromagnetic laws” [1].

Because any theory of gravitation consistent with special relativity cannot be an action-at-a-distance theory, in many ways, Maxwell’s theory, being the first relativistic physical theory, implied the existence of gravitational waves (GWs) in general relativity (GR). Indeed, years before Einstein derived the

wave equation in the linearised version of his field equations and discussed the generation of GWs as one of the first consequences of his new theory of gravity [2, 3], Henri Poincaré proposed the existence of *les ondes gravifiques* purely based on consistency of gravity with special relativity [4]. However, for many years GWs caused much controversy and a lot of doubts were cast on their existence [5–8]. The year 1959 was, in many ways, the turning point — it was the year of publication of a seminal paper by Bondi, Pirani and Robinson [6] on the exact plane wave solution with cylindrical symmetry and the energy carried by the waves [9]. This paper proved that wave solutions exist not just in the weak-field approximation and that GWs in GR carry energy and angular momentum away from their sources. These results cleared the way for Joseph Weber [10] to start pioneering experimental efforts. The discovery of the Hulse-Taylor binary [11], a system of two neutron stars in orbit around each other, led to the first observational evidence for the existence of gravitational radiation [12–14]. The loss of energy and angular momentum to GWs causes the two stars in this system to slowly spiral in towards each other. Since 1974, few other pulsar binaries have been discovered. For the most relativistic binary the observed rate of change of the period agrees with the GR prediction to better than 0.03% [15].

Once the most obvious theoretical impediments in defining gravitational radiation were tackled and observational evidence of the existence of the radiation was firmly established, serious research on the modeling of astrophysical and cosmological sources of GWs began along side experimental and data-analysis efforts to detect GWs. This chapter examines the last thirty years of endeavours that have brought the field to the dawn of the first, direct detections of GWs, hopefully marking the one-hundred year anniversary of the first articles by Einstein on gravitational radiation [2, 3].

Impressive theoretical advances and a few breakthroughs have occurred since the publication of the two notable reviews: *Gravitational Radiation* in 1982 [16] and *Three-Hundred Years of Gravitation* in 1987 [17]. Since then, a network of ground-based, GW laser interferometers has been built and has taken data ¹. Sophisticated and robust analytical techniques have been developed to predict highly-accurate gravitational waveforms emitted by compact-object binary systems (compact binaries, for short) during the inspiral, but also plunge, merger and ringdown stages (see Secs. 6.2 and 6.3). After many years of attempts, today numerical-relativity (NR) simulations ² are routinely employed to predict merger waveforms and validate analytical models of binary systems composed of black holes (BHs) and/or

¹ See the chapter on Receiving Gravitational Waves in this volume.

² See also the chapter on Numerical Relativity in this volume.

neutron stars (NSs). Simulations of binary systems containing NSs are becoming more realistic, and robust connections to astrophysical, observable phenomena (i.e., electromagnetic counterparts) are under development (see Sec. 6.3). The internal structure of NSs has still remained a puzzle, but there are hints of superfluidity of neutrons in the core. Neutron-star normal modes are now understood in far more detail and a new relativistic instability, that could potentially explain NSs in X-ray binaries, was discovered (see Sec. 6.4). Supernova simulations are getting more sophisticated and are able to include a variety of micro- and macro-physics (full GR, neutrino transport, weak interaction physics, magnetohydrodynamics), but not all in a generic 3-dimensional simulation with realistic equations of state. Many challenges remain, including understanding the basic supernova mechanism of core collapse and bounce (see Sec. 6.4). Thirty years ago, only a few rough predictions of GW signals from the primordial dark age of the Universe existed. Today we know a plethora of physical mechanisms in the early Universe that could generate GWs (see Sec. 6.5). Because of the weakness of GW signals, scientists working closely with the experiments have established strong collaborations with theorists, astrophysicists and cosmologists, so that searches for GWs are fully optimised (see Secs. 6.3, 6.4 and 6.5). Concurrently with the construction of initial interferometers, geometrical approaches to optimizing data analysis were developed, which now form the backbone of all GW data-analysis quests. As we shall discuss, searches with initial LIGO and Virgo detectors have already produced astrophysically and cosmologically significant upper limits. Pulsar Timing Arrays have reached unprecedented sensitivity levels and could detect a stochastic background from a population of supermassive black holes over the next five years.

Although the progress has been tremendous and the field has reached an unprecedented degree of maturity, several challenges still need to be tackled to take full advantage of the discovery potential of ground- and space-based detectors, and pulsar timing arrays. Part of this chapter is also devoted to highlight those challenges.

Later in this chapter we will discuss sources that can be observed in different types of detectors. These include ground-based interferometers such as initial and Advanced LIGO (iLIGO and aLIGO), Virgo and Advanced Virgo (AdV), KAGRA and Einstein Telescope (ET) (see Fig. 6.6), space-based detectors LISA and eLISA (see Fig. 6.7) and Pulsar Timing Arrays (PTA) and the Square Kilometre Array (SKA) ³.

Lastly, while this Chapter was being finalised, the BICEP2 experiment

³ ET is a third generation detector concept being studied in Europe whose conceptual design study was completed in 2011 [18]. The European Space Agency has selected GW Observatory as the

claimed to have observed the polarisation of the cosmic microwave background (CMB) photons (the so-called B-modes), caused by primordial GWs [19]. If confirmed, this result will constitute a landmark discovery in cosmology and GW science, enabling us to probe epochs very close to the Big Bang. However, at this stage it is not clear if the observed signal is truly primordial in nature and not due to astrophysical foregrounds and synchrotron emission by intervening dust [20, 21]. Measuring the imprint of primordial GWs on the CMB is different from, but equally relevant to, the detection of GWs with ground- and space-based detectors or PTAs. Indeed, detectors like BICEP2 infer the presence of GWs through their interaction with the CMB radiation at the time the latter was produced. They do not detect GWs passing by the detector on the Earth today. LIGO, Virgo, KAGRA, eLISA, PTA, etc., will probe contemporary GWs, yielding spectral and sky position data, and a plethora of new and unique information about our Universe and its contents. The focus of this Chapter is on the new window on the Universe that those detectors will enable us to open.

6.2 Analytical approximation methods

Progress over the past three decades: There is no doubt that the field of analytical relativity has matured considerably and has made tremendous progress since the notable Les Houches school on *Gravitational Radiation* in 1982 [16]. During the last thirty years there have been significant advances on the problems emphasised in the historic discussion organised and moderated by A. Ashtekar at the end of the school. The validity of the quadrupole formula for gravitational radiation far away from a binary source was questioned by some of the participants at the Les Houches school, appealing to the ongoing debate at that time [22–29] relating to the difficulties in describing nonlinearities in GR within a precise mathematical framework. At the Les Houches school, the Paris group (Damour, Deruelle, ...) proposed a consistent framework in terms of which to formulate questions about the two-body dynamics and GW emission. The Paris group was motivated by the impressive observational work related to the discovery of the Hulse-Taylor binary pulsar [11] and wanted to develop a mathematical framework that could match the standards set by the ever more accurate pulsar-timing data. Eventually, as we shall discuss below, a precise mathematical framework was also needed for *direct* detection of gravitational waves on the ground, because

science theme for the 3rd large mission (L3) in its future science program, scheduled for a launch in 2034. eLISA is the current straw man design for L3.

in this case nonlinearities play a role that is much more crucial than in binary pulsar observations.

Between 1980 and 1992 important theoretical foundations in gravitational radiation and post-Newtonian (PN) theory were carried out by a number of researchers [30–43]. However, during those years, the analytical work on the two-body problem was considered mostly academic. It was not clear how relevant it would be to push calculations beyond the quadrupole formula for the direct observation of GWs. The first important turning point was in 1993 when [44] pointed out the importance of computing the GW phasing beyond the leading order. Many crucial developments took place in the subsequent years [45–60]. The second important turning point, which brought theory and observations closer, occurred in the mid and late 1990s when the construction of LIGO, Virgo, GEO600 and TAMA 300 detectors started [61]. The TAMA 300 and LIGO detectors took the first data in 1999 [62] and 2002 [63], respectively. (The first ever coincident operation of a pair of interferometers was between the Glasgow 10 m and Garching 30 m prototypes [64].) The third turning point happened in the late 1990’s and early 2000’s when, pressed by the construction of GW interferometers, the analytical effective-one-body (EOB) approach [65, 66] made a bold prediction for the late inspiral, merger and ringdown waveform emitted by comparable-mass binary BHs. The EOB formalism builds on PN and perturbation theory results, and it is guided by the notion that non-perturbative effects can be captured analytically if the key ingredients that enter the two-body dynamics and GW emission are properly resummed about the (exact) test-particle limit results. Moreover, in the early 2000’s, a pragmatic, numerical and analytical, hybrid approach aimed at predicting the plunge and merger waveform was bravely carried out [67, 68]. This approach, called the Lazarus project, consisted of evolving the binary system in full numerical relativity (NR) for less than an orbit just prior to merger before stopping the evolution, extracting the spacetime metric from the results of the simulation of a deformed BH, and using perturbation theory calculations to complete the evolution during ringdown. The fourth relevant turning point occurred in 2005, when after more than thirty years of attempts, the first numerical-relativity simulations of binary BHs at last unveiled the merger waveforms [69–71]. Since then, synergies and interplays between different analytical and numerical techniques to solve the two-body problem in GR have grown considerably. A few paradigms were broken, in particular the nature of the binary BH merger waveform, which turned out to be much simpler than what most people had expected or predicted. Finally, recent years have seen remarkable interactions between GW data analysts, astro-

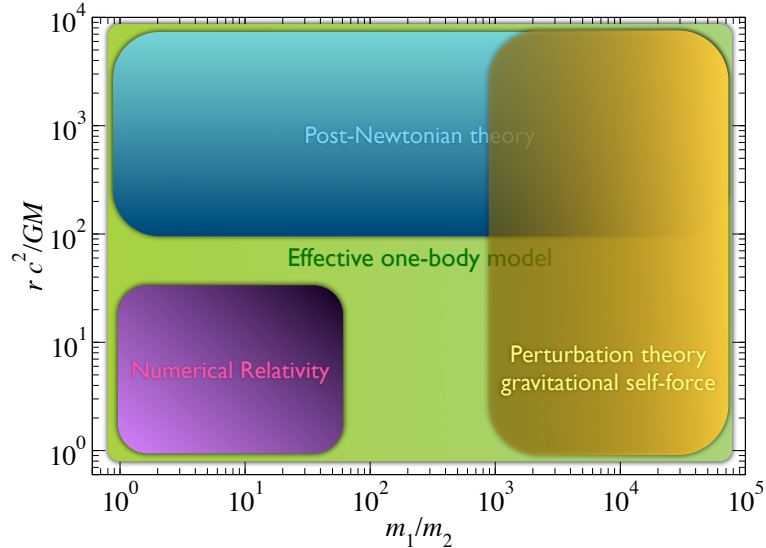


Figure 6.1 Current range of validity of the main analytical and numerical methods to solve the two-body problem.

physicists and theorists to construct templates to be used for the searches, making analytical relativity a crucial research area for experiments that will soon revolutionise our understanding of the Universe.

In the rest of this section we shall discuss the main approximation methods that have been developed to study the two-body problem in GR, highlighting some of the key theoretical ideas that have marked the last thirty years. As we shall see, in all the approximation schemes one needs to develop a conceptual and consistent framework and solve difficult technical problems. Since Einstein did not conceive the theory of GR starting from approximations to it, we shall see in relation to GWs what we gain and what we lose from the original theory when investigating it through approximation methods.

Physical scales and methods in the two-body problem: Three main methods have been proposed to tackle the two-body problem in GR: the PN approach, perturbation theory (and the gravitational self-force formalism), and NR. The first step towards setting up those approximation methods consists in identifying some small (dimensionless) parameters. In Fig. 6.1 we show the range of validity of each method using the parameters $rc^2/(GM)$ and $m_1/m_2 \geq 1$, where m_1 and m_2 are the binary's component masses, $M = m_1 + m_2$ is its total mass and r is the separation between the two bodies. If

we consider astrophysical sources that are held together by gravitational interactions, then, as a consequence of the virial theorem, $v^2/c^2 \sim GM/(rc^2)$, where v is the characteristic velocity of the bodies in the binary.

The PN formalism expands the dynamics and gravitational waveforms in powers of v/c . It is valid for any mass ratio but, in principle, only for slow motion, which, for self-gravitating objects, also implies large separations. Perturbation theory is suitable to describe the motion and radiation of a small body moving around a large body. It expands the Einstein equations around the BH metric in powers of the mass ratio m_2/m_1 . At leading order the small-body moves along geodesics of the background spacetime and can reach any speed $v \lesssim c$. When taking into account the back-reaction of the gravitational field of the small body on its motion, one needs to develop a consistent framework free of divergences. This is done within the gravitational self-force (GSF) formalism. Finally, NR solves the Einstein equations on a computer. In principle, it could be used for any mass ratio, binary separation and velocity. However, the computational cost and the requirements on the accuracy of the numerical solutions limit its range of validity. For the past thirty years the two-body problem has been tackled keeping in mind that each method has a domain of validity displayed in Fig. 6.1. As we shall see below, by proceeding without blinkers, recent work at the interfaces between the different methods has demonstrated that the limits of validity of those approaches are more blurred than expected — for example PN calculations can be pushed into the mildly relativistic regime $v/c \lesssim 0.1$ and GSF predictions could be used also for intermediate (or perhaps even comparable) mass binary systems. Moreover, an analytical formalism, namely, the EOB approach, exists that can incorporate the results of the different methods in such a way as to span the entire parameter space and provide highly-accurate templates to search for BH binaries in GW data.

Because of space limitations, the presentation of the different approximation methods will be sketchy and incomplete. The reader is referred to the original articles, reviews [72–77] and books [78–81] for more details.

6.2.1 Post-Newtonian formalism

The Einstein field equations $R_{\alpha\beta} - g_{\alpha\beta}R/2 = 8\pi GT_{\alpha\beta}/c^4$ can be recast in a convenient form introducing the field $h^{\alpha\beta} = \sqrt{-g}g^{\alpha\beta} - \eta^{\alpha\beta}$, which is a measure of the deviation of the background from Minkowskian metric $\eta_{\alpha\beta}$, and imposing the harmonic gauge condition $\partial_\beta h^{\alpha\beta} = 0$ [78],

$$\square h^{\alpha\beta} = \frac{16\pi G}{c^4}|g|T^{\alpha\beta} + \Lambda^{\alpha\beta} \equiv \frac{16\pi G}{c^4}\tau^{\alpha\beta}, \quad (6.1)$$

where \square is the D'Alambertian operator in flat spacetime, $g \equiv \det(g_{\alpha\beta})$, $T^{\alpha\beta}$ is the matter stress-energy tensor and $\Lambda^{\alpha\beta}$ depends on non-linear terms in $h^{\mu\nu}$ and $g^{\mu\nu}$ and their derivatives. By imposing no-incoming-radiation boundary conditions, one can formally solve Eq. (6.1) in terms of retarded Green functions

$$h^{\alpha\beta}(t, \mathbf{r}) = \frac{16\pi G}{c^4} \square_{\text{ret}}^{-1} \tau^{\alpha\beta} = -\frac{4G}{c^4} \int \frac{\tau^{\alpha\beta}(t - |\mathbf{r} - \mathbf{r}'|/c, \mathbf{r}')}{|\mathbf{r} - \mathbf{r}'|} d^3 r'. \quad (6.2)$$

Limiting to leading order in G and considering $r \equiv |\mathbf{r}| \gg d$ (i.e., the field point is at a far greater distance compared to the size d of the source), we can expand the integrand in powers of $1/r$ and find at leading order

$$h^{\alpha\beta}(t, \mathbf{r}) = -\frac{4G}{c^4 r} \int T^{\alpha\beta}(t - r/c + \mathbf{n} \cdot \mathbf{r}'/c, \mathbf{r}') d^3 r', \quad (6.3)$$

where $\mathbf{n} = \mathbf{r}/r$. Let us assume that the source is a PN source (i.e., it is slowly moving, weakly stressed and weakly self-gravitating). This means that $|T^{0i}/T^{00}| \sim \sqrt{|T^{ij}/T^{00}|} \sim \sqrt{|U/c^2|} \ll 1$, where U is the source's Newtonian potential. It is customary to indicate the magnitude of the above small quantities with a small parameter ϵ , which is essentially v/c where v is the characteristic, internal velocity of the source. Assuming that the source's size is d and it oscillates at frequency ω , the characteristic speed of the source is $v \sim \omega d$. From analogy to the electromagnetic case, we expect $\lambda_{\text{GW}} \sim (c/v)d$. For slow motion $v/c \ll 1$, thus $\lambda_{\text{GW}} \gg d$ and the source is located well within one wavelength. Historically, the region at a distance $r \ll \lambda_{\text{GW}}$ from the source, extending to \mathcal{R} with $\mathcal{R} \ll \lambda_{\text{GW}}$, has been denoted the *near zone*, whereas the region which extends to $r \gg \lambda_{\text{GW}}$ is denoted the *wave zone* (see Fig. 6.2).

Using the conservation of the energy-momentum tensor at linear order in G , that is $\partial_\alpha T^{\alpha\beta} = 0$, and expanding the integral (6.3) in powers of v/c , one can obtain the gravitational field at linear order in G as a function of the derivatives of the source multipole moments [30]. As originally derived by Einstein [3] and then by Landau and Lifshitz, at lowest order in the wave-generation formalism, the gravitational field in the transverse-traceless (TT) gauge and in a suitable radiative coordinate system $X^\mu = (cT, \mathbf{X})$ reads (“far-field quadrupole formula”)

$$h_{ij}^{\text{TT}} = \frac{2G}{c^4 R} \sum_{k,l} \mathcal{P}_{ijkl}(\mathbf{N}) \left[\frac{d^2}{dT^2} Q_{kl} \left(T - \frac{R}{c} \right) + \mathcal{O}\left(\frac{1}{c}\right) \right] + \mathcal{O}\left(\frac{1}{R^2}\right), \quad (6.4)$$

where $R = \sqrt{\sum_i X_i^2}$ is the distance to the source, $\mathbf{N} = \mathbf{X}/R$ is the unit vector from the source to the observer, and $\mathcal{P}_{ijkl} = \mathcal{P}_{ik}\mathcal{P}_{jl} - \mathcal{P}_{ij}\mathcal{P}_{kl}/2$ is

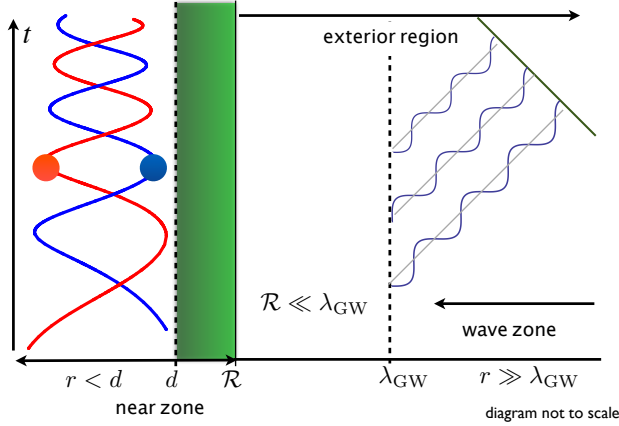


Figure 6.2 Schematic diagram of an inspiraling binary showing various scales used in the PN formalism.

the TT projection operator, where $\mathcal{P}_{ij} = \delta_{ij} - N_i N_j$ is the operator that projects onto the plane orthogonal to \mathbf{N} . The radiative coordinate system X^μ can be related to the source-rooted coordinate system $x^\mu = (ct, \mathbf{x})$ [73]. The source quadrupole moment at Newtonian order is

$$Q_{ij}(t) = \int_{\text{source}} d^3x' \rho(t, \mathbf{x}') \left(x'_i x'_j - \frac{1}{3} \delta_{ij} x'^2 \right), \quad (6.5)$$

where ρ is the Newtonian mass density. The gravitational field (6.4) is generally referred to as Newtonian because the evolution of the quadrupole moment of the source is computed using Newton's law of gravity.

Several methods have been proposed for going beyond the leading-order result to solve Eq. (6.2) approximately. In the near zone the solution $h_{\mu\nu}$ can be written in terms of instantaneous potentials, while in the wave zone retardation effects must be taken into account. Note that at higher orders gravitational waves can themselves act as sources; so $\tau^{\alpha\beta}$ in Eq. (6.2) contains both compact and non-compact support terms.

The multipolar post-Minkowskian–post-Newtonian formalism: Early on Epstein and Wagoner [82], and Thorne [30] proposed a PN extension of the Landau-Lifshitz derivation and computed the $\mathcal{O}(v^2/c^2)$ corrections to the quadrupole formula for binary systems. However, in their approach the formal application of the PN expansion leads to divergent integrals. Building on pioneering work by Bonnor et al. [83, 84] and Thorne [30], Blanchet and Damour [34, 39, 85] introduced a GW generation formalism in which the corrections to the leading quadrupolar formalism are obtained in a mathemat-

ically well-defined way. In this approach the wave-zone expansion, in which the external vacuum metric is expanded as a multipolar post-Minkowskian (MPM) series (i.e., a non-linear expansion in G), is matched to the near zone expansion, in which a PN expansion (i.e., a non-linear expansion in $1/c$) is applied, the coefficients being in the form of a multipole expansion. The multipolar expansions employ a multipole decomposition in irreducible representations of the rotation group. The gravitational field all over space can be obtained by matching the near-zone to the wave-zone fields and the matching can be accomplished at all orders, as shown by Blanchet and collaborators [86–89]. We shall denote this approach the MPM-PN formalism.

Wave-zone multipolar post-Minkowskian approximation: In the multipolar post-Minkowskian expansion, as one moves away from a weakly self-gravitating source, the spacetime quickly approaches the Minkowskian spacetime. At a distance r from the source with mass M , the deviations from the metric scale like r_s/r with $r_s = 2GM/c^2$. Thus, in the region $d < r < +\infty$, one can solve the vacuum Einstein equations iteratively in powers of G . Indeed, one sets $\sqrt{-g}g^{\alpha\beta} = \eta^{\alpha\beta} + Gh_1^{\alpha\beta} + G^2h_2^{\alpha\beta} + \dots$, that is $h^{\alpha\beta} = \sum_{n=1} G^n h_n^{\alpha\beta}$, substitutes this expression in the Einstein's equations (6.1) in vacuum, obtaining

$$\square h^{\alpha\beta} = \Lambda^{\alpha\beta} = N^{\alpha\beta}(h, h) + M^{\alpha\beta}(h, h, h) + \mathcal{O}(h^4), \quad (6.6)$$

and equates terms of the same order in G .

At linear order in G , the most general homogeneous solution satisfying the harmonic gauge can be written in terms of symmetric trace-free tensors (STF), which are a complete basis of the rotation-group's representation, that is $h_1^{\alpha\beta} = \sum_{\ell=0} \partial_L [K_L^{\alpha\beta}(t - r/c)/r]$ where $L = i_1 \cdots i_\ell$ denotes a multi-index composed of ℓ STF indices i_1, \dots, i_ℓ , ranging from 1 to 3. More explicitly, one finds that the most general solution satisfying the gauge condition is given by $h_1^{\alpha\beta} = k_1^{\alpha\beta} + \partial^\alpha \varphi_1^\beta + \partial^\beta \varphi_1^\alpha - \eta^{\alpha\beta} \partial_\rho \varphi_1^\rho$, where $k_1^{\alpha\beta}$ and φ_1^α can be expressed in terms of two *source* multipole moments, $\{I_L, J_L\}$, that encode properties of the source and four multipole functions, $\{W_L, X_L, Y_L, Z_L\}$, that parameterise gauge transformations. Eventually, these six moments can be reduced to two gauge-inequivalent canonical ones $\{M_L, S_L\}$. At quadratic order in G , one needs to invert the equation $\square h_2^{\alpha\beta} = N^{\alpha\beta}(h_1, h_1)$. Because $h_1^{\alpha\beta}$ is known only in the exterior region ($r > d$), one cannot employ retarded or advanced Green functions for which it is necessary to know the solution everywhere in space. However, at each finite PN order only a finite number of multipole moments contribute. So, one applies a multipolar post-Minkowskian expansion outside the source for $d/r < 1$ and introduces

a regularisation to extend $N^{\alpha\beta}(h_1, h_1)$ at the origin. Blanchet and Damour proposed that at each order G^n the function $\Lambda_n^{\alpha\beta}$ be multiplied by r^B , B being a complex number whose real part is positive and sufficiently large, so that $r^B \Lambda_n^{\alpha\beta}$ is regular at the origin. Then, the solution of $\square h_n^{\alpha\beta} = r^B \Lambda_n^{\alpha\beta}$ is obtained by using retarded Green functions, analytic continuation in the complex B -plane and extracting the coefficient of the zeroth power of r ($B = 0$), that is $u_n^{\alpha\beta} = \text{FP}_{B=0} \left\{ \square_{\text{ret}}^{-1}[r^B \Lambda_n^{\alpha\beta}] \right\}$, where FP stands for finite part [34]. The most general solution is obtained by adding to the inhomogeneous solution $u_n^{\alpha\beta}$ the homogeneous solution $v_n^{\alpha\beta}$, such that the harmonic gauge condition $\partial_\alpha h_n^{\alpha\beta} = 0$ is satisfied. Thus, $h_n^{\alpha\beta} = u_n^{\alpha\beta} + v_n^{\alpha\beta}$. The solution $h_n^{\alpha\beta}$ depends on the canonical multipole moments M_L and S_L , which at this stage do not know anything about the matter source. They only parameterise the most general solution of the Einstein equations in vacuum.

Near-zone post-Newtonian approximation: In the near zone one wants to obtain the solution of Eq. (6.2) in a multipolar PN expansion. Expanding $h^{\alpha\beta}$ and $\tau^{\alpha\beta}$ in powers of $1/c$, that is $h^{\alpha\beta} = \sum_{n=2}^{(n)} h^{\alpha\beta}/c^n$ and $\tau^{\alpha\beta} = \sum_{n=-2}^{(n)} \tau^{\alpha\beta}/c^n$, substituting them in the Einstein equations (6.1) and equating terms of the same order in $1/c$, one finds the following relation [80] $\nabla^2[(n)h^{\alpha\beta}] = 16\pi G [(n-4)\tau^{\alpha\beta}] + \partial_t^2[(n-2)h^{\alpha\beta}] \equiv (n)f^{\alpha\beta}$. If one were solving the above differential equation via Poisson integrals, the presence of non-compact-support terms at some order in the PN expansion would prevent the integral from converging at spatial infinity. The convergence problem becomes even more severe when the multipolar expansion $1/|\mathbf{r} - \mathbf{r}'| = 1/r + \mathbf{r} \cdot \mathbf{r}'/r^3 + \dots$ is applied. These were the problems that affected the original method of Epstein, Wagoner and Thorne. They were overcome by applying a more sophisticated mathematical method to invert the Laplacian and find the correct solution. This method is a variant of the analytic continuation technique developed by Blanchet and Damour in the wave zone, and it was carried out in [86–90]. Basically, one multiplies the function $(n)f^{\alpha\beta}$ by r^B , where B is a negative real number whose modulus is sufficiently large that the integral is regular at spatial infinity. Then, the inhomogeneous solution is derived by analytic continuation in the complex B -plane and extracting the coefficient of the pole at $B = 0$, that is $(n)u^{\alpha\beta} = \text{FP}_{B=0} \left\{ (\nabla^2)^{-1}[(n)f^{\alpha\beta} r^B] \right\}$. The most general solution is obtained by adding the homogeneous solution $(n)v^{\alpha\beta}$ that is regular at the origin $r = 0$, to the inhomogeneous solution, that is $(n)h^{\alpha\beta} = (n)u^{\alpha\beta} + (n)v^{\alpha\beta}$. As derived in [86–91], the solution in the near zone that matches the external field and satisfies correct boundary conditions at infinity involves a specific

homogenous solution which can be expressed in terms of STF tensors as $\sum_{\ell=0} \partial_L [F_L^{\alpha\beta}(t - r/c)/r - F_L^{\alpha\beta}(t + r/c)/r]$ and it is fixed by matching it to the post-Minkowskian solution. In the region $d < r < \mathcal{R}$ the multipolar PN and post-Minkowskian series are both valid and one can resort to the standard method of matched asymptotic expansion to relate them, obtaining the solution all over space, $0 < r < +\infty$. In particular, the matching allows expression of the canonical multipole moments M_L and S_L (or the source multipole moments $\{I_L, J_L, W_L, X_L, Y_L, Z_L\}$) in terms of integrals that extend over the matter and gravitational fields described by the PN-expanded $\tau^{\alpha\beta}$.

Direct integration of the relaxed Einstein equations: A different formalism that also cures the convergence issues that plagued previous brute-force, slow-motion approaches to gravitational radiation from isolated sources, was developed by Will, Wiseman and collaborators [54, 92, 93]. It is called the Direct Integration of the Relaxed Einstein Equation (DIRE). It differs from the MPM-PN approach in the definition of the source multipole moments. In both formalisms, the moments are generated by the PN expansion of $\tau^{\alpha\beta}$ in Eq. (6.2). However, in the DIRE formalism they are defined by compact-support integrals terminating at the radius \mathcal{R} enclosing the near zone, while in the MPM-PN approach, as we have discussed, the moments are defined by integrals covering the entire space and are regularised using the finite-part procedure.

Gravitational waveform in the wave zone: When neglecting terms of order $1/R^2$ or higher, the general expression of the TT waveform that goes beyond the leading-order term (6.4) reads

$$h_{ij}^{\text{TT}} = \frac{4G}{c^2 R} \sum_{k,q} \mathcal{P}_{ijkq}(\mathbf{N}) \sum_{\ell=2}^{+\infty} \frac{1}{c^\ell \ell!} \left[N_{L-2} U_{kqL-2} - \frac{2\ell N_{mL-2} \varepsilon_{mn(k} V_{q)nL-2}}{c(\ell+1)} \right], \quad (6.7)$$

where the integer ℓ refers to the multipolar order, ε_{ijk} is the Levi-Civita antisymmetric symbol, parentheses denote symmetrisation and U_L and V_L are the multipole moments at infinity (called *radiative* multipole moments), which are functions of the retarded time $T - R/c$. The radiative multipoles U_L and V_L can be expressed in terms of the canonical multipole moments M_L and S_L as $U_L(T) = d^\ell M_L/dT^\ell + \mathcal{F}_L[M(T'), S(T')]$ and $V_L(T) = d^\ell S_L/dT^\ell + \mathcal{G}_L[M(T'), S(T')]$ where \mathcal{F}_L and \mathcal{G}_L are multi-linear retarded functionals of the full past behaviour, with $T' < T$. For example, the radiative mass-type

multipole reads

$$U_L = \frac{d^\ell M_L}{dT^\ell} + \frac{2GM}{c^3} \int_0^\infty d\tau M_L^{(\ell+2)}(T_R - \tau) \left[\log\left(\frac{c\tau}{2r_0}\right) + \kappa_\ell \right] + \mathcal{O}\left(\frac{1}{c^5}\right), \quad (6.8)$$

where $T_R = T - R/c$, r_0 is an arbitrary length scale and κ_ℓ are constants. The term at order $1/c^3$ in the equation above describes the effect of back scattering of the gravitational waves on the Schwarzschild-like curvature associated with the total mass M of the source, the so-called *tail terms* [37, 94]. At order $1/c^5$, one has another hereditary term called the *memory term*, which is generated by non-linear interactions between multipole moments [42]. At order $1/c^6$, tails back scatter again with the Schwarzschild-like curvature generating *tail-of-tail terms* [95].

Gravitational-wave flux at infinity: The GW energy flux (or luminosity) \mathcal{L} can be expressed in terms of the radiative multipole moments. It reads:

$$\begin{aligned} \mathcal{L} = & \sum_{\ell=2} \frac{G}{c^{2\ell+1}} \left[\frac{(\ell+1)(\ell+2)}{(\ell-1)\ell\ell!(2\ell+1)!!} \left(\frac{dU_L}{dT} \right)^2 \right. \\ & \left. + \frac{4\ell(\ell+2)}{c^2(\ell-1)(\ell+1)!(2\ell+1)!!} \left(\frac{dV_L}{dT} \right)^2 \right]. \end{aligned} \quad (6.9)$$

and at leading order, using $U_{ij} = d^2Q_{ij}/dT^2 + \mathcal{O}(1/c^3)$, the luminosity reduces to the famous ‘‘Einstein quadrupole formula’’

$$\mathcal{L} = \frac{G}{5c^5} \left[\frac{d^3Q_{ij}}{dT^3} \frac{d^3Q_{ij}}{dT^3} + \mathcal{O}\left(\frac{1}{c^2}\right) \right]. \quad (6.10)$$

Gravitational radiation reaction: The gravitational radiation acts back on the motion of the binary through a radiation-reaction force. To have an explicit temporal representation of the waveform h_{ij}^{TT} and the fluxes, one needs to solve the problem of motion of the source, including radiation-reaction effects. The first relativistic terms in the equations of motion, at the 1PN order, were derived by Lorentz and Droste [96]. Then Einstein, Infeld and Hoffmann obtained the full 1PN corrections using the surface-integral method [97], in which the equations of motions are deduced from the vacuum field equations and they are valid for any compact object (NS, BH, etc.). Petrova [98], Fock [99] and Papapetrou [100] also obtained the equations of motion for the centres of extended bodies at 1PN order. Kimura, Ohta and collaborators introduced the ADM Hamiltonian formalism for doing PN

computations [101, 102] and started the computation of the equations of motion for nonspinning bodies at 2PN order [103, 104]. The equations of motion for nonspinning point masses through 2.5PN order in harmonic coordinates were obtained by Damour and Deruelle [31, 33], who built on the nonlinear iteration of the metric proposed by Bel et al. [105]. The gravitational radiation-reaction force in the equations of motion at 2.5PN order made it possible to unambiguously test general relativity through the observation of the secular acceleration in the orbital motion of binary pulsars [106]. Quite importantly, because of the *effacement principle*, the 2.5PN equations of motion are independent of the internal structure of the bodies [107]. In fact, the latter effect appears only at 5PN order for compact bodies. The 2.5PN equations of motion for point masses were also derived using extended compact objects by Kopeikin [108]. Itoh, Futamase and Asada [109] also computed the equations of motion through 2.5PN order, using a variant of the surface-integral method. In Table 6.1 we summarise the current status of the computation of the two-body equations of motion.

Advances in regularisation method: In the MPM-PN approach the two bodies are treated as point particles using delta functions. As a consequence, singularities appear when computing the near-zone metric and the equations of motion, because the gravitational field needs to be computed at the location of the particles. Thus, it is necessary to introduce a regularisation. Until the early 2000's the Hadamard regularisation was employed [110], but it does not provide unambiguous results at 3PN order, and so dimensional regularisation, which is a well-known regularisation scheme in particle physics, was adopted [111].

Canonical Hamiltonian approach: Another analytical approach that has been very effective in computing the two-body equations of motion at high PN orders is the canonical Hamiltonian approach. The canonical Hamiltonian formulation of GR was developed in 1958–1963 by Dirac [112–114], Arnowitt, Deser, Misner (ADM) [115, 116], and Schwinger [117], with important contributions by deWitt [118], and Regge and Teitelboim [119] in the 60s and 70s. The original motivation of the formulation was the quantisation of GR.

Assuming asymptotically flat spacetime and an asymptotically Minkowskian reference frame, one considers the 4-dimensional metric $g_{\alpha\beta}$ and the extrinsic curvature K_{ij} of the spacelike hypersurface $x^0 = \text{const}$. The Lagrangian describing non-spinning point particles interacting gravitationally

is

$$L = \sum_A \mathbf{p}_A \frac{d\mathbf{x}_A}{dt} + \int d^3x (\pi^{ij} g_{ij,0} - N_\alpha \mathcal{H}^\alpha) - \oint d^2s_i \partial_j (g_{ij} - g_{kk} \delta_{ij}), \quad (6.11)$$

where the surface integral is computed at infinity on the spacelike hypersurface $x^0 = \text{const}$, $\pi^{ij} = -\sqrt{g}(K^{ij} - g^{ij}K)$ is the variable conjugate to g_{ij} , $K = g^{ij}K_{ij}$, $N_0 = (-g^{00})^{-1/2}$ and $N_i = g_{0i}$ are the shift and lapse functions, respectively, and \mathcal{H}_α are the four-momentum densities, which depend on the intrinsic curvature of the spacelike hypersurface $x^0 = \text{const}$ and on the matter energy-momentum tensor. The Hamiltonian can be derived from the Lagrangian through a Legendre transformation. It reads

$$H = \int d^3x N_\alpha \mathcal{H}^\alpha + \oint d^2s_i \partial_j (g_{ij} - g_{kk} \delta_{ij}), \quad (6.12)$$

where the second term on the right hand side is the usual ADM energy. Variations of the Lagrangian (6.11) with respect to g_{ij} and π^{ij} give the field equations, while variations with respect to N_α yields the constraint equations $\mathcal{H}^\alpha = 0$. ADM introduced suitable coordinate conditions that allow solution of the field and constraint equations for the metric coefficients such that they become Minkowskian asymptotically. By adopting such a coordinate system and imposing the constraint equations, one obtains the *reduced* Hamiltonian $H_{\text{reduced}} = E[h_{ij}^{\text{TT}}, \pi^{ij \text{ TT}}, \mathbf{x}_A, \mathbf{p}_A]$, which contains the full information for the dynamical evolution of the canonical field variables h_{ij}^{TT} and $\pi^{ij \text{ TT}}$ and the canonical particle variables \mathbf{x}_A and \mathbf{p}_A . The reduced Hamiltonian has been explicitly computed by solving the constraint equations in a PN expansion and by adopting a suitable regularisation procedure. It contains a matter piece, an interaction piece that yields the radiation-reaction force, and a radiation piece. The energy and angular momentum losses can be computed through surface integrals in the wave zone. The ADM Hamiltonian has been successfully extended to gravitationally interacting spinning particles using a tetrad generalisation of the ADM canonical formalism. This allowed the computation of spin-orbit and spin-spin couplings at quite high PN orders. So far, the ADM Hamiltonian approach has been developed mostly for the conservative dynamics through high PN orders [32, 50, 51, 101, 102, 111, 120–126].

Effective-field theory approach: The two-body equations of motion and gravitational radiation have also been computed using Feynman diagrams, in GR by Bertotti and Plebanski [127], Hari Dass and Soni [128], and in scalar-tensor theories by Damour and Esposito-Farese [129]. An important turning

point occurred in 2006, when Goldberger and Rothstein proposed a more systematic use of Feynman diagrams within effective field theory (EFT) to describe non-relativistic extended objects coupled to gravity [130]. As discussed above, there are three relevant scales in the two-body problem: r_s , the internal structure scale or the size of the compact object; r , the orbital separation, and $\lambda_{\text{GW}} \sim r(c/v)$, the radiation wavelength, where v is the typical velocity of the body in the binary. To carry out calculations in a systematic manner at high orders in v , Goldberger and Rothstein took advantage of the separation among those scales to set up a tower of effective field theories that account for effects at each scale [131].

When using the EFT approach to describe the object's size r_s , one does not need to resort to a specific model of the short-scale physics to resolve the point-particle singularity. Instead, one integrates out the internal structure of the object by matching onto an effective theory that captures the relevant degrees of freedom. Thus, one systematically parameterises the ignorance of the internal structure by building an effective point-particle Lagrangian that includes the most general set of operators consistent with the symmetry of GR (i.e., with general coordinate invariance). The operators in the point-particle Lagrangian have coefficients which encapsulate the properties of the internal structure of the extended objects. Moreover, short-distance divergences can be regularised and renormalised using standard methods in quantum field theory. Given a model for the internal structure, the value of the coefficients in the point-particle Lagrangian can be adjusted by a short-distance matching calculation so that they reproduce the observables of the isolated object. The resulting effective point-particle Lagrangian correctly describes length scales all the way to the orbital separation r . Then, to describe the binary problem at the scale r , it would be necessary to go beyond the point-particle effective Lagrangian and integrate out all modes of the graviton with wavelengths between the scales r_s and r , so that one obtains an effective Lagrangian of composite particles interacting with long wavelength modes of the gravitational field.

So far, the EFT approach has recovered and confirmed the PN results that were previously obtained with the MPM-PN, DIRE and ADM canonical Hamiltonian methods for the two-body equations of motion up to 3.5PN order when spins are neglected [132, 133]. When spin effects are included, the EFT approach has extended the knowledge of the conservative dynamics and multipole moments to high PN orders [134–145].

Summary of results and final remarks: In Table 6.1 we summarise the impressive current status of PN calculations for the conservative dynamics,

Table 6.1 *State-of-the-art of PN calculations for compact binaries with comparable masses. We list main references that contributed to the current accuracy. Unless otherwise specified, $n/2$ -PN refers to the PN term of formal order $\mathcal{O}(1/c^n)$ relative to the leading non-spinning term.*

	No Spin	Spin-Linear	Spin-Squared	Tidal
	4PN ^a	3.5PN	3PN	7PN ^b
Conservative Dynamics	[121, 122, 133] [126, 158–164]	[52, 54, 141] [140, 165–169]	[52, 54, 138] [137, 170–172]	[155–157]
Energy Flux at Infinity	3.5PN [95, 173, 174]	4PN [175–178]	2PN [53, 54, 179–181]	6PN [182]
RR Force	4.5PN [37, 93, 183–185]	4PN [186–188]	4.5PN [189]	6PN [155]
Waveform Phase ^c	3.5PN [190]	4PN [175, 177, 178]	2PN [54, 179–181, 191]	6PN [182, 192]
Waveform Amplitude ^e	3PN ^d [194–197]	2PN [191, 198]	2PN [53, 54, 191, 198]	6PN [156, 182]
BH Horizon Energy Flux ^g	5PN [199]	3.5PN [200, 201]	4PN ^f [200, 201]	— —

^a Partial higher-order PN terms in the two-body energy for circular orbits have been computed both analytically and numerically [146–151]. Bini-Damour work built on Refs. [152–154].

^b 2PN tidal effects in the conservative dynamics are known explicitly only for circular orbits.

^c We refer to quasi-circular orbits only.

^d The -2 spin-weighted $(2, 2)$ mode is known through 3.5PN order [193].

^e We refer to quasi-circular orbits only.

^f Spin couplings beyond the squared ones have also been computed.

^g We count the PN order with respect to the leading-order luminosity at infinity. BH horizon flux terms start at 4PN and 2.5PN orders in the non-spinning and spinning case, respectively.

equations of motion and waveforms, for compact objects with and without intrinsic rotation (or spin) and tidal effects. We indicate with $n/2$ -PN the PN term of formal order $\mathcal{O}(1/c^n)$ relative to the leading non-spinning term 4. (For PN results of highly eccentric systems the reader may consult [73] and references therein.)

In summary, during the last thirty years there has been tremendous progress

⁴ The spin of a rotating body is on the order $S \sim mlv_{\text{rot}}$, where m and l denote the mass and typical size of the body, respectively, and where v_{rot} represents the velocity of the body's surface. Here, we consider bodies which are both compact, $l \sim Gm/c^2$, and maximally rotating, $v_{\text{rot}} \sim c$. For such objects the magnitude of the spin is roughly $S \sim Gm^2/c$.

in the PN computation of the two-body equations of motion and gravitational radiation. Results obtained using different analytical techniques (i.e., point particles described by Dirac delta-functions, surface-integral methods, post-Minkowskian and PN expansions, canonical Hamiltonian formalism, and EFT approach) have been compared with each other and agree. We stressed at the beginning of Sec. 6.2 that Einstein did not conceive the theory of GR starting from approximations to it. In spite of this, the PN approximation to the two-body dynamics is able to capture all relevant features of the weak-field, slow-motion dynamics and it can approximate quite well the theory of GR as long as the motion of comparable-mass compact objects is not highly relativistic and PN corrections at the highest order currently known are included. Future work at the interface between numerical and analytical relativity will be able to determine more precisely the PN region of accuracy, but this will imply doing very long NR simulations (i.e., simulations over hundreds of orbits) for generic binary configurations.

As we shall discuss in Sec. 6.3.4, current PN results allow us to compute the GW phasing with sufficient accuracy to detect quasi-circular, neutron-star inspirals and extract physical parameters if neutron stars carry mild spins. Moreover, the knowledge of higher-order PN calculations has made it possible to test the reliability of the PN expansion as the two bodies approach each other and also understand the practicability of extending those calculations at any PN order. It turns out that as one approaches the last stages of inspiral crucial quantities that enter the computation of the waveforms start being very sensitive to the PN truncation error, leading to unreliable results. As we shall see below, by wisely combining different analytical techniques one can avoid such shortcomings and further improve the accuracy of the two-body dynamics and GW emission up to coalescence.

6.2.2 Perturbation theory and gravitational self force

Extreme-mass-ratio inspirals composed of a stellar-mass compact object orbiting a supermassive or massive BH are promising sources for space-based and (future) ground-based detectors. The orbits are expected to be highly eccentric, non-equatorial and relativistic. To detect such binary systems and extract the strong-field information encoded in the spacetime around the larger body, one needs to model very accurately the equations of motion of the smaller body orbiting the BH and develop a consistent, appropriate wave-generation formalism. The PN framework, which is limited to slow velocities, is not suitable in this case. One needs to include relativistic effects at all orders and expand the field equations in the binary mass ratio (see

Fig. 6.1). Henceforth, we let m denote the mass of the small object, M the mass of the central object and $q = m/M$ the mass ratio. Typically, extreme mass-ratio binaries have $q \lesssim 10^{-5}$. If $g_{\mu\nu}$ is the metric of the background spacetime, the perturbation produced by the particle is $h_{\mu\nu} = g_{\mu\nu} - g_{\mu\nu}$, where $g_{\mu\nu}$ is the metric of the perturbed spacetime. The metric perturbation can be written as $h_{\alpha\beta} = \sum_{n \geq 1} h_{\alpha\beta}^{(n)}$ with $h_{\alpha\beta}^{(n)} \propto q^n$. In the limiting case of a very small test mass orbiting a heavy central mass, one works at first order in q and obtains equations for the linear perturbations of the background geometry roughly of the kind $\square_g h_{\alpha\beta}^{(1)} \sim T_{\alpha\beta}[z] \sim \mathcal{O}(m)$, where $T_{\alpha\beta}$ is the energy-momentum tensor of the small body and z^μ its worldline. [Essentially one obtains Eq. (6.1) with $\eta_{\mu\nu}$ replaced by the background metric $g_{\mu\nu}$ and the higher-order terms $\Lambda_{\mu\nu}$ neglected.] Those equations were derived in 1950's and 1970's for the metric perturbations by Regge-Wheeler and Zerilli (RWZ) [202, 203] in the Schwarzschild case, and for the curvature perturbations by Teukolsky [204] in the Kerr case. Using suitable gauges, those equations (or variants of them [205]) can be integrated analytically, for quasi-circular orbits, by PN expansion in powers of v/c , v being the velocity of the small body, obtaining the gravitational radiation and luminosity at very high PN orders. (Strictly speaking one computes analytically the Green function associated with the master equations.) In Table 6.2 we summarise the current status of PN calculations in BH perturbation theory. Furthermore, at leading order in the computation of the radiation field, one can assume that the small test mass moves along an adiabatic sequence of geodesics of the fixed background spacetime and compute the gravitational radiation numerically solving the RWZ and Teukolsky equations [55, 56, 206–208]. Much progress has been made in the last twenty years to evolve those equations in a robust, accurate and fast way [209–216], and compute the gravitational waveform $h_{\alpha\beta}^{(1)}$ in the wave zone. Today, time-domain RWZ and Teukolsky equations can compute not only the waveform emitted during the very long inspiral stage, but also the plunge, merger and ringdown stages [216–221].

The perturbation sourced by the small test mass not only produces outgoing radiation in the wave zone that removes energy and angular momentum from the particle, but also produces a field in the near zone that acts on the test mass (i.e., the GSF) and gradually diverts it from its geodesic motion. Besides conservative terms, the GSF contains dissipative contributions that are responsible for the radiation-reaction force. The finite-mass corrections to the orbital motion due to the GSF are important for detection of extreme mass-ratio binaries and extraction of parameters. Although at any

Table 6.2 *State-of-the-art of PN calculations in BH perturbation theory (i.e., for an extreme mass-ratio compact binary) in the case of quasi-circular orbits. We list main references that contributed to the current accuracy. Unless otherwise specified, $n/2$ -PN refers to the PN term of formal order $\mathcal{O}(1/c^n)$ relative to the leading non-spinning term.*

	No Spin	Spin-Linear	Spin-Squared
Energy Flux at Infinity	22PN [55, 59, 222–226]	4PN [57, 58, 60]	4PN [60, 227]
BH Horizon Flux ^b	6PN [152, 228, 229]	6.5PN [152, 229, 230]	6.5PN ^a [152, 229, 230]

^a Spin couplings beyond the squared ones are also present.

^b We count the PN order with respect to the leading-order luminosity at infinity. BH horizon flux terms start at 4PN and 2.5PN orders in the non-spinning and spinning case, respectively.

given time the GSF yields fractional corrections to the motion of the small body on the order of $q \ll 1$, these corrections accumulate over the very large number of cycles ($\sim 1/q$), thus producing effects that cannot be neglected.

The computation of the GSF is not an easy task because the field generated by the particle's motion diverges on the particle's worldline. Indeed, the gravitational field is infinite at the particle's position. Thus, one first needs to isolate the field's singular part. Quite interestingly, a careful analysis shows that the singular piece does not affect the motion of the particle, but only contributes to the particle's inertia and it renormalises its mass. The regular field is solely responsible for the GSF.

The case of a point electric charge moving in flat spacetime is well understood and dates back to work by Lorentz, Abrahams, Poincaré and Dirac [231]. The extension to curved spacetime has not been straightforward [232–234]. The proper definitions of the singular and regular Green functions from the Hadamard elementary functions for the wave equation in curved spacetime were obtained only in 2003 by Detweiler and Whiting [235]. In curved spacetime the GSF is non-local in time. It is given by a tail integral describing radiation that is first emitted by the particle and then comes back to the particle after interacting with the spacetime curvature. Because the regular field that is fully responsible for the GSF satisfies a homogeneous wave equation, it is a free radiation-field that interacts with the particle and carries information about its past. We now follow [76] and sketch the derivation of the GSF equation at first order.

The gravitational perturbations produced by a point particle of mass m can be described by the trace-reversed potentials $\gamma_{\mu\nu} = h_{\mu\nu} - 1/2(g^{\rho\lambda}h_{\rho\lambda})g_{\mu\nu}$. Imposing the Lorenz gauge $\gamma^{\mu\nu}_{;\mu} = 0$, one finds that the trace-reversed potentials satisfy the equation $\square\gamma^{\alpha\beta} + 2R_{\mu}^{\alpha\nu}\gamma^{\mu\nu} = -16\pi GT^{\alpha\beta}/c^4$, where covariant differentiation uses the background metric $g_{\mu\nu}$, $\square = g^{\mu\nu}\nabla_{\mu}\nabla_{\nu}$, $T^{\alpha\beta}$ being the point-mass's energy momentum tensor. The solutions for the potentials are obtained in terms of retarded Green functions $G_{+}^{\alpha\beta}$ as $\gamma^{\alpha\beta}(x) = 4m \int_{\gamma} G_{+}^{\alpha\beta}(x, z)u^{\mu}u^{\nu}d\tau$ where the integral is done on the body worldline and $u^{\mu} = dz^{\mu}/d\tau$. The perturbations $h_{\mu\nu}$ are derived by inverting the equation $\gamma_{\mu\nu} = h_{\mu\nu} - 1/2(g^{\rho\lambda}h_{\rho\lambda})g_{\mu\nu}$. Furthermore, the equation of motion of the small body are obtained: (i) imposing that the body follows geodesics in the metric $g_{\mu\nu}$ of the perturbed spacetime, (ii) removing the singular part $h_{\mu\nu}^S$ from the retarded perturbation and (iii) postulating that it is the regular part $h_{\mu\nu}^R$ that acts on the small body. They read

$$a^{\mu} = -\frac{1}{2}(g^{\mu\nu} + u^{\mu}u^{\nu})(2h_{\nu\lambda\rho}^{\text{tail}} - h_{\lambda\rho\nu}^{\text{tail}})u^{\lambda}u^{\rho}, \quad (6.13)$$

with

$$h_{\mu\nu\lambda}^{\text{tail}} = 4m \int_{-\infty}^{\tau^-} \nabla_{\lambda}(G_{+\mu\nu\mu'\nu'} - \frac{1}{2}g_{\mu\nu}G_{+\rho\mu'\nu'}^{\rho})(z(\tau), z(\tau'))u^{\mu'}u^{\nu'}d\tau', \quad (6.14)$$

where $\tau^- = \tau - \epsilon$ is introduced to avoid the singular behaviour when $\tau' = \tau$, $z(\tau)$ is the current position of the particle; all tensors with unprimed indices are evaluated at the current position, while tensors with primed indices are evaluated at prior positions $z(\tau')$. Finally, on the particle worldline the regular field is $h_{\mu\nu;\lambda}^R = -4m(u_{(\mu}R_{\nu)}{}_{\rho\lambda\xi} + u_{\lambda}R_{\mu\rho\nu\xi})u^{\rho}u^{\xi} + h_{\mu\nu\lambda}^{\text{tail}}$.

The equation of motion (6.13) was first derived in 1996 by Mino, Sasaki and Tanaka [233], and then by Quinn and Wald [234]. It is known as the MiSaTaQuWa equation of motion. It is important to notice that whereas in the original derivation the MiSaTaQuWa equation appears as the geodesic equation in the metric $g_{\mu\nu} + h_{\mu\nu}^{\text{tail}}$, in the interpretation by Detweiler and Whiting, it is a geodesic equation in the (physical) metric $g_{\mu\nu} + h_{\mu\nu}^R$, which is regular on the worldline of the body and satisfies the Einstein equations in vacuum. The derivation in [233, 234] is limited to point masses, but Gralla and Wald [236], and Pound [237] demonstrated that the MiSaTaQuWa equation applies to any compact object of arbitrary internal structure. The MiSaTaQuWa equation of motion is not gauge invariant [238] and relies on the Lorenz gauge condition. To obtain physically meaningful results, one needs to combine the MiSaTaQuWa equation of motion with the metric perturba-

tions $h_{\mu\nu}$ to obtain gauge invariant quantities that can be related to physical observables.

Although considerable progress has been made in the last several years to develop methods to calculate the metric perturbation and GSF at first order [238, 239], the majority of the work has focused on computing the GSF on a particle that moves on a *fixed* worldline of the background spacetime — for example for a static particle [240], radial [241], circular [242, 243] and eccentric [244, 245] geodesics in Schwarzschild. Methods to compute the GSF on a particle orbiting a Kerr BH have been proposed (e.g., see [246]) and actual implementations are underway. Recently, [247] has carried out the first calculation, in Schwarzschild spacetime, that takes into account changes in the particle’s worldline as the GSF acts on the particle. It is important to stress that it is computationally very intensive to integrate the Einstein equations for very long inspiraling orbits. For this reason approximation methods have also been developed. Assuming that secular effects associated with the GSF accumulate on time scales much longer than the orbital period, one can employ the adiabatic approximation [248–252], which uses a field that is sourced by a geodesic and neglects periodic effects and the conservative portion of the GSF. For some choices of the binary parameters the adiabatic approximation can be sufficiently accurate for detection, but it has been shown [253] to be generically inaccurate for extracting binary parameters.

The GSF program is not yet complete. To obtain sufficiently accurate templates produced by extreme mass-ratio binaries, the GSF needs to be computed at first order in q , but the gravitational energy flux at second order in q . This implies that the metric perturbations need to be computed at second order. The formalism to derive metric perturbations at second order has been developed [254–256], calculations are underway and might be completed in a few years. Nevertheless, steady advances in the knowledge of the GSF have already been used to derive interesting, physical effects and higher-order PN terms, as we now discuss.

Barack and Sago [244] combined the conservative pieces of the GSF and metric perturbations to calculate the frequency shift in the innermost, stable circular orbit that originates from the GSF of the small body in Schwarzschild spacetime (see [257] for the extension to the Kerr spacetime). In [258] a similar shift was computed in the rate of periastron advance for eccentric orbits. In 2008 Detweiler pointed out [243] that the time component of the velocity vector, u^t , of a small test mass in the Schwarzschild spacetime is gauge invariant with respect to transformations that preserve the helical symmetry of the perturbed spacetime. The inverse of u^t is an observable, as it is

the gravitational redshift experienced by photons emitted by the orbiting body and observed at a large distance on the orbital axis. The redshift has been computed numerically through a GSF calculation as a function of the (gauge invariant) orbital frequency and it has been compared to analytical predictions [146, 150, 151] and used to extract yet unknown higher-order PN terms beyond the test-particle limit [146, 147, 149, 259, 260]. The latter was possible through the first-law of binary BH dynamics [147, 260, 261]. Quite importantly, the redshift factor has been shown to be simply related to the binding energy and angular momentum of circular-orbit binaries [260]. Thus, the knowledge of the redshift can be employed to compute relativistic effects linear in q in the (specific) binding energy and angular momentum [148, 262, 263]. Other dynamical invariants have also been derived [264–266].

Lastly, in the absence of GSF results at second order in q and of comparisons to NR simulations for intermediate mass-ratio binaries, it is difficult to assess the region covered by GSF results in Fig. 6.1. It is generally believed that the knowledge of relativistic effects at first order in q in the conservative dynamics and second order in q in the dissipative sector would be able to describe only waveforms from extreme-mass ratio inspirals having $q \lesssim 10^{-5}$. However, results at the interface between GSF, PN theory and NR, are suggesting that leading order GSF results may have a much larger range of validity including intermediate mass-ratio binaries and perhaps even comparable mass binaries when q is replaced by the symmetric mass ratio $mM/(m+M)^2$ [267–269]. Approximations to GR continue to be surprisingly successful.

6.2.3 The effective-one-body formalism

In 1998-2000, motivated by the construction of LIGO and Virgo detectors and the absence of merger waveforms for comparable-mass binary BHs from NR, an analytical approach that combines the PN expansion and perturbation theory, known as the effective-one-body (EOB) approach [65, 66], was introduced. This novel approach was aimed at modeling analytically both the motion and the radiation of coalescing binary systems over the entire binary evolution (i.e., from the inspiral to the plunge, then the merger and the final ringdown). Several predictions [66, 270] of the EOB approach has been broadly confirmed by the results of NR simulations. These include: (i) the blurred, adiabatic transition from the inspiral to a plunge, which is merely a continuation of the inspiral, (ii) the extremely short merger phase, (iii) the simplicity of the merger waveform (i.e., the absence of high-frequency fea-

tures in it, with the burst of radiation produced at the merger being filtered by the potential barrier surrounding the newborn BH), (iv) estimates of the radiated energy during the last stages of inspiral, merger and ringdown (0.6% to 5% of the binary total mass depending on BH spin magnitude) and spin of the final BH (e.g., $0.8M_{\text{BH}}^2$ for an equal-mass binary, M_{BH} being the final BH mass), and (v) prediction that a Kerr BH will promptly form at merger even when BHs carry spin close to extremal. Soon after its inception, the EOB model was extended to include leading-order spin effects [271] and higher-order PN terms that meanwhile became available [272].

We now describe how the EOB formalism is able, in principle, to predict the full waveform emitted by coalescing binary systems using the best information available from analytical relativity. In Sec. 6.3.4, we shall show that the EOB approach can be made highly accurate by calibrating it to NR simulations, so that it can be used for detection and parameter estimation by ground- and space-based GW detectors.

There are three key ingredients that enter the EOB approach: (i) the conservative, two-body dynamics (or Hamiltonian), (ii) the radiation-reaction force and (iii) the gravitational waveform emitted during inspiral, merger and ringdown. In building these ingredients the EOB formalism relies on the assumption that the comparable-mass case is a smooth deformation of the test-particle limit. Moreover, each ingredient is crafted through a resummation of the PN expansion to incorporate non-perturbative and strong-field effects that are lost when the dynamics and the waveforms are Taylor-expanded in PN orders. The construction of the three ingredients leveraged on previous results. The finding of the EOB Hamiltonian was inspired by results in the 1970's aimed at describing the binding energy of a two-body system composed of comparable-mass, charged particles interacting electromagnetically [273]. The resummation of the radiation-reaction force was initially inspired by the Padé resummation of the energy flux [274]. The description of the merger-ringdown waveform was inspired by results in the 1970's on the radial infall of a test particle in a Schwarzschild BH [275], where it was found that the direct gravitational radiation from the particle is strongly filtered by the potential barrier once the test particle is inside it. The construction of the EOB merger-ringdown waveform was also inspired by results in the close-limit approximation [276], in which one switches from the two-body to the one-body description close to the peak of the BH potential barrier. The recent description of the EOB inspiral-plunge waveform [277] was inspired by the multiplicative (or factorised) structure of the waveform in the test-particle limit case. We now review the three basic ingredients.

In the physical, *real* description, the centre-of-mass conservative dynam-

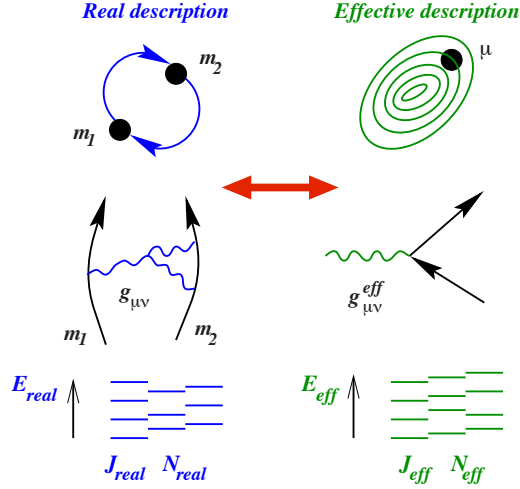


Figure 6.3 The real and effective descriptions in the EOB formalism.

ics of two particles of masses m_1 and m_2 and spins \mathbf{S}_1 and \mathbf{S}_2 is described by the PN-expanded Hamiltonian $H_{\text{PN}}(\mathbf{Q}, \mathbf{P}, \mathbf{S}_1, \mathbf{S}_2)$, where \mathbf{Q} and \mathbf{P} are the relative position and momentum vectors. The basic idea of the EOB approach is to construct an auxiliary, *effective* description of the real conservative dynamics in which an effective particle of mass $\mu = m_1 m_2 / (m_1 + m_2)$ and effective spin $\mathbf{S}_*(\mathbf{S}_1, \mathbf{S}_2)$ moves in a deformed, Kerr-like geometry $g_{\mu\nu}^{\text{eff}}(M, \mathbf{S}_{\text{Kerr}}; \nu)$, with mass $M = m_1 + m_2$ and spin $\mathbf{S}_{\text{Kerr}}(\mathbf{S}_1, \mathbf{S}_2)$, such that the effective conservative dynamics is equivalent (when expanded in powers of $1/c$) to the original, PN-expanded dynamics. The deformation parameter is the symmetric mass ratio $\nu = \mu/M$, ranging from $\nu = 0$ (test particle limit) to $\nu = 1/4$ (equal masses). Exactly solving the problem of a spinning, effective particle in this deformed, Kerr-like geometry amounts to introducing a particular *non-perturbative* method for re-summing the PN-expanded equations of motion.

As done originally in [65], even if the problem is purely classical, it is quite instructive to obtain such a mapping between the real and effective dynamics by thinking quantum mechanically. For simplicity, let us restrict ourselves to non-spinning particles. Instead of considering the classical Hamiltonians $H_{\text{real}}(\mathbf{Q}, \mathbf{P})$ and $H_{\text{eff}}(\mathbf{q}, \mathbf{p})$ and their bounded orbits, we consider the energy levels $E_{\text{real}}(N_{\text{real}}, J_{\text{real}})$ and $E_{\text{eff}}(N_{\text{eff}}, J_{\text{eff}})$ of the quantum bounded states associated with the Hamiltonian operators. The energy levels depend on the principal quantum number N and the total-angular-momentum quantum number J , and they can be computed in a gauge-invariant manner within the

Hamilton-Jacobi formalism, where N and J correspond to classical action variables. We sketch in Fig. 6.3 the real and effective descriptions. Because in quantum mechanics the action variables are quantised in integers, it is most natural to map the real and effective descriptions, requiring that the quantum numbers be the same (i.e., imposing $N_{\text{real}} = N_{\text{eff}}$ and $J_{\text{real}} = J_{\text{eff}}$), but allowing the energy axis to change. Doing the mapping explicitly, [65] found the following, simple relation between the real and effective non-relativistic energies ($E_{\text{real}}^{\text{nr}} \equiv E_{\text{real}} - Mc^2$ and $E_{\text{eff}}^{\text{nr}} \equiv E_{\text{eff}} - \mu c^2$) $E_{\text{eff}}^{\text{nr}} = E_{\text{real}}^{\text{nr}}[1 + \nu/2(E_{\text{eff}}^{\text{nr}}/\mu c^2)]$, which can be re-written as

$$\frac{E_{\text{eff}}}{\mu c^2} = \frac{E_{\text{real}}^2 - m_1^2 c^4 - m_2^2 c^4}{2m_1 m_2 c^4}. \quad (6.15)$$

Remarkably, the relation (6.15) coincides with the one found in quantum electrodynamics [273], resumming part of the Feynman diagrams when mapping the one-body relativistic Balmer formula onto the two-body one, which describes charged particles of comparable masses interacting electromagnetically (e.g., positronium). (The mapping between the effective and real Hamiltonians can be also obtained through a suitable canonical transformation [65].) The improved resummed or EOB Hamiltonian, obtained by inverting the expression Eq. (6.15), reads [65]

$$H_{\text{EOB}} = Mc^2 \left[\sqrt{1 + 2\nu \left(\frac{H_{\text{eff}}}{\mu c^2} - 1 \right)} - 1 \right], \quad (6.16)$$

with

$$H_{\text{eff}}(\mathbf{r}, \mathbf{p}) = \mu c^2 \sqrt{A(r) \left[1 + \frac{\mathbf{p}^2}{\mu^2 c^2} + (B(r)^{-1} - 1) \frac{(\mathbf{n} \cdot \mathbf{p})^2}{\mu^2 c^2} + \mathcal{Q}_4(\mathbf{p}) \right]}, \quad (6.17)$$

where $A(r)$ and $B(r)$ are the radial potentials of the effective metric $ds_{\text{eff}}^2 = -A(r)c^2 dt^2 + B(r) dr^2 + r^2 d\Omega^2$ and $\mathcal{Q}_4(\mathbf{p})$ is a non-geodesic term quartic in the linear momentum that appears at 3PN order [272]. The metric potentials differ from the Schwarzschild ones by terms proportional to ν . They can be computed in a PN series by matching the effective and real dynamics, thus $A_k(r) = \sum_{i=0}^{k+1} a_i(\nu)/r^i$ and $B_k(r) = \sum_{i=0}^k b_i(\nu)/r^i$. The EOB Hamilton equations read

$$\frac{d\mathbf{r}}{dt} = \frac{\partial H_{\text{real}}}{\partial \mathbf{p}}, \quad \frac{d\mathbf{p}}{dt} = -\frac{\partial H_{\text{real}}}{\partial \mathbf{r}} + \mathcal{F}, \quad (6.18)$$

where \mathcal{F} denotes the radiation-reaction force that can be expressed, assuming the energy balance equation and quasi-circular orbits, in terms of the GW

energy flux at infinity [66, 274] and through the BH horizons [278, 279]. Using -2 spin-weighted spherical harmonics ${}_{-2}Y_{\ell m}(\theta, \phi)$, the gravitational polarisations can be written as $h_+(\theta, \phi; t) - i h_\times(\theta, \phi; t) = \sum_{\ell, m} {}_{-2}Y_{\ell m}(\theta, \phi) h_{\ell m}(t)$. The most recent description of the EOB inspiral-plunge modes proposed in [217, 277] read (symbolically)

$$h_{\ell m}^{\text{inspiral-plunge}}(t) = h_{\ell m}^{(N, \epsilon)} \hat{S}_{\text{eff}}^{(\epsilon)} T_{\ell m} e^{i\delta_{\ell m}} f_{\ell m} N_{\ell m}, \quad (6.19)$$

where the term $h_{\ell m}^{(N, \epsilon)}$ is the leading Newtonian mode, ϵ denotes the parity of the mode, the factor $T_{\ell m}$ resums the leading order logarithms of tail effects, the term $e^{i\delta_{\ell m}}$ is a phase correction due to sub-leading order logarithms, while the function $f_{\ell m}$ collects the remaining PN terms. Finally, the term $N_{\ell m}$ is a non-quasi-circular correction that models deviations from quasi-circular motion [280], which is assumed when deriving all the other factors in Eq. (6.19).

Inspired by results in the 1970's [275], the EOB approach assumes that the merger is very short in time, although broad in frequency, and builds the merger-ringdown signal by attaching a superposition of quasi-normal modes (QNMs) [66] to the plunge phase of the signal. Following the close-limit result [276], in a first approximation the plunge and QNM signals are matched at the light ring (i.e., at the unstable photon circular orbit), where the peak of the potential barrier around the newborn BH is located. Thus, the EOB merger-ringdown waveform is built as a linear superposition of QNMs of the final Kerr BH [66, 281]

$$h_{\ell m}^{\text{merger-RD}}(t) = \sum_{n=0}^{N-1} A_{\ell mn} e^{-i\sigma_{\ell mn}(t-t_{\text{match}}^{\ell m})}, \quad (6.20)$$

where N is the number of overtones [282, 283], $A_{\ell mn}$ is the complex amplitude of the n -th overtone, and $\sigma_{\ell mn} = \omega_{\ell mn} - i/\tau_{\ell mn}$ is the complex frequency of this overtone with positive (real) frequency $\omega_{\ell mn}$ and decay time $\tau_{\ell mn}$. The complex QNM frequencies are known functions of the mass and spin of the final Kerr BH.

Finally, the full inspiral-plunge-merger-ringdown EOB waveform is obtained by joining the inspiral-plunge waveform $h_{\ell m}^{\text{inspiral-plunge}}(t)$ and the merger-ringdown waveform $h_{\ell m}^{\text{merger-RD}}(t)$ at the matching time $t_{\text{match}}^{\ell m}$ as [66]

$$h_{\ell m}^{\text{EOB}}(t) = h_{\ell m}^{\text{inspiral-plunge}}(t) \theta(t_{\text{match}}^{\ell m} - t) + h_{\ell m}^{\text{merger-RD}}(t) \theta(t - t_{\text{match}}^{\ell m}), \quad (6.21)$$

where $\theta(t)$ is the Heaviside step function. For $t > t_{\text{match}}$ the GW emission is no-longer driven by the orbital motion, but by the ringing of spacetime itself and the production of QNMs.

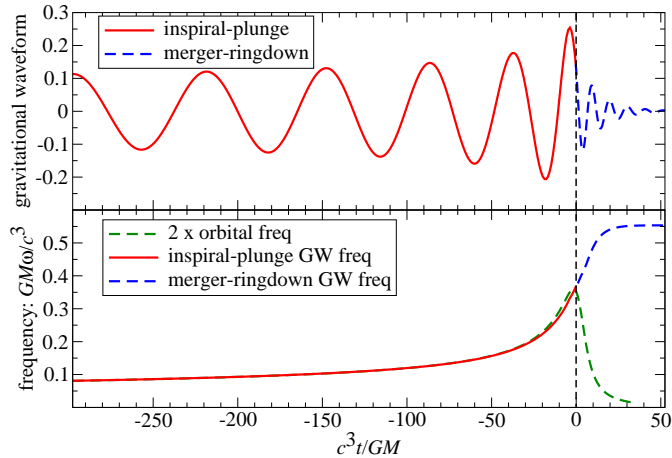


Figure 6.4 Gravitational waveform (upper panel), GW and twice orbital-angular frequencies (lower panel) from inspiral, plunge, merger and ringdown stages of a non-spinning, equal-mass binary BH as predicted in the EOB approach [65, 66].

In Fig. 6.4 we show in the top panel the first, full EOB waveform for a non-spinning, equal-mass binary BH obtained in [66] (see [270] for first, full EOB spinning, precessing waveforms). In the lower panel we show the EOB GW and twice orbital-angular frequencies, the former flattening at late times at the least damped QNM of the newborn BH, the latter having a peak around the EOB light ring. During the inspiral and plunge stages the GW emission is driven by the motion of the effective particle. As the effective particle passes through the EOB light ring, the direct GW emission from the effective particle is filtered by the potential barrier around the newborn BH, and the GW radiation is driven by the perturbed spacetime geometry through the emission of QNMs. Soon after the NR breakthrough, [281] compared EOB to NR waveforms finding very reasonable agreement for the late inspiral, plunge, merger and ringdown stages. In particular, the EOB light ring was found to be located very close to the peak of the NR waveform and close to the location of the common apparent horizon, supporting the idea that GW radiation is quickly described by a superposition of QNMs as the two BHs merge. In Sec. 6.3.4 we shall discuss more recent, sophisticated comparisons and also calibrations of EOB waveforms. The EOB inspiraling dynamics has been compared directly to the one produced in NR simulations through the computation of the periastron advance and the binding energy. The agreements are remarkable [267, 284, 285], even when no information from NR is used to improve the EOB model.

The possibility of analytically modeling the merger waveform in the EOB approach stems from the waveform's simplicity. Does the simplicity imply that nonlinearities of GR do not play an important role? Not at all. Comparisons between numerical and analytical PN and EOB waveforms during the last 15–20 orbits of evolution have demonstrated that the best agreement with NR results is obtained when corrections up to the highest PN order available today are included. Thus, as expected, non-linear effects are present and dominant in the strong-field regime. The waveform simplicity is the result of (i) the presence of only one characteristic scale close to merger, when radiation reaction, orbital and spin precession time scales become of the same order of magnitude, (ii) the formation of a potential barrier around the newborn BH filtering the direct radiation from the merger *burst*, and (iii) the highly dissipative nature of disturbances in the BH spacetime because of QNMs.

The EOB conservative dynamics and waveforms have been extended to spinning BHs in [271, 286–291] and [292], respectively. In particular, motivated by the construction of a EOB Hamiltonian for spinning systems, that reduces to the Hamiltonian of a spinning particle in the extreme-mass ratio limit, [287] worked out, for the first time, the Hamiltonian of a spinning particle in curved spacetime at all orders in PN theory and linear in the particle's spin. The EOB approach has also been extended to NS binary systems, incorporating tidal effects in the dynamics and waveforms [156, 157].

To gain more insight and improve the transition from merger to ring-down [216, 217, 219–221] combined the EOB approach to numerical studies in BH perturbation theory. Concretely, they used the EOB formalism to compute the trajectory followed by an object spiraling and plunging into a much larger BH, and then used that trajectory in the source term of either the time-domain RWZ [202, 203] or Teukolsky equation [204]. Solving those equations is significantly less expensive than evolving a BH binary in full numerical relativity. The possibility of using the test-particle limit to infer crucial information about the merger waveform of bodies of comparable masses follows from the universality of the merger process throughout the binary parameter space. The EOB approach has also been employed to generate quasi-circular, equatorial, very long, inspiraling waveforms in the extreme mass-ratio limit, with accuracy comparable to the ones produced by the Teukolsky-equation code [293, 294]. Finally, the EOB formalism has been improved by taking advantage of important developments in the GSF formalism and its interface with PN theory [260]. In particular, using those results, the potentials entering the EOB metric have been derived at PN orders higher than previously known [148, 163, 262, 295].

6.3 Compact-object binaries

Binary systems of compact objects⁵ are the prime target for observation of almost all GW detectors. Loss of energy and angular momentum to GWs causes the companion stars of a binary system to spiral in toward each other, making the system more relativistic, in turn leading to a greater luminosity and a faster rate of inspiral. Indeed, a binary is a good example of a positive feedback system wherein radiation back-reaction makes the system more luminous. After evolving adiabatically over millions of years, in the end, the two stars merge in a violent event, emitting extremely luminous gravitational radiation.

The leading order expression for the GW luminosity of a system, Eq. (6.10), can be used to make an order of magnitude estimate of how bright compact binaries can be and why they are the prime sources of GWs. To leading order the luminosity of a system composed of masses m_1 and m_2 (total mass $M = m_1 + m_2$), separated by a distance d , on a circular orbit can be worked out from Eq. (6.10) to be [73] $\mathcal{L} = (32c^5\nu^2/5G)(v/c)^{10}$, where $\nu = m_1m_2/M^2$ is the symmetric mass ratio and $v = \sqrt{GM/d}$ is the orbital velocity. \mathcal{L} is a steep function of v and depends quadratically on the mass ratio. Therefore, the source luminosity is greatest necessarily for relativistic, comparable mass systems. Most binary systems in the Universe are asymmetric in mass and far from being relativistic: for the Jupiter-Sun system $v/c \sim 3 \times 10^{-5}$ (and $\nu \sim 10^{-3}$), for the Hulse-Taylor binary, J1913+16, $v/c \sim 10^{-3}$ [13] and for the AM CVn system RX J0806+1527 [296, 297] — the most luminous source of GWs known today and expected to be observable in eLISA [298] — it is $v/c \sim 4 \times 10^{-3}$.

Neutron stars and BHs are the most compact objects in the Universe, with orbital velocities that can reach close to the speed of light; therefore, the most luminous sources are also the most compact and strongly-gravitating systems. Indeed, when BH binaries merge $v/c \sim 1/\sqrt{2}$ (see, e.g., Eq. (3.2) of [299]) and luminosities could reach the phenomenal levels of $\sim 4 \times 10^{50} \text{ W} \sim 10^{24} \text{ L}_\odot$, independent of the total mass of the binary.

6.3.1 Characteristic evolution time scales and strain amplitude

A binary predominantly emits GWs at twice its orbital frequency. As the system loses angular momentum and energy to gravitational radiation its frequency increases. Noting that the luminosity in GWs is balanced by the

⁵ Compactness of a body of mass M and size r_s is defined as $\mathcal{C} \equiv GM/(c^2r_s)$. For BHs $\mathcal{C}_{\text{BH}} = 0.5$, for NSs, depending on the EoS, $\mathcal{C}_{\text{NS}} \sim 0.2\text{--}0.4$, while for the Sun $\mathcal{C}_\odot \ll 1$.

loss in binding energy $E = -\nu Mv^2/2$, that is $\mathcal{L} = -\dot{E}$, at leading order in the PN expansion, the orbital angular frequency evolution reads

$$\dot{\omega} = \frac{\dot{E}}{dE/d\omega} = \frac{96}{5c^5}(G\mathcal{M})^{5/3}\omega^{11/3}, \quad (6.22)$$

where we have substituted $v = (GM\omega)^{1/3}$. The quantity $\mathcal{M} \equiv \nu^{3/5}M$ is called the *chirp mass* and it turns out that at leading PN order a number of quantities depend on this specific combination of the component masses. Starting from a certain initial angular frequency ω_0 , the time τ it takes for the system to merge (i.e., $\omega \rightarrow \infty$) can be estimated from $\tau = \int_{\omega_0}^{\infty} d\omega/\dot{\omega}$:

$$\tau = \frac{5c^5 \omega_0^{-8/3}}{256(G\mathcal{M})^{5/3}} \simeq 1000 \text{ s} \left(\frac{1.22 M_{\odot}}{\mathcal{M}} \right)^{5/3} \left(\frac{10 \text{ Hz}}{f_0} \right)^{8/3}, \quad (6.23)$$

where $f_0 = \omega_0/\pi$ is the GW frequency, equal to twice the orbital frequency, and a chirp mass of $1.22 M_{\odot}$ corresponds to a binary consisting of two $1.4 M_{\odot}$ NSs. The Hulse-Taylor binary, with two NSs of masses $\sim 1.4 M_{\odot}$ each and orbital period of 7.75 Hrs, will merge in about 300 million years⁶, its cousin J0737-3039 [300], with NSs of masses $1.35 M_{\odot}$ and $1.25 M_{\odot}$ and orbital period of 2.5 Hrs, will merge in 85 million years, while J0806+1527, with two white dwarfs of roughly $0.5 M_{\odot}$ and orbital period of 321 s, will merge in ~ 0.5 Myr.

For a source at a distance R from Earth, we can estimate the strain amplitude h from its luminosity. Comparing Eqs. (6.4) and (6.10) we can approximate $\mathcal{L} \sim c^3(R\dot{h})^2/20G$. Writing $\dot{h} \sim \omega h$, it follows that at leading order in the PN expansion

$$h \sim \frac{\sqrt{32}}{\pi c^4} \frac{(G\mathcal{M})^{5/3}\omega^{2/3}}{R}. \quad (6.24)$$

For a NS binary at 100 Mpc the amplitude of the waveform at 100 Hz is $h \sim 4 \times 10^{-23}$.

6.3.2 Frequency-mass diagram

In Fig. 6.5 we plot several characteristic frequencies of equal-mass systems on (quasi-)circular orbits and illustrate time scales over which they evolve. The frequency range 1 nHz–100 nHz is targeted by pulsar timing arrays (PTA), 30 μ Hz–1 Hz by space-based interferometers and 1 Hz–10 kHz by ground-based or underground detectors. Dotted lines are frequencies starting

⁶ The Hulse-Taylor binary has quite a large eccentricity ($e \simeq 0.62$), which needs to be taken into account while computing the merger time scale.

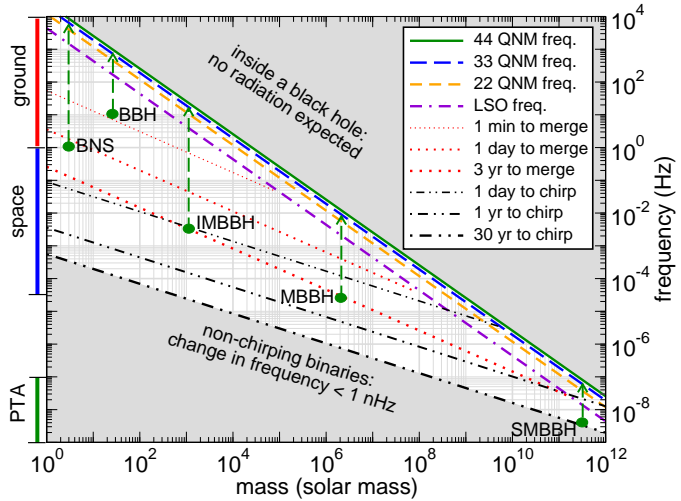


Figure 6.5 Frequency-mass diagram for equal-mass compact binaries.

from which a binary would last for 1 min, 1 day and 3 years until merger. As a binary evolves, its orbital frequency changes. For equal-mass sources that begin above the “30 yr (1 yr, 1 day) to chirp” line, it will be possible to measure their chirp mass and luminosity distance after a 30-year (1-yr, 1-day) observational period; for systems that begin below the “30 yr (1 yr, 1 day) to chirp” line, it will not be possible to infer the two quantities even after 30 years (respectively, 1 yr and 1 day).

During the final stages of the evolution, the component stars of a binary are no longer able to stay on stable orbits. They plunge towards each other when the orbital frequency is larger than a certain value, which we assume, for simplicity, to be that corresponding to the last stable orbit (LSO) of a Schwarzschild BH, i.e. $f_{\text{merge}} \simeq c^3/(6^{3/2}\pi GM) \simeq (M/10M_\odot)^{-1} 440 \text{ Hz}$. A binary’s GW luminosity reaches its peak soon after it reaches the LSO. The merged object in all cases, except for very low total-mass NS binaries, is a highly deformed BH that quickly settles down to a quiescent Kerr state, emitting a characteristic spectrum of damped sinusoidal GWs — the quasi-normal modes (QNMs) [301]. The complex frequencies of the QNMs depend on the mass and spin of the final BH. Figure 6.5 shows, for a non-spinning BH, frequency of the dominant quadrupole mode (i.e., $\ell = 2, m = 2$ mode labeled ‘22 QNM freq.’) and two of the higher-order modes (labelled ‘33 QNM freq.’ and ‘44 QNM freq.’, see [282] for QNM frequencies) that are expected to carry a significant amount of energy. Although BHs have an infinite sequence of modes of higher frequencies, numerical simulations of BH mergers reveal that they are devoid of any appreciable energy in modes

with $\ell > 4$ [302] and so we do not expect sources to radiate significantly in the top shaded region.

6.3.3 Zoo of compact-object binaries

Compact binaries occur in a very large range of masses and mass ratios. In Fig. 6.5 we show a few examples, but only for equal-mass, non-spinning systems: (i) a NS binary of total mass $3 M_\odot$ (BNS) that would be visible for about 15 minutes from 10 Hz in aLIGO/AdV and a few days from 1 Hz in ET, and it would chirp up in far less than a day from 1 Hz, (ii) a $20 M_\odot$ BH binary (BBH) that lasts for almost 40 seconds from 10 Hz in aLIGO/AdV and ~ 5 hours from 1 Hz in ET, (iii) a $10^3 M_\odot$ intermediate-mass BH binary (IMBBH) that would chirp up in just one day from 3 mHz, but takes 3 years to merge, sweeping the bands of both eLISA and ground-based detectors, (iv) a $2 \times 10^6 M_\odot$ massive BH binary (MBBH) in the eLISA band that would chirp up in less than a year, but takes 3 years to merge, starting at $30 \mu\text{Hz}$ and (v) a $3 \times 10^{11} M_\odot$ supermassive BH binary in the PTA band that takes 100's of years to merge, but would just chirp up in 30 years.

Stellar-mass binaries: Binaries of stellar-mass compact objects could contain two NSs, a NS and a BH or two BHs. Advanced LIGO and Virgo are well positioned to observe all such systems. In the case of a binary composed of two NSs the merger dynamics can be quite complex and depends on the binary's total mass M , the mass of the final remnant M_f and the maximum NS mass M_{\max}^{NS} allowed by the (unknown) NS EoS. For majority of mergers the final remnant is expected to be a BH with or without an accretion disk, except on rare occasions when $M_f < M_{\max}^{\text{NS}}$, the final remnant can be a NS [303–305]. A BH with an accretion disk might promptly form if $M_{\max}^{\text{NS}} < M \lesssim 3 M_\odot$ and the component masses are different from each other. However, if $M_{\max}^{\text{NS}} < M \lesssim 3 M_\odot$ and the component masses are similar, a transient object called a *hypermassive* NS may form [304, 306]. The hypermassive NS is expected to be a non-axisymmetric ellipsoid supported against collapse by a combination of thermal pressure and differential rotation [305] and can delay BH formation for 1 ms to 1 s [305, 307]. This phase could witness quite a lot of rotational energy emitted as GWs, with a spectrum that is characteristic of the NS EoS [308, 309]. A BH without an accretion disk is not a very likely outcome, but it can happen if $M \gtrsim 3 M_\odot$ [303, 304, 310]. The hypermassive NS phase and BHs with accretion disks could both be accompanied by significant emission of electromagnetic radiation [311].

In the case of NS-BH binaries and binary BHs, the merger essentially

produces a highly deformed BH that quickly settles down to a quiescent Kerr state by emitting QNM radiation. In the case of NS-BH mergers with mild mass ratios (say, $m_{\text{NS}}/m_{\text{BH}} \gtrsim 1/3$ for a non-spinning BH), the NS is tidally disrupted before the LSO and forms an accretion disk, which can generate electromagnetic signals; for smaller mass ratios the NS directly plunges into the BH without forming an accretion disk [312–314].

It is apparent from Fig. 6.5 that every binary in the band of ground-based detectors will merge within just a few days. How many such mergers might we expect each year within a given volume of the Universe? From the small number of observed pulsar binaries it is not possible to reliably estimate the merger rate. The estimated median rate is about one event per year in 100 Mpc³, but it could be a factor 100 smaller or 10 greater due mainly to uncertainties in the distance to radio pulsars, their radio luminosity function, opening angle of the radio beam and incompleteness of radio surveys [315]. Rate predictions based on the evolution of populations of massive-star binaries (called *population synthesis*) is also highly uncertain due to poor knowledge of the relevant astrophysics (e.g., supernova kick velocities and stellar metallicity). The upshot of these predictions is that aLIGO, with a horizon distance⁷ of ~ 450 Mpc for binary NS mergers, might observe between 0.4 to 400 mergers per year [315].

There is currently no evidence for compact binaries in which one or both of the components is a BH. Population synthesis models predict a median rate of 5 binary BH mergers and 30 NS-BH mergers per Gpc³/year; also in this case the uncertainties are large. Advanced LIGO, with a horizon distance of 2.2 Gpc and 930 Mpc for these sources, could detect 10 and 20 mergers per year, respectively [315]. Metallicity of stars plays a key role in the evolution of massive stars. Black holes could be far more common in the Universe for low metallicities because stars would lose far less of their mass by stellar wind due to lower opacities and lead to more massive remnants towards the end of main sequence evolution. Expected binary BH detection rates in aLIGO for low metallicities are a factor 10 larger [317] and binary NS rates a factor 10 smaller. More recently, it has been noted that high mass X-ray binaries, such as IC10 X-1 and NGC300 X-1, could be progenitors of BH binaries, in which case their merger rate could be far higher [318].

⁷The *horizon distance* of a detector is defined as the distance at which a face-on binary located directly above the plane of the detector produces a SNR of 8. The *reach* of a detector is the distance at which a randomly oriented and located source produces the same SNR; the reach of a detector is a factor 2.26 smaller than its horizon distance [316]. A detector has roughly 50% efficiency, i.e. is able to see half of all sources, within its reach [316].

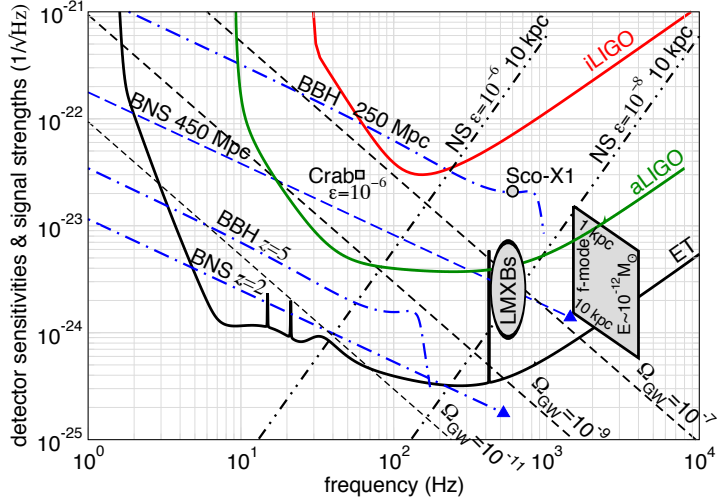


Figure 6.6 Sources of GWs for the ground-based detectors iLIGO, aLIGO and ET. For continuous waves and stochastic backgrounds the characteristic amplitude of the signals are plotted assuming an integration time of 1 year.

Supermassive and intermediate-mass black-hole binaries: There is growing evidence that certain galactic nuclei contain binary supermassive BHs [319] and eLISA would observe binary mergers if their total mass is in the range $10^4\text{--}10^7 M_\odot$ (see Fig. 6.5). The merger rate of binaries of interest to eLISA is highly uncertain. This is because there are only a handful of such candidate binaries that would merge within the Hubble time [320]. eLISA could observe $\sim 10\text{--}100$ mergers per year, depending on the model that is used for the formation and growth of massive BHs [321, 322]. PTAs are expected to detect in five years or more the background produced by a population of $> 10^7 M_\odot$ supermassive BH binaries [323]; while they are not likely to observe mergers, they could detect individual systems if binaries of appropriate masses exist at redshifts $z \sim 0.1\text{--}1$, with orbital periods of $\sim 1\text{--}30$ years [324].

Although there is strong observational evidence for the existence of stellar-mass ($5\text{--}30 M_\odot$) and supermassive ($\gtrsim 10^6 M_\odot$) BHs, little is known about BHs of intermediate mass $\sim 10^2\text{--}10^5 M_\odot$, not to mention their binaries. However, there are hints that certain ultra-luminous X-ray sources (e.g., HLX-1 in ESO 243-49 [325]) might host intermediate mass BHs. If a population of such objects exists and they grow by merger of smaller BHs, then, depending on their masses, ET and eLISA will be able to detect them (see

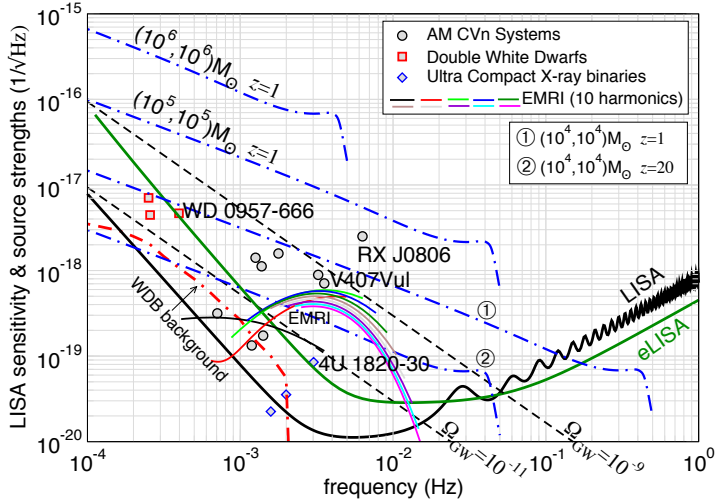


Figure 6.7 Sources of GWs for the space-borne detectors LISA and eLISA. For double white dwarfs, AM CVn systems, X-ray binaries and the stochastic background, the characteristic amplitude is computed assuming an integration time of 1 year.

Fig. 6.5). Their merger rates are highly speculative and range from 10 to 100 per year [322, 326, 327].

Extreme mass-ratio binaries: When one of the companion masses is far smaller than the other (e.g., a $10 M_{\odot}$ BH orbiting a $10^6 M_{\odot}$ BH), we have the problem of a test body in *near geodesic* motion in BH geometry. Such binaries are called *extreme mass-ratio binaries*, as the mass ratio could be stupendously small $\sim 10^{-6}\text{--}10^{-4}$. eLISA would be best suited to observe the inspiral of stellar and intermediate-mass BHs into massive $10^4\text{--}10^7 M_{\odot}$ BHs (see Fig. 6.5). Supermassive BHs in galactic nuclei are believed to grow by the infall of stellar mass and intermediate-mass BHs. Such events could be observed by eLISA at cosmological distances. For instance, the inspiral of a $10 M_{\odot}$ BH into a $10^6 M_{\odot}$ supermassive BH at 1 Gpc would be visible in eLISA. The rates in this case too are highly uncertain and range from a few to several hundreds per year [322, 328, 329].

Figures 6.6 and 6.7 plot the characteristic amplitude $h_c \equiv \sqrt{f}|H(f)|$, where $H(f)$ is the Fourier transform of the signal, for several non-spinning, equal-mass binaries with random orientation and sky position; for BH-BH binaries we use the inspiral-merger-ringdown signal, for BNS systems we have plotted only the inspiral part of the signal terminated at the LSO frequency because the spectrum of the merger signal is known only numerically and it

varies largely, depending on the microphysics and NS EoS. Also plotted are the detector noise amplitude spectra of three generations of ground-based interferometers in Fig. 6.6 and two versions of LISA in Fig. 6.7.

Figure 6.8 plots the horizon distance, computed using the full inspiral-merger-ringdown EOB waveforms, for aLIGO as a function of the intrinsic mass of the binary, for several mass ratios $q = m_1/m_2 \geq 1$. In the equal-mass case we also show the horizon distance using only the inspiral phase of the signal. We see that the inclusion of the merger and ringdown portions of the signal has a significant effect in the horizon distance for $\gtrsim 40 M_\odot$ binaries [270, 330, 331].

Black-hole binaries of mass 50–2000 M_\odot can be detected by aLIGO/AdV at redshifts $z \sim 0.3$ –1.4. The largest confirmed BH mass in the stellar range is $\sim 15 M_\odot$ [332], but there are hints of even heavier BHs of 23–34 M_\odot [333]. Theoretically, low metallicity massive stars could lead to BHs of $50 M_\odot$ or higher [317]. For binary systems of total mass 50–100 M_\odot , detectors are sensitive to the final moments of merger, when the strong field dynamics dominates the evolution. Comprehensive studies have shown that depending on the mass ratio, full inspiral-merger-ringdown waveforms should be used as matched filters when $M \gtrsim 10$ –15 M_\odot , if one wishes a loss in detection rate of no more than 10% [299]. Space-based detectors would observe the merger dynamics from $\sim 10^5$ – $10^7 M_\odot$ binaries, with SNRs ~ 300 for sources at $z \sim 3$ [322, 334]. These SNRs are so large that templates would need to be improved beyond their current status, so as not to bias the estimation of the system’s masses and its position on the sky.

6.3.4 Interface between theory and observations

A search for GWs from sources with known amplitude and phase evolution can make use of *matched filtering*, which involves cross-correlating the detector output with a copy of our best guess of the expected signal called a *template*. If the template matches the signal well, then the correlation between the noisy signal and the template builds up with time, giving rise, on the average, to a positive output. Matched filtering, however, is very sensitive to the signal’s phase evolution; even tiny phasing errors in the template can destroy the cross correlation. It is critical to have accurate templates so that the SNR lost due to incorrect templates is negligible.

For low-mass, inspiraling binary systems, carrying very mild spins, i.e., for NS-NS binaries, any 3.5PN approximant is accurate enough for detection [299], a remarkable result of the PN formalism. Until what time in the binary evolution (or, equivalently, for which total mass of the binary) is it

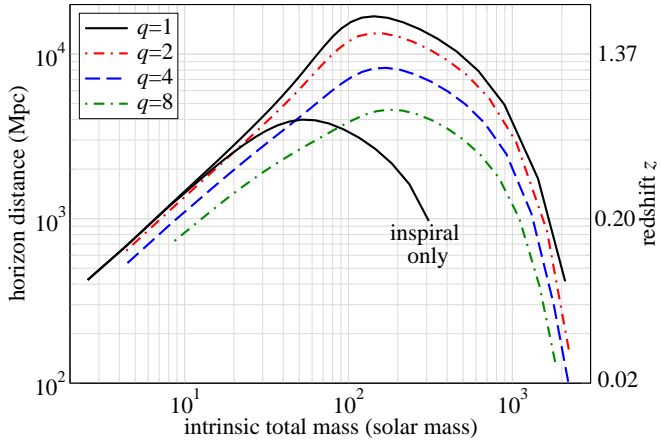


Figure 6.8 Plots of the horizon distance of aLIGO as a function of the intrinsic total mass of a binary using (non-spinning) inspiral-merger-ringdown EOB waveforms calibrated to NR simulations [302]. We also plot the horizon-distance when we only include the inspiral phase terminated at the LSO of Schwarzschild.

safe to employ PN approximants in GW searches? Is there one particular PN approximant that is more accurate than others for any mass ratio and spin? Such questions remained unsolved for many years and were among the motivations of the EOB formalism in late 1990’s. To cope with those uncertainties, for a few years before the NR breakthrough, *detection-template families* were developed [280, 335–337] and some of them were used in LIGO searches [338, 339]. To incorporate possible systematics present in PN approximants, those template families either extended the binary parameter space to unphysical regions or incorporated higher-order physical effects, so that they could reach higher overlaps with both PN approximants and EOB waveforms. Eventually, after the NR breakthrough in 2005, PN approximants started to be compared to highly accurate NR waveforms [340, 341] and also to EOB waveforms calibrated to NR waveforms [299]. It was found that for $M \gtrsim 10\text{--}15 M_{\odot}$, non-quasi-circular effects cannot be neglected and templates that include inspiral, merger and ringdown should be employed to avoid a large loss in the detection rate [299]. It was also found that PN approximants did not perform very well for large mass ratios, i.e., for NS-BH binaries or IMBHs. This is because in the PN approach, exact, known results in the test-particle limit are expanded in a PN series, washing out crucial non-perturbative information — a drawback that was another motivation for the EOB formalism.

In recent years, a variety of studies have been carried out at the interface between analytical and numerical relativity. The results have indicated that the best way to provide accurate templates for a successful detection and extraction of binary parameters is to combine the knowledge from all the available methods: PN, GSF and NR. One could try to directly combine PN-computed waveforms with NR waveforms, thus building a hybrid waveform. However, if the goal is to produce *highly* accurate templates, this method would still require high computational cost, because the different PN approximants agree sufficiently well with each other *only* at large separations, thus the hybridisation should start hundreds of GW cycles before merger [342–344]. An alternative avenue is provided by the EOB approach.

Analytical vis-a-vis numerical relativity: As earliest comparisons with NR waveforms demonstrated [281, 345] (cf. Sec. 6.2.3), the EOB formalism is able to describe waveforms emitted during the inspiral, plunge, merger and ringdown stages using *only* analytical information. Those first comparisons employed the 3.5PN EOB dynamics and leading-order PN waveforms. Subsequent studies carried out with highly accurate NR waveforms revealed the necessity of including higher-order PN terms in the EOB dynamics, energy flux and waveforms if the goal is to develop highly accurate templates for aLIGO/AdV searches. As a consequence, higher-order PN terms (in particular, the test-particle limit terms) are included in the gravitational modes $h_{\ell m}$ [277, 292, 346]. Since PN corrections are not yet fully known in the two-body dynamics, higher-order PN terms are included in the EOB dynamics with arbitrary coefficients [302, 346–354], which are then calibrated by minimising the phase and amplitude difference between EOB and NR waveforms aligned at low frequency. Those coefficients have been denoted *adjustable or flexible parameters*. In particular, EOB non-spinning waveforms (including the first four subdominant modes) have been developed with any mass ratio and shown to be indistinguishable from highly-accurate NR waveforms with mass ratios 1–6 up to SNRs of ~ 50 [355]. Note, however, that current NR waveforms cover the full detector bandwidth only for binaries with total mass larger than $M \gtrsim 100M_\odot$, thus those results are not yet conclusive. EOB waveforms are also stable with respect to the length of the numerical waveforms [344]. EOB waveforms for non-precessing systems with any mass ratio and spin have also been developed and calibrated to existing, highly accurate numerical waveforms, which, however, do not yet span the overall parameter space [354]. EOB waveforms for precessing systems can be built from those for non-precessing ones [356]; they capture remarkably well the spin-induced modulations in the long inspiral of NR waveforms and

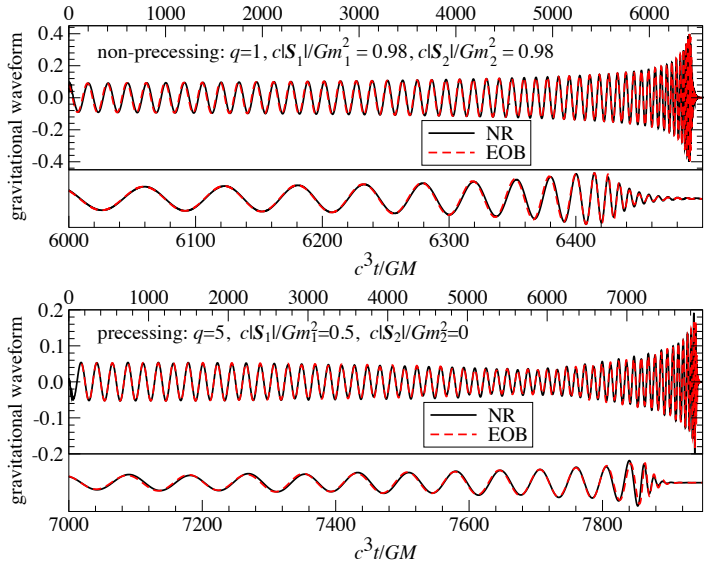


Figure 6.9 State-of-the-art comparison [354] between (calibrated) EOB and NR waveforms for quasi-extremal, non-precessing spins (top panel) and precessing spins (bottom panel); lower parts show final few cycles.

will be calibrated and improved in the near future. In Fig. 6.9 we show the agreement between state-of-the-art EOB [279] and NR waveforms for an equal-mass BH-BH binary with both spins aligned with the orbital-angular momentum and quasi-extremal (top panel), and a single-spin binary BH with mass ratio 5, precessing with mild spin magnitude (bottom panel).

Starting with [345, 357], a more phenomenological avenue has also been followed to produce inspiral-merger-ringdown waveforms. In this case, the original motivation was to provide aLIGO/AdV detectors with inspiral, merger and ringdown waveforms that could be computed efficiently during searches and be used to detect high-mass coalescing compact binaries. The full waveforms are constructed by first matching inspiral PN templates and NR waveforms in either the time or frequency domain, and then fitting this hybrid waveform in the frequency domain to a stationary-phase-approximation based template, augmented by a Lorentzian function for the ringdown stage. As NR waveforms started spanning larger regions of the parameter space, the phenomenological waveforms have been improved [358], and extended to non-precessing [359] and precessing [360] binary BHs.

Today, highly accurate NR waveforms, having several tens (~ 70) of GW cycles and generic BH–spin orientations, can be produced by the pseudo-spectral Einstein code (SpEC) of the Simulating eXtreme Spacetime (SXS)

collaboration [361]. Although such waveforms are not long enough and do not span the entire parameter space to be employed as search templates, they do allow testing of the stability of calibrated analytical waveforms with respect to the length of the simulations, improvement of the accuracy of analytical templates and also discrimination between different PN/EOB approximants. We expect that longer and more accurate numerical waveforms will be produced even more efficiently in the near future. Furthermore, the production of many short numerical waveforms with finite-difference codes [362] will continue to help with extracting interesting information about the characteristics of the merger signal. Eventually, all those advances will reduce systematics in the analytical waveforms, so that they can be used not only to observe GWs with advanced detectors, but can also be employed in the future by space-based detectors to extract binary parameters and to test general relativity at high SNRs ($\sim 10^3$).

6.3.5 Results from LIGO and Virgo

Data from several science runs of iLIGO and Virgo have been analysed to search for compact binary coalescences. No GW signals were found, but the results were used to set upper limits on merger rates and exclusion distances to short-hard gamma ray bursts (GRBs). The searches have used PN templates for “low-mass” binaries [363] with total mass $< 25 M_\odot$ and component masses $> 1 M_\odot$ and EOB templates calibrated to NR waveforms [347] for “high-mass” binaries [364] with total mass in the range $[25, 100] M_\odot$ and mass ratio in the range $1 \leq m_1/m_2 \leq 6$. The horizon distance to low-mass systems during iLIGO Science Run S6 and Virgo Science Run VSR3 was 40 Mpc, 80 Mpc and 90 Mpc, for binaries with $(1.35+1.35)M_\odot$, $(1.35+5.0)M_\odot$ and $(5.0+5.0)M_\odot$, respectively. The corresponding upper limits, in units of $\text{Mpc}^{-3} \text{Myr}^{-1}$, were 130, 31 and 6.4 [363]. These limits were derived for binaries with non-spinning components; if spins are included the upper limits are 15% higher for binaries containing one or more BHs. The horizon distance to high-mass binaries [364] ranged from 230 Mpc for a $(14+14) M_\odot$ binary to nearly 600 Mpc for a $(50+50) M_\odot$ binary; the corresponding upper limits, in units of $\text{Mpc}^{-3} \text{Myr}^{-1}$, were 0.87 and 0.07. Additionally, searches for intermediate mass BHs with component masses $50 M_\odot$ to $350 M_\odot$ were carried out [365] using an excess-power algorithm in the time-frequency plane, setting upper limits in the range $0.14\text{--}13 \text{ Mpc}^{-3} \text{Myr}^{-1}$ for equal-mass binaries.

The upper limits from the low-mass searches are roughly two orders of magnitude away from the expected “realistic” merger rates [315]. Advanced

detectors, at their design sensitivity [366], will improve the distance reach by a factor of ~ 10 , and an increase in search volume by a factor of 1000. We can, therefore, expect the network of aLIGO/AdV/KAGRA to be making detections once they reach their design sensitivities. The current plan [366] is to collect data intermittently for periods of 3 to 6 months each year, when the detectors are commissioned from their initial sensitivity in late 2015 to their design sensitivity by the end of the decade; detectors are expected to be in continuous operation after 2020. There is a fair chance that the first detections might happen around 2017, when the distance reach for binary NSs is expected to reach ~ 100 Mpc (or horizon distance of 250 Mpc). Initial detections, with two or three detectors, might only have a moderate SNR ($\sim 12\text{--}15$) and it might only be possible to localise events to within hundreds of square degrees. The addition of KAGRA and a new detector in India [367] will help improve the angular resolution of the network to tens of square degrees and facilitate easier EM follow-up of mergers. The analysis methods deployed in the searches have proven their ability to make use of the predicted waveforms to identify events and measure their parameters and compute the false alarm probability and statistical significance of detected events. The best example of this is the GW100916 event (popularly called the *Big Dog* event) that was secretly injected into the iLIGO-Virgo data streams as part of the *Detection Challenge* (<http://www.ligo.org/news/blind-injection.php>). It was successfully identified by the on-line and off-line analysis pipelines, attributing a very high significance to the detected event [363].

Finally, new collaborative efforts have been established to coordinate activities between GW data analysts (or astronomers), numerical relativists and analytical relativists which have enabled testing of data analysis pipelines, production of a variety of NR simulations of binary BHs, and building of more robust models for use in searches and in extracting astrophysical information from the data [368–371].

6.3.6 Science targets and challenges

Gravitational waves from compact sources will unravel many unsolved problems in astronomy, fundamental physics and cosmology. In this section we will discuss science targeted by GW observations and the challenges that must be addressed in achieving those targets.

Science targets

Formation and evolution of stellar mass compact binaries: Coalescing compact binaries form from massive stars. Their formation involves a number of stellar processes. These include the evolution of the two stars through the main sequence; gravitational collapse; supernova of the more massive star and associated kick that could disrupt the binary; evolution of the binary through the common envelope phase, wherein the larger giant star transfers mass to its compact companion; the second supernova and associated kick [372]. The property of the final compact binary remnant depends on all these factors, as well as on the metallicity, chemical composition, masses and spins of the progenitors and the initial separation of the stars [317]. Understanding the formation and evolution of compact object stars is an open problem in astrophysics as many of the mechanisms mentioned above are poorly understood, not accessible from observations and difficult to model.

Different evolutionary models of compact binaries predict different coalescence rates for the three types of compact binary mergers. By determining the rates for these different populations it will be possible to discriminate amongst the many competing models that are currently prevalent. Determining the mass function and spin distributions (i.e., spin magnitudes and relative orientations) and mass ratios of companion stars, will add more discriminatory power to single out the correct model that describes the formation and evolutionary mechanisms [373]. Some models also predict a gap in the largest NS mass allowed by the EoS and the smallest mass of a BH formed by stellar evolution. Gravitational-wave observations could help verify the existence of such a mass gap [374].

Gamma-ray bursts: Observing GWs in coincidence with GRBs will have a tremendous impact on understanding the progenitors of GRBs and how they are powered. Moreover, coincident observation of GRBs and GWs will help identify the host galaxy of a GW source and measure its redshift. If progenitors of short GRBs (shGRBs) are binary NS mergers [375], then this would help measure both the luminosity distance and redshift to the source, *without* the use of the cosmic distance ladder [376, 377]. Clearly, such observations will have a great potential for precision cosmography [378–380].

If binary NS mergers are progenitors of shGRBs then in addition to beamed emission of gamma-rays, they could also emit isotropic radiation at optical and infra-red wavelengths. The neutron-rich material that is ejected in the process of merger could produce heavy nuclei that decay by r-process radioactivity, powering a transient optical and infra-red source called *kilonova* [311]. Follow-up observations with the Hubble Space Telescope of the shGRB 130603B at a redshift of $z = 0.356$ is the first evidence of a kilonova

[381, 382], with apparent magnitude of 25.8. At 200 Mpc, the distance reach of ground-based advanced detectors to binary NS mergers, such transients would have an apparent magnitude of about 23 and be observable by some of the ground-based optical and near-IR telescopes, but sky localisation of GW events will be a challenge.

Cosmology: Compact binary sources are quite unique for cosmology as they are standard candles [376]: for binaries that chirp up during the course of observation one can measure the source's luminosity distance from GW observations alone. Weak gravitational lensing would bias distance measurements of individual sources [383], but a large population of events, as might be expected in the case of ET, can average out lensing biases [379]. If the host galaxy of a merger event is identified and its redshift measured, then we can use a population of binary coalescence events to infer cosmological parameters. In fact, GW observations might also measure the redshift through galaxy clustering using wide-field galaxy surveys [376, 377]. Moreover, tidal effects can be used to determine the source's redshift provided the NS EoS is known [384].

There is strong observational evidence that galactic centres, including the Milky Way [385], host supermassive BHs of $10^6\text{--}10^{12} M_\odot$. When and how did such BHs form? Did the BHs precede the galaxies or did they form after the galaxies were assembled? What were their initial masses and how did they grow? These are among the most pressing unsolved questions in cosmology. Gravitational-wave observations by PTAs, eLISA and ground-based interferometers will together cover the entire spectrum of BH binaries up to $z \sim 5\text{--}20$, redshifts so large that the Universe was in its infancy assembling the first stars and galaxies.

Neutron-star equation of state: By determining the EoS of NSs we can infer the composition and structure of NS cores, which has remained largely unknown nearly half-a-century after the discovery of the first pulsar, although astronomical observations have begun to indicate hints of neutron superfluidity in the core [386, 387]. Tidal interaction in compact binaries, where one or both of the companions is a NS, depends on the EoS. Tidal effects are imprinted in the inspiral phasing starting at 5PN order beyond the leading term and in the merger and post-merger dynamical phases, as well. Advanced LIGO/AdV could distinguish between extreme models of equations of state by observing ~ 25 NS binary inspirals [388], while ET should measure the EoS quite accurately with a single loud event [389].

Testing gravitational dynamics: Signals from coalescing compact binaries can be used to probe the strong-field dynamics of gravity and as such facilitate tests of GR and its alternatives. Proposed tests either assume that GR is correct and look for small deviations from GR [390, 391], or begin with an alternative theory of gravity and determine the degree to which observations favour the alternative [392, 393]. Orbits of small BHs plunging into massive BHs are very complex and capture the non-linear dynamics of gravity. By observing the emitted radiation one can map out the geometry of the massive objects that reside in galactic nuclei and check if it agrees with the Kerr geometry or if BHs have extra “hair” [394–396]. An alternative approach checks for consistency of GWs from QNMs emitted during the ringdown phase of a BH binary merger [397].

Challenges

Critical problems in numerical relativity: It is important to continue to test the accuracy of analytical inspiral-merger-ringdown waveforms by comparing them to long NR waveforms and to characterise any systematic biases in parameter estimation that might result due to inaccurate modeling. If BHs carry large spins, waveforms emitted by NS-BH and BH-BH binaries with mass ratios $\gtrsim 4$ will have modulations due to spin-induced precession, which accumulate mostly during the long inspiral. Thus, more comprehensive studies are needed to understand the dynamics as a function of mass ratio, BH spins and EoSs of NSs. Moreover, at present, accurate NR waveforms span the entire aLIGO/AdV bandwidth only if their total mass is larger than $\sim 100 M_\odot$ and their mass ratio is $\lesssim 10$. Longer waveforms for larger mass ratios and generic spin configurations would be highly challenging, but they will be invaluable in validating analytical models, even if they sparsely sample the full parameter space.

Binary neutron star and NS-BH merger simulations that use realistic EoSs and include neutrino transport and other microphysics will be necessary to extract the best science from the data. Such simulations will also provide more accurate templates for the merger and bar-mode instability phases to infer redshifts from GW observations alone. Analytical and semi-analytical models of NS-NS and NS-BH mergers will be crucial for parameter estimation and Bayesian hypothesis testing. This will be a huge challenge for the bar-mode instability regime where the signal does not seem to have any phase coherence (see, e.g., simulations in [308, 309]). Even so, accurate modeling of the expected spectrum or time-frequency content of the signal can be useful in understanding the physics of dynamical instabilities. Several

related questions remain open such as the role of large NS magnetic fields and spins in the merger dynamics of binary NSs and NS-BHs [311].

Critical problems in analytical relativity: As discussed in Sec. 6.2.1, advances in PN theory over the last thirty years will enable the detection of BNS inspirals (if NSs carry mild spins) with negligible loss in detection rates and in extraction of binary parameters. When spins are present, the PN phasing and amplitude are not known as accurately as in the non-spinning case, causing PN approximants to differ substantially even during the inspiral phase [398]. Thus, spin couplings through at least 4.5PN order beyond the leading order are required in the conservative dynamics and gravitational flux at infinity, and through a similar PN order in the BH-absorbed horizon flux. Once available, spin couplings will also be employed in the EOB formalism to further improve inspiral-merger-ringdown waveforms. Considering that today the two-body, non-spinning conservative dynamics is known at 4PN order, it will be relevant to derive the energy flux at 4PN order to allow the computation of the phase evolution at 4PN order, further validating analytical templates against NR waveforms.

Recent results that take advantage of GSF calculations have allowed the computation of new terms in the conservative dynamics at PN orders higher than 4PN. However, if we consider that to fully complete the computation of the dynamics at 3PN and 4PN orders, it was necessary to overcome novel, specific subtleties that appeared at those PN orders (notably, at 3PN order one had to replace the Hadamard regularisation with dimensional regularisation and at 4PN order it was necessary to introduce a non-local in time action to properly include tail effects), it is difficult to imagine that, in the future, PN calculations could be systematically and automatically extended to an *arbitrarily high* PN order by simply using algebraic computer programs. This limitation does not depend on the particular technique that is used (MPM-PN or DIRE formalisms, EFT or Hamiltonian canonical formalism), but it seems simply a consequence of quibbles and complexities of the nonlinearities of GR. It is worth noticing that at present it does not also seem necessary to have Taylor-expanded PN results at arbitrarily high PN orders to detect the signals and to extract the best science. A combination of PN, perturbative, and NR results and resummation techniques can effectively work around the problem.

As discussed in Sec. 6.2.2, to obtain sufficiently accurate templates for extreme mass-ratio binaries, the metric perturbations need to be computed at second order. The formalism has been developed, calculations are underway and hopefully will be completed in the next few years.

Refining analytic source models and waveforms: Current searches in ground-based detectors assume that compact binaries are on quasi-circular orbits when they enter the detector sensitivity band (see, e.g., [364]). This is very likely a good approximation for binaries formed in fields as radiation back reaction circularises a binary much faster than the orbit decays [399, 400]. However, eccentric binaries may form through Kozai mechanism or dynamical capture in dense stellar environments [401–404] and in this case the eccentricity can be large at merger. Eccentric-binary event rates are very uncertain. Eccentric-binary waveforms are not required for detection in aLIGO/AdV/KAGRA, unless the eccentricity at 20 Hz is larger than 0.1. Faithful models that take into account eccentricity would be needed to detect GWs from highly eccentric binaries or to accurately estimate parameters of mildly eccentric binaries.

Except for [63], past analysis pipelines have mostly searched for binaries composed of non-spinning objects in the two-dimensional space of component masses [364]. It is important to explore the relevance of including spins for detection. Several studies have indicated that due to degeneracies in the binary parameter space, template families containing a single effective spin could be sufficient to detect waveforms emitted by double-spin binary systems [336, 337, 405–407]. Moreover, precession-induced modulations can be incorporated in template waveforms in an efficient way, reducing also the dimensionality of the parameter space [336, 337, 356, 374, 408]. However, we still miss a comprehensive study that spans the entire parameter space and determines, after taking into account how the improvements in sensitivity can be set aside by increases in false alarm probability, in which region of the parameter space single- and/or double-spin, non-precessing or precessing searches, are needed (for first steps in this direction see [409, 410]). Furthermore, studies are needed on the systematic biases in the estimation of parameters due to the use of incomplete waveform models, especially when spin-induced modulations in NS-BH and BH-BH are included. At present EOB waveforms for spinning BH binaries are computationally expensive to generate (although far faster than doing NR simulations) and hence not suitable for use in Markov Chain Monte Carlo-based parameter estimation methods. Quite importantly, accelerated waveform generation techniques that use reduced-order algorithms or singular-value decomposition techniques have been proposed to address such problems [411–415].

Finally, using PN results and NR simulations, analytical templates that extend up to merger and include tidal effects are under development [416, 417]. They will be needed to extract the best information on tidal effects and EoS in NS-NS and NS-BH coalescences. Including tidal effects in *point-*

particle templates calibrated to highly accurate BH-BH waveforms from NR (e.g., EOB waveforms) is the best way of controlling systematic errors due to lack of knowledge of higher-order point-particle terms in the PN expansion. In fact, employing inspiraling, point-particle PN templates augmented by tidal effects, leads to large systematic biases and limits the extraction of tidal information [418, 419].

Lastly, all sources of systematic effects in GR waveforms need to be under control if one wants to measure possible deviation from GR. Current waveforms are likely not to satisfy this requirement in the majority of the parameter space for ground-based and especially space-based detectors. A comprehensive study that also employs accurate waveforms from alternative theories of gravity both for the inspiral, but also the plunge and merger stages, is needed to understand how much one should to reduce systematic errors in GR waveforms and to be able to observe deviations from GR.

Synergy between EM and GW observations: Following up GW events using EM telescopes, and likewise analysing GW data at the time of EM transients, will be invaluable in enhancing the scientific returns of observations. Since the EM sky is full of transient events, understanding which EM transients to follow-up in GW data is important as otherwise coincidences will lose significance. While many EM transients are easily identifiable, challenges remain in unraveling the nature of astronomical transients [420]. A study of the fraction of EM transients that might look like GW progenitors, and hence contribute to false coincidences, is desirable.

EM followups of GW events rely on accurate estimation of source position [421]. What are the methods by which we might be able to improve sky localisation? For example, sub-dominant harmonics in systems with large mass ratios [422, 423] and binaries with rapidly spinning components [424], could both enhance sky resolution and galaxy surveys could help target specific sky patches [425]. A proper understanding of biases in the estimation of sky position due to inaccurate waveform models or the use of galaxy catalogues is necessary.

Pulsar timing arrays are approaching astrophysically relevant sensitivity levels and setting limits on the detectability of binary supermassive BH binaries [426]. SKA could observe continuous waves from an isolated supermassive BH binary, if one exists in the relevant frequency range, within $z \lesssim 1$ [427]. The challenge here would be to control systematics in pulsar timing noise and to discover a large number of (~ 100) stable (timing noise $\lesssim 20$ ns) millisecond pulsars.

6.4 Isolated compact objects

Over the past 30 years, astronomy has made great strides in observing compact objects and their environments and equally raised new puzzles about the interior structure of NSs. In particular, X- and gamma-ray observations have identified new potential sources of GWs. On the theoretical front, there is now a vast amount of literature aiming to understand the structure and composition of NS cores and observational signatures expected of them. Supernova simulations have become more sophisticated, with predictions of GW amplitudes that are far more pessimistic now than it was thought three decades ago, but challenges have remained in producing realistic simulations that resolve all the relevant scales and include all the macro- and micro-physics. Gravitational-wave observations with initial interferometers at design sensitivity have broken new ground, setting the best upper limits on the strength of GWs from known pulsars. These observations are already constraining theoretical models and advanced interferometers will greatly improve upon them. In this section we will take a census of the most important GW sources of isolated compact objects, current observational status and science targets and challenges for future observations.

6.4.1 A menagerie of neutron-star sources

Neutron stars in isolation with a time-varying quadrupole moment are potential sources of GWs. The birth of a NS in a supernova, a non-axisymmetric spinning NS, a NS accreting from a companion in a low-mass X-ray binary, differentially rotating NSs, could all produce GWs.

For an isolated body the energy available for radiation is in the form of its gravitational binding energy, rotational energy or energy stored in its magnetic field. Most of the available energy might be emitted in a burst of GWs, resulting in a source with a large amplitude, or else the energy might leak out slowly over a long period of time, giving a continuous, but low-amplitude, source of radiation.

Supernovae: Neutron stars are born in the aftermath of the gravitational collapse of a massive star of $\sim 8\text{--}100 M_{\odot}$ or when the core of a white dwarf becomes more massive than the Chandrasekhar limit of $1.4 M_{\odot}$. Supernovae were the prime targets for the first GW detectors and they are still among the most important sources. The Galactic supernova rate is uncertain and is thought to be between 0.01–0.1 per year, but the rate within about 5 Mpc could be one per few years [428].

In supernovae, GWs are emitted at the expense of the gravitational bind-

ing energy. The time scale over which the radiation is emitted is the dynamical free-fall time $\tau_{\text{FF}} \sim \sqrt{4\pi/G\rho_{\text{NS}}}$, where $\rho_{\text{NS}} \sim 5 \times 10^{17} \text{ kg m}^{-3}$ is the mean density of a NS⁸. Thus the time scale for collapse is $\tau_{\text{FF}} \sim 2 \text{ ms}$ and the frequency of GWs would be $f \sim \tau_{\text{FF}}^{-1} \sim 500 \text{ Hz}$. Numerical simulations also reveal that the time domain waveform is a short burst and the energy in the burst is spread over a frequency range of 200 Hz to 1 kHz, with the peak of the radiation at $f_{\text{peak}} \simeq 500 \text{ Hz}$ [429, 430]. If a fraction $\epsilon \sim 10^{-8}$ of the rest mass energy of the star is converted to GWs then the characteristic amplitude of the signal would be $h_c \sim 2 \times 10^{-22} \text{ Hz}^{-1/2}$. From Fig. 6.6 we see that a Galactic supernova from a random sky position would be easily observable in aLIGO, producing an SNR⁹ of $\sim \sqrt{2/5} h_c / \sqrt{S_h(f_{\text{peak}})} \sim 30$. At 4 Mpc, the distance at which the rate could be one per few years, the characteristic amplitude would be $h_c \sim 5 \times 10^{-24} \text{ Hz}^{-1/2}$, which would be observable in ET with a similar SNR if $\epsilon \sim 10^{-6}$.

Spinning neutron stars: A NS that is perfectly spherically symmetric or spinning about its symmetry axis emits no radiation since its quadrupole moment would not vary with time. Non-axisymmetric NSs would produce radiation at twice the spin frequency. The amplitude of GWs for a NS at a distance R , is [80] $h_0 = 4\pi^2 G \epsilon I_{zz} f^2 / (c^4 R)$, where f is the frequency of GWs and $\epsilon \equiv (I_{xx} - I_{yy})/I_{zz}$ is the NS ellipticity given in terms of the principal moments of inertia with respect to the rotation axis, I_{xx} , I_{yy} and I_{zz} . Typical NS moments of inertia are $I \sim 3 \times 10^{38} \text{ kg m}^2$, so a NS at 10 kpc, spinning at 50 Hz (GW frequency of 100 Hz) and an ellipticity of 10^{-6} , has an amplitude of $h_0 \simeq 3 \times 10^{-27}$.

Since GWs from spinning NSs are essentially continuous waves (CW), Fourier transforming the signal would focus all its power into one frequency bin. The SNR grows as the square-root of the integration period. Thus, the characteristic strain amplitude h_c of a signal integrated over a time T is $h_c = h_0 \sqrt{T}$, which for the example considered above is $h_c \sim 1.7 \times 10^{-23} \text{ Hz}^{-1/2}$, for $T = 1 \text{ yr}$. For the Crab (B0531+21), the youngest known pulsar, at a distance of 2 kpc and spin frequency of 30 Hz, $h_c \sim 3 \times 10^{-23} \text{ Hz}^{-1/2}$, for the same ellipticity. Figure 6.6 plots the characteristic amplitude as a function of GW frequency for two choices of ellipticities, $\epsilon = 10^{-6}$ and 10^{-8} , and for NSs at 10 kpc, located and oriented randomly with respect to the detector and for an integration time of 1 year. Neutron stars of spin frequencies in the range

⁸The density of the pre-collapse star is not relevant as most of the energy in GWs is emitted in the final moments of the collapse and core bounce.

⁹Laser interferometers have the best response to burst sources that occur directly above their plane, but for an event at a random position on the sky and for waves of arbitrary polarisation the response and the SNR are a factor $\sqrt{2/5}$ smaller.

20–400 Hz (GW frequencies of 40–800 Hz) would be accessible to advanced detectors if their ellipticities are $\epsilon \gtrsim 1.6 \times 10^{-5} (f/100 \text{ Hz})^{-2} (R/10 \text{ kpc})$.

Nearly 2000 pulsars are currently known¹⁰ and it is estimated that our galaxy is host to $\sim 10^9$ NSs. The fraction of NSs accessible to the gravitational window is uncertain. The biggest uncertainty is the ellipticity that can be sustained in a NS, with largest estimates of $\epsilon \sim 10^{-4}$ [431], but more typically $\epsilon \sim 10^{-6}$ or smaller [432]. Statistical arguments suggest that a NS with ellipticity $\epsilon = 10^{-6}$ could be close enough to have an amplitude of $h_{\max} \simeq 1.6 \times 10^{-24}$ in the frequency range 250–680 Hz [433].

Figure 6.7 shows the expected amplitude for several known AM CVn systems, white dwarf binaries, and X-ray binaries in the eLISA band. The latter sources are often referred to as *calibration sources*, because eLISA should see them at these amplitudes.

Pulsar Glitches and Magnetar Flares: Radio pulsars have very stable spins and their periods (P) change very slowly over time. Their small spin-down rate ($\dot{P} \lesssim 10^{-12}$), is occasionally marked by a sudden increase in angular frequency Ω , an event that is called a *glitch* [434]. To date more than 300 glitches have been observed in about 100 pulsars [435]. Vela (B0833-45) is a nearby ($R \sim 300 \text{ pc}$) pulsar in which 16 glitches have been observed since its discovery in 1969. The magnitude of a glitch is measured in terms of the fractional change in the angular velocity, which is found to be in the range $\Delta\Omega/\Omega \sim 10^{-5}\text{--}10^{-11}$. Some time after a glitch, the pulsar returns to its regular spin-down evolution. Pulsar glitches are not the only transient phenomena observed in NSs. Sources of giant X- and gamma-ray flashes are thought to arise in highly magnetised NSs, called *magnetars*, with B-fields $\sim 10^{15}\text{--}10^{16}$ Gauss. The source of high-energy radiation is believed to be powered by the decay of the magnetic field associated with stellar quakes [436].

Pulsar glitches and magnetar flares could excite a spectrum of normal mode oscillations of the ultra dense NS core, the characteristic mode frequencies varying over a range of 1.5–6 kHz and damping times $\tau \sim \text{ms}$, depending on the mode in question and the NS EoS [437]. The energy in normal modes could be emitted as a narrow-band burst of exponentially damped sinusoidal GWs. Figure 6.6 shows plausible characteristic amplitudes produced by normal modes of energy $10^{-12} M_\odot$, for mode frequencies in the range of 1.5–4 kHz and NS distances in the range 1 kpc to 10 kpc. Third generation detectors like ET should be able to detect such amplitudes in coincidence with radio observations.

¹⁰ ATNF pulsar catalogue: <http://www.atnf.csiro.au/people/pulsar/psrcat/>

Low Mass X-ray Binaries: Low-Mass X-ray Binaries (LMXBs) are accreting NSs or BHs that emit bursts of X-ray flashes lasting for about 10 s and repeat once every few hours or days, with millisecond oscillations in burst intensity [438]. X-ray bursts are believed to be caused by thermonuclear burning of infalling matter, while oscillations are suspected to be caused by the NS spin. About 100 galactic LMXBs are known to-date as well as many extra-galactic ones. Inferred spin frequencies of NSs in LMXBs seem to have an upper limit of about 700 Hz [438], although this is nowhere close to the value at which centrifugal break-up would limit the star’s spin frequency. It has been proposed that GWs might be responsible for limiting the spin frequencies of NSs in LMXBs [439–441].

The expected characteristic amplitude of gravitational radiation is shown in Fig. 6.6 for the well-known LMXB Sco X-1 and for the known Galactic population of LMXBs. Advanced detectors could detect Sco X-1 if it is losing all of its accreted angular momentum to GWs (which is unlikely to be the case), while ET targets the full galactic population [442].

6.4.2 Results from *LIGO* and *Virgo*

Searches for burst signals: Searches for bursts of GWs essentially fall into one of two classes: all sky, blind searches and astrophysically triggered searches. In the first approach there is no a priori information about what and when to look for. The goal of this approach is to detect radiation from unmodeled, or poorly modeled, transient sources, as well as hitherto unknown sources, that last for less than ~ 1 second. Since no assumption about the nature of GWs is made, this approach has the greatest serendipitous discovery potential. The search algorithm uses wavelet transforms to look for excess power [443] and the sensitivity of the search is characterised in terms of the root-sum-square strain amplitude h_{rss} of the signal¹¹. Analysing data from the various science runs has determined that the rate of strong GW bursts (i.e., bursts with $h_{\text{rss}} > 10^{-19} \text{ Hz}^{-1/2}$ in the frequency region from 70 Hz to 3 kHz) reaching the Earth is less than 1.3 events per year at 90% confidence [444]. For hypothesised standard candle sources that emit $1 M_\odot$ equivalent of energy in GWs as sine-Gaussian waveforms, the inferred rate density of events in the local Universe, in units of $\text{Mpc}^{-3} \text{ yr}^{-1}$, is less than 10^{-6} in the frequency range 100–200 Hz and less than 10^{-2} in the frequency range 1–2 kHz. Alternatively, generic burst sources within 10 kpc emitted

¹¹ The strain amplitude h_{rss} is defined as: $h_{\text{rss}} = \sqrt{\int [|h_+(t)|^2 + |h_\times(t)|^2] dt}$.

less than $\simeq 2 \times 10^{-8} M_{\odot}$ in GWs in the frequency range 100–200 Hz; that limit increases to $\simeq 10^{-5} M_{\odot}$ at 1 kHz [444].

In the second approach, analysis is carried out around the time of an astrophysical transient, such as a supernova or a magnetar flare. Knowledge of the epoch and sky position of the event helps reduce the amount of data that needs to be searched for, which in turn decreases the false alarm probability and improves the search sensitivity. Searches have been carried out at the time of pulsar glitches [445], magnetar flares [446] and GRBs [447]. Of particular significance is the search for GWs around the time of GRB070201 [448]. The event in this case was a shGRB that is believed to have followed either from giant quakes in highly magnetised NSs or from merging binary NSs. Location of GRB070201 coincides with the spiral arms of the Andromeda galaxy (M31) at 780 kpc. LIGO detectors, which were taking data at the time of this event, would have quite easily detected signals from a merging NS binary at this distance, but not bursts associated with a magnetar flare. The analysis found no plausible GW candidates within a 180 s window around the time of the GRB and in particular excluded binary NS-NS and NS-BH mergers at M31 with more than 99% confidence [448]. The analysis also concluded that isotropic energy in GWs from the source, if it were at M31, was most likely less than $4.4 \times 10^{-4} M_{\odot}$, lending support for the possibility that this was the first Soft Gamma Repeater flare observed outside the Milky Way.

More recently, searches have also been performed around the times of 128 long GRBs and 26 shGRBs [447]; no GW candidates of any significance were found, which meant that the bursts could not have occurred closer than a certain distance determined by the horizon distance of the detectors in the direction of the GRBs. The maximum exclusion distance for the population of shGRBs was 80 Mpc, which is not surprising since the closest known shGRB is at a distance of ~ 500 Mpc. However, extrapolating current results to advanced detectors, it seems quite plausible that GWs coincident with GRBs could be detected within 2.5–5 years of observing [447, 449], or place upper bounds on the number of GRBs arising from merging binaries.

Searches for continuous waves: Most CW signals are monochromatic in the rest frame of their sources. Their detection is complicated by the fact that the signal received at the detector is modulated due to the Earth’s motion. Because of Doppler modulation in frequency, the spectral lines of fixed frequency sources spread power into many Fourier bins about some mean frequency. Although the modulation of the signal makes the search prohibitively expensive, imprinted in the modulation is the source’s position on the sky; it will be possible to resolve the source’s location subject to

Rayleigh criterion, $\delta\theta = 2\pi\lambda/L$, where $\delta\theta$ is the angular resolution, λ is the wavelength of the radiation and $L = 2$ AU is the baseline for an observation period of 1 year. At a frequency of 100 Hz, $\delta\theta \sim 2''$. In the case of CW sources, two different types of searches have been performed: searches for known pulsars (with precisely known sky position and frequency evolution) and blind searches (sources with unknown sky position and spin frequency).

Searches for CW signals from known, isolated pulsars, not being limited by computational resources, have achieved the best possible sensitivity [450]. In particular, upper limits on the strength of GWs from the Crab and Vela pulsars are now determined by these observations to be well below the level expected from the observed rate at which these pulsars are spinning down. The loss in energy to GWs in Crab is less than 1% of the rotational energy lost due to the observed spin down [450]; the corresponding number for Vela is 10% [445]. A search for CW signals in the frequency range of 100–300 Hz from the compact central object, believed to be a NS, in the supernova remnant Cassiopeia A at 3 kpc, has set best upper limit on the strain amplitude of $\sim 3 \times 10^{-24}$ and equatorial ellipticity of $0.4\text{--}4 \times 10^{-4}$, as well as setting the first ever limit on the amplitude of r-modes in this young NS [451].

Given the possibility that the strongest CW sources may be electromagnetically quiet or previously undiscovered, an all sky, all frequency search for such unknown sources is very important, though computationally formidable. Clever and computationally efficient algorithms and distributed volunteer-computing `Einstein@Home` [452] have made the searches ever more sensitive, and have been successful in discovering new radio pulsars in old radio data (see, e.g., [453, 454]). A blind GW search using `Einstein@Home` excluded signals in the 50 Hz to 1.2 kHz band, with upper limits on strain amplitudes $\sim 10^{-24}\text{--}10^{-23}$ depending on the frequency of the source. For example, strain amplitudes greater than 7.6×10^{-25} were excluded at 152.5 Hz (frequency where LIGO S5 run had the best sensitivity), over a 0.5 Hz-wide band [455]. This means there are no NSs at this frequency within 4 kpc and spinning down faster than 2 nHz s^{-1} and ellipticities greater than 2×10^{-4} . Targeted searches for sources within 8 pc of the Galactic centre Sag A*, in the frequency range of 78–496 Hz, and maximum spin down rates of $\sim -8 \times 10^{-8} \text{ Hz s}^{-1}$ have achieved the best sensitivities for blind searches, ruling out NSs with GW amplitude $\sim 3 \times 10^{-25}$ around 150 Hz in this region of the sky (for details and caveats see [456]).

Advanced detectors will beat the spin down limit of several pulsars [450]. For the fastest pulsars in the frequency range 200–400 Hz, advanced detectors will reach ellipticity limits of $\sim 10^{-8}$ (or a differential radius of 100

microns in 10 km!), significantly below the spin-down limits; ET will be sensitive to ellipticities as low as 10^{-9} [18].

6.4.3 Science targets and challenges

Neutron stars are the most compact objects with matter known today. They have strong surface gravity that is responsible for very intense sources of X-rays and gamma-rays. Their dense cores could be superfluid and might consist of hyperons, quark-gluon plasma or other exotica [438] and are, therefore, laboratories of high energy nuclear physics. Observing a representative sample of the galactic population of NSs could transform astrophysical studies of compact objects, but there are still some challenges in theoretical modeling of NSs and analysis of data.

Science Targets

Physics of low-mass X-ray binaries: Detecting GWs from LMXBs should help to understand the mechanism is behind limiting spin frequencies in LMXBs. The centrifugal breakup of NS spins for most EoS is ~ 1500 Hz, far greater than the maximum spin of ~ 700 Hz inferred from X-ray observations [457]. It has, therefore, been a puzzle as to why NS spin frequencies are stalled. One reason for this could be that some mechanism operating in the NS is emitting GWs and the resulting loss in angular momentum explains why NSs cannot be spun up beyond a certain frequency. The exact mechanism causing the emission of GWs can account for this amplitude if NS can support an effective ellipticity of $\epsilon \sim 10^{-8}$. This ellipticity could be produced by a time-varying, accretion-induced quadrupole moment [440], or by relativistic instabilities (e.g. r-modes) [458], or by large toroidal magnetic fields [459]. Targeted observations of known LMXBs could confirm or rule out astrophysical models of such systems.

Understanding supernovae: Supernovae produce the Universe's dust and some of its heavy elements; their cores are laboratories of complex physical phenomena requiring general relativity, nuclear physics, magneto-hydrodynamics, neutrino viscosity and transport and turbulence to model them. Much of the physics of supernovae is poorly understood: How non-axisymmetric is the collapse? How much energy is converted to GWs and over what time scale? What causes shock revival in supernovae that form a NS: neutrino, acoustic and/or magneto-rotational mechanisms? Depending on the supernova mechanism, the predicted energy in GWs from supernovae varies by

large factors (see, e.g., [460, 461]), indicating the complexity of the problem in numerical simulations. Until we know the mechanism that revives the stalled shock it will not be possible to correctly predict the amplitude of the emitted gravitational radiation or its time-frequency structure. Gravitational-wave observations could provide some of the clues for solving these questions [430, 462]. Moreover, GWs could also be produced by neutrino emission during the supernova explosion and the signal spectrum could extend down to ~ 10 Hz [463]. More realistic studies are needed to quantify this signal.

Testing neutron-star models: Models of NSs are mostly able to compute their maximum ellipticity by subjecting the crust to breaking strains with predicted ellipticities ranging from $\epsilon \sim 10^{-4}$ (for exotic EoS) [431] to 10^{-7} for conventional crustal shear [464]. Large toroidal magnetic fields of order 10^{15} G could sustain ellipticities of order 10^{-6} [465] and accretion along magnetic fields might produce similar, or a factor 10 larger, deformations [466]. The large range in possible ellipticities shows that GW observations could have a potentially high impact and science return in this area. Confirmed detections of NSs with known distances will severely constrain models of the crustal strengths and a catalogue of CW sources would help understand the galactic supernova rate and their demographics could lead to insights on the evolutionary scenarios of compact objects.

Challenges

Interfacing theory with searches: Models that can accurately predict the spectrum and complex mode frequencies will be very useful in searches for GW signals at the time of glitches in pulsars and flares in magnetars [437]. In fact, robust predictions can also help to tune detectors to a narrower band, where signals are expected, with greater sensitivity. To take advantage of such techniques, which will become feasible in the era of routine observations, models would need to become realistic and reliable.

Supernova simulation is one area where a breakthrough in understanding the core bounce that produces the explosion could be critical to produce reliable models. At present, it is not clear if models will ever be able to produce waveforms that can be deployed as matched filters. A catalogue of predicted waveforms are routinely used to calibrate the sensitivity of a search (see, e.g., [444]). Accurate models of the frequency range and spectral features of the emitted radiation will obviously aid in better quantification of the search sensitivity.

The problem of blind searches: Looking for CWs in GW data is a computationally formidable problem [467–469]. Blind searches have to deal with many search parameters, such as the sky position of the source, its spin frequency and one or more derivatives of the spin frequency [468]. The number of floating point operations grows as the 5th power of the integration time T for a blind search with unknown sky position, unknown spin frequency and one spin-down parameter [470]. Most blind searches are able to coherently integrate the data for about a few hours to days (depending on the number of spin-down parameters searched for) [455, 456] and the sensitivity of searches will always be limited by the available computing resources. Algorithms that can integrate for longer periods are desirable, as are multi-step hierarchical searches that could achieve optimal sensitivity given the computational power.

6.5 Gravitational radiation from the early Universe

During the past 30 years, several new predictions for GW signals from the primordial Universe have been made, greatly stimulated by the construction and operation of the first GW detectors and the planning of future experiments.

The epoch of big-bang nucleosynthesis (BBN), when light elements first formed, is the earliest epoch of the Universe that we understand today with any confidence. The Universe was only a second old at this epoch, it was radiation dominated and had a temperature of ~ 1 MeV. In contrast, the Universe was much older (age of $\sim 10^5$ – 10^6 years) and cooler (temperature of ~ 1 eV), when the CMB radiation, measured today with amazing accuracy, was emitted. It is expected that the Universe is filled with cosmic neutrinos produced when the Universe's temperature was 1 MeV, but this has not been observed, yet. In fact, no primordial background, of radiation or particles, produced before the epoch of CMB has ever been detected.

6.5.1 Primordial sources and expected strengths

Gravitational waves emitted prior to BBN in the so-called *dark age* would travel unscathed, due to their weak interaction with matter, and provide us with a view of the Universe at that time.

A rapidly varying gravitational field during inflation can produce a stochastic background of GWs by parametric “amplification” of quantum, vacuum fluctuations [471, 472]. Today this background would span the frequency range of 10^{-16} – 10^{10} Hz, which covers the frequency band of current and

future detectors on the ground and in space (see Figs. 6.6 and 6.7). This is the same mechanism that is believed to have produced the scalar density perturbations that led to the formation of large scale structures in the Universe. Single-field, slow-roll models of inflation predict that the GW background today slightly decreases as the frequency increases, $\Omega_{\text{GW}} = \Omega_0(f/f_{\text{eq}})^{n_T}$, for $f > f_{\text{eq}}$ with $n_T \lesssim 0$, while it rises as a power-law, $\Omega_{\text{GW}} = \Omega_0(f/f_{\text{eq}})^{-2}$, for $f < f_{\text{eq}}$ [473, 474], where $\Omega_{\text{GW}}(f) = d\rho_{\text{GW}}(f)/d\log f/\rho_C$ [475], with $\rho_C = 3H_0^2/(8\pi G)$, being H_0 the present value of the Hubble parameter. The transition frequency $f_{\text{eq}} \simeq 10^{-16}$ Hz corresponds to the Hubble radius at the time of matter-radiation equality, redshifted to the current epoch. The value of Ω_0 is not known, but the current upper limit on the tensor-to-scalar ratio from the CMB [476] implies $\Omega_0 \lesssim 10^{-15}$. A cosmological GW background would leave an imprint in the CMB polarisation map [477, 478] and, as mentioned in Sec. 6.1, the BICEP2 [19] experiment has claimed a detection of this signature. However, further scrutiny suggests that at this time BICEP2 result cannot be excluded from being of astrophysical origin [20, 21]. Concurrently with the construction of ground-based detectors and the planning of next generation of experiments, studies of the GW background from inflation have been refined and several physical effects that may impact the high-frequency portion of the spectrum have been predicted [479–482].

The preheating phase, which occurs at the end of inflation, is a highly non-thermal phase that creates transient density inhomogeneities with time-varying mass multipoles, which would generate a stochastic background of GWs [483]. Symmetry breaking phase transitions or the ending stages of brane inflation might witness the creation of cosmic (super)strings [484–486]. Due to their large tension these strings undergo relativistic oscillations and thereby produce GWs, which causes them to shrink in size and disappear. However, they could be constantly replaced by smaller loops that brake off from loops of size larger than the Hubble radius. In this way, a network of cosmic (super)strings could generate a stochastic GW background but they could also produce bursts of gravitational radiation when cusps and kinks form along strings [487–491]. Likewise, a strong first order phase transition could create bubbles of true vacuum, which collide with each other and produce a GW background [492, 493]. For more details on the mechanisms responsible for gravitational radiation in the early Universe, we refer the reader to the following reviews [473, 474, 494, 495] and references therein.

6.5.2 Results from LIGO and Virgo

Stochastic signals are a type of continuous waves, but with two important differences. In general they do not arrive from any particular direction and, by definition, have no predictable phase evolution. Therefore, conventional matched filtering would not work and sliding data of one detector relative to another (to account for the difference in arrival time) has no particular advantage. Even so, data from one detector could serve as a “template” to detect the same stochastic signal present in another detector. If the detectors are located next to each other and have the same orientation then a simple cross-correlation of their outputs weighted by their noise spectral densities would result in optimal SNR [496]. The problem with two nearby detectors is that they will have a common noise background that would contaminate the correlated output. By placing detectors far apart, one could mitigate the effect of common noise, but in that case wavelengths smaller than the distance between the detectors will not all be coherent in the two detectors, which effectively reduces the sensitivity bandwidth. This is appropriately taken into account in the cross-correlation statistic of a pair of detectors by using what is called the *overlap reduction function* [497], which is a function of frequency that accounts for the lack of coherence in stochastic signals in detectors of different orientations and separated by a given distance [475]. Additionally, since the template is essentially noisy, the amplitude SNR grows as the *fourth-root* of the product of the effective bandwidth Δf of the detector and the duration T over which the data is integrated [496]. In the case of PTAs, the detection technique is similar; instead of a pair of detectors one constructs the correlation between the timing residuals of many stable millisecond pulsars.

The energy density in GWs is related to the strain power spectrum $S_{\text{GW}}(f)$ by [475] $S_{\text{GW}}(f) = 3H_0^2 \Omega_{\text{GW}}(f)/(10\pi^2 f^3)$. The *characteristic amplitude* h_c of a stochastic background, i.e. the strain amplitude produced by a background after integrating for a time T over a bandwidth Δf , is given by $h_c^2 = \sqrt{T \Delta f} S_{\text{GW}}$. In Figs. 6.6 and 6.7 we plot (in dotted lines) $h_c(f)$ for several values of Ω_{GW} assumed to be independent of f , setting $T = 1 \text{ yr}$ and $\Delta f = 100 \text{ Hz}$. Due to the overlap reduction function, the SNR is built up mostly from the low-frequency part of the signal such that $\lambda_{\text{GW}} \gtrsim d/2$, where d is distance between detectors. A stochastic signal would be detectable if it stays above the noise curve roughly over a frequency band $\Delta f \simeq f$. Advanced detectors should detect $\Omega_{\text{GW}} \geq 10^{-9}$ at tens of Hz, while ET, due to its much improved low-frequency sensitivity and collocated detectors, could detect $\Omega_{\text{GW}} \sim 10^{-11}$, while eLISA could detect $\Omega_{\text{GW}} \geq 10^{-12}$ at mHz fre-

quencies. For an integration time of $T = 5$ yr and bandwidth of $\Delta f = 6$ nHz, a stochastic background with $\Omega_{\text{GW}} = 2.5 \times 10^{-10}$ would be detectable in PTA with an SNR of 5, assuming 20 millisecond pulsars that have an rms stability of 100 ns [498, 499]. SKA will improve the sensitivity of PTAs by two orders of magnitude to $\Omega_{\text{GW}} \sim \text{few} \times 10^{-13}$ [500].

Gravitational radiation from the early Universe does not only generate stochastic backgrounds: bursts from cusps and kinks along cosmic (super)strings produce power-law signals in the frequency domain [490] that can be searched for using matched-filtering techniques. Data from several science runs of iLIGO and Virgo detectors have been analysed to search for signals from the early Universe. In those science runs, the detectors' sensitivity has passed the BBN bound [501, 502] in the frequency band around 100 Hz, $\Omega_{\text{GW}} < 6.9 \times 10^{-6}$, but not yet the CMB bound [503]. The results have started to exclude regions of the parameter space of expected signals from cosmic (super)strings [502, 504, 505], and have constrained the equation of state of the Universe during the dark age [502, 506]. Moreover, pulsar timing observations have set physically meaningful upper limits for the supermassive BH binary background ($\Omega_{\text{GW}} < 1.3 \times 10^{-9}$ at 2.8 nHz) [507] and cosmic (super)strings [508].

6.5.3 Science targets and challenges

Stochastic GW signals might carry signature of unexplored physics in the energy range $\sim 10^9$ GeV to $\sim 10^{16}$ GeV. The detection of GWs from the dark age could therefore be revolutionary. The spectrum of the detected radiation could reveal phase transitions that might have occurred in the Universe's early history, unearth exotic remnants like cosmic (super)strings, prove that a cosmic inflationary phase existed and that gravity can be reconciled with quantum mechanics. No other observation can ever take us closer to the origin of our Universe and hence the science potential of discovering primordial GWs will be immense. However, the challenges in this area are equally formidable.

As mentioned before, one of the biggest problems in identifying a stochastic GW background is how to disentangle it from the environmental and instrumental noise backgrounds. At present, data from two or more detectors are cross correlated to see if there is any statistical excess. If the detectors are geographically widely separated then one could reasonably hope for the environmental noise backgrounds in different instruments not to correlate, although correlations could exist due to large scale magnetic fields, cosmic rays and anthropogenic noise and the like. When the number of detectors

grows, noise correlations go down. However, because of the overlap reduction function, the sensitivity to a stochastic background diminishes quickly with geographically separated detectors. Due to environmental and instrumental noise, searching for stochastic backgrounds in collocated detectors like ET or eLISA will be a real challenge.

In the case of PTAs, the problem is less severe as one is looking for correlations in the residuals of the arrival times of radio pulses from an array of millisecond pulsars, after subtracting the model of the pulsar from the original data. In principle, any systematics in timing residuals could be mitigated by integrating the correlation over long periods, but the problem here is that the time scale for integration tends to be large (i.e., tens of years).

In the case of the GW background from inflation, CMB bounds on inflationary potentials are not very informative on the value of Ω_0 except for placing an upper limit. In the absence of probes from epochs prior to BBN, it is very hard to infer the equation of state of the Universe between the end of inflation to the epoch when the radiation era started. Thus, it is difficult to predict the spectral slope of the relic GW background from BBN (when the Universe was certainly radiation dominated) to the scales where PTA, space-based and ground-based detectors are sensitive [506]. It is customary and (perhaps) natural to assume that the slope is the same over the huge range of frequency, spanning twenty orders of magnitude, and that it can be determined by CMB observations. However, as we look backward past BBN, a stiff energy component might overtake radiation as the dominant component in the cosmic energy budget [509–513], without coming into conflict with any current observational constraints. The detection of the B-mode polarisation in the CMB will certainly have a huge impact, determining Ω_0 , but we will still not know whether the slope remains the same for twenty orders of magnitude.

Predictions for the GW background from preheating at the end of inflation [483, 495] lie typically (except for some choices of parameters in hybrid inflation) in the MHz frequency range where no GW detectors exist or are currently planned. Experimental proposals would need to be made, but since, when holding Ω_{GW} fixed, the noise spectral density decreases as the frequency increases, the requirements on the detector sensitivity can be very hard to achieve. Finally, depending on string parameters, both the stochastic background and single powerful bursts from cusps and kinks of cosmic (super)strings could be observed by PTAs, eLISA and the aLIGO/AdV/KAGRA network. More robust predictions of (super)string loop sizes (large versus small loop sizes at birth) will be important to restrict regions of parameter space that are searched over (see [495] and references therein).

Acknowledgements

We are greateful to Luc Blanchet, Eric Poisson and Riccardo Sturani for carefully reading and providing comments on the manuscript. We have benefited from useful discussions with Leor Barack (who supplied a Mathematica code to compute EMRI spectra in Figure 6.7), Chris Messenger, Bernard Schutz and Patrick Sutton. A.B. acknowledges partial support from NSF Grant No. PHY-1208881 and NASA Grant NNX09AI81G. B.S.S. acknowledges support from STFC (UK) grant ST/L000962/1, ST/L000342/1 and ST/J000345/1.

References

- [1] Maxwell, J. 1865. *Phil. Trans. R. Soc. Lond.*, **155**, 459–512.
- [2] Einstein, A. 1916. *Sitzungsberichte der Königlich Preussischen Akademie der Wissenschaften Berlin*, 688–696.
- [3] Einstein, A. 1918. *Sitzungsberichte der Königlich Preussischen Akademie der Wissenschaften Berlin*, 154–167.
- [4] Poincaré, H. 1905. *Comptes Rendus Acad Sci. paris*, **140**, 1504–1508.
- [5] Einstein, A., Rosen, N. 1937. *Journal of Franklin Institute*, **223**, 43–54.
- [6] Bondi, H., Pirani, F., Robinson, I. 1959. *Proc. Roy. Soc. Lond.*, **A251**, 519.
- [7] Kennefick, D. 2007. *Traveling at the speed of thought: Einstein and the quest for gravitational waves*. Princeton University Press, Princeton.
- [8] Saulson, P. R. 2011. *General Relativity and Gravitation*, **43**, 3289–3299.
- [9] Bondi, H., van der Burg, M., Metzner, A. 1962. *Proc. Roy. Soc. Lond.*, **A269**, 21–52.
- [10] Weber, J. 1960. *Phys. Rev.*, **117**, 306.
- [11] Hulse, R. A., Taylor, J. H. 1975. *Astrophys. J.*, **195**, L51–L53.
- [12] Taylor, J., Fowler, L., McCulloch, P. 1979. *Nature*, **277**, 437–440.
- [13] Weisberg, J. M., Taylor, J. H. 2005. The Relativistic Binary Pulsar B1913+16: Thirty Years of Observations and Analysis. Page 25 of: Rasio, F. A., Stairs, I. H. (eds), *ASP Conf. Ser. 328: Binary Radio Pulsars*. Astronomical Society of the Pacific, Aspen, Colorado, USA.
- [14] Weisberg, J. M., Nice, D. J., Taylor, J. H. 2010. *Astrophys. J.*, **722**, 1030–1034.
- [15] Kramer, M. 2013. Probing gravitation with pulsars. Page 19 of: van Leeuwen, J. (ed), *IAU Symposium*, vol. 291.
- [16] Deruelle, N., Piran, T. (eds). 1982. *Gravitational Radiation (Les Houches Winter School, 1982)*. Amsterdam: North Holland.
- [17] Hawking, S. W., Israel, W. (eds). 1987. *Three hundred years of gravitation*. Cambridge: Cambridge University Press.
- [18] Abernathy, M., et al. 2011. *Einstein gravitational wave Telescope: Conceptual Design Study*. Available from *European Gravitational Observatory*, document number ET-0106A-10.
- [19] Ade, P., et al. 2014. *BICEP2 I: Detection Of B-mode Polarization at Degree Angular Scales*. arXiv:1403.3985.
- [20] Mortonson, M. J., Seljak, U. 2014. *A joint analysis of Planck and BICEP2 B modes including dust polarization uncertainty*. arXiv:1405.5857.

- [21] Flauger, R., Hill, J. C., Spergel, D. N. 2014. *Toward an Understanding of Foreground Emission in the BICEP2 Region.* arXiv:1405.7351.
- [22] Wagoner, R., Will, C. 1976. *Astrophys.J.*, **210**, 764–775.
- [23] Ehlers, J., Rosenblum, A., Goldberg, J., Havas, P. 1976. *Astrophys.J.*, **208**, L77–L81.
- [24] Ehlers, J. 1980. Isolated systems in general relativity. Pages 279–294 of: Ehlers, J., Perry, J. J., Walker, M. (eds), *Ann. New York Acad. Sc.* **336**.
- [25] Walker, M., Will, C. 1980. *Phys. Rev. Lett.*, **45**, 1741–1744.
- [26] Walker, M., Will, C. M. 1980. *Astrophys.J.*, **242**, L129–L133.
- [27] Damour, T., Deruelle, N. 1981. *Phys. Lett.*, **A87**, 81.
- [28] Futamase, T., Schutz, B. F. 1983. *Phys. Rev. D*, **28**, 2363–2372.
- [29] Futamase, T. 1983. *Phys. Rev. D*, **28**, 2373–2381.
- [30] Thorne, K. S. 1980. *Rev. Mod. Phys.*, **52**, 299–339.
- [31] Damour, T., Deruelle, N. 1985. *Ann. Inst. H. Poincaré*, **44**, 107–132.
- [32] Damour, T., Schäfer, G. 1985. *General Relativity and Gravitation*, **17**, 879.
- [33] Damour, T., Deruelle, N. 1986. *Ann. Inst. H. Poincaré Phys. Théor.*, **44**, 263–292.
- [34] Blanchet, L., Damour, T. 1986. *Phil. Trans. Roy. Soc. Lond. A*, **320**, 379.
- [35] Blanchet, L. 1987. *Proc. R. Soc. A*, **409**, 383–399.
- [36] Damour, T., Schaefer, G. 1988. *Nuovo Cim.*, **B101**, 127.
- [37] Blanchet, L., Damour, T. 1988. *Phys. Rev. D*, **37**, 1410–1435.
- [38] Blanchet, L., Schaefer, G. 1989. *Mon. Not. Roy. Astron. Soc.*, **239**, 845–867.
- [39] Blanchet, L., Damour, T. 1989. *Annales Inst. H. Poincaré Phys. Théor.*, **50**, 377–408.
- [40] Damour, T., Iyer, B. R. 1991. *Ann. Inst. Henri Poincaré, A*, **54**, 115–164.
- [41] Lincoln, C., Will, C. 1990. *Phys. Rev. D*, **42**, 1123–1143.
- [42] Blanchet, L., Damour, T. 1992. *Phys. Rev. D*, **46**, 4304–4319.
- [43] Thorne, K. S. 1992. *Phys. Rev. D*, **45**, 520–524.
- [44] Cutler, C., Apostolatos, T. A., Bildsten, L., Finn, L. S., Flanagan, E. E., et al. 1993. *Phys. Rev. Lett.*, **70**, 2984–2987.
- [45] Blanchet, L., Schaefer, G. 1993. *Class. Quant. Grav.*, **10**, 2699–2721.
- [46] Iyer, B. R., Will, C. 1993. *Phys. Rev. Lett.*, **70**, 113–116.
- [47] Blanchet, L., Damour, T., Iyer, B. R. 1995. *Phys. Rev. D*, **51**, 5360–5386.
- [48] Blanchet, L., Damour, T., Iyer, B. R., Will, C. M., Wiseman, A. 1995. *Phys. Rev. Lett.*, **74**, 3515–3518.
- [49] Blanchet, L., Iyer, B. R., Will, C. M., Wiseman, A. G. 1996. *Class. Quant. Grav.*, **13**, 575–584.
- [50] Jaranowski, P., Schaefer, G. 1997. *Phys. Rev. D*, **55**, 4712–4722.
- [51] Jaranowski, P., Schaefer, G. 1998. *Phys. Rev. D*, **57**, 7274–7291.
- [52] Kidder, L. E., Will, C. M., Wiseman, A. G. 1993. *Phys. Rev. D*, **47**, 4183–4187.
- [53] Kidder, L. E. 1995. *Phys. Rev. D*, **52**(Jul), 821–847.
- [54] Will, C. M., Wiseman, A. G. 1996. *Phys. Rev. D*, **54**, 4813–4848.
- [55] Poisson, E. 1993. *Phys. Rev. D*, **47**, 1497–1510.
- [56] Tagoshi, H., Nakamura, T. 1994. *Phys. Rev. D*, **49**, 4016–4022.
- [57] Poisson, E. 1993. *Phys. Rev. D*, **48**, 1860–1863.
- [58] Shibata, M., Sasaki, M., Tagoshi, H., Tanaka, T. 1995. *Phys. Rev. D*, **51**, 1646–1663.
- [59] Tagoshi, H., Sasaki, M. 1994. *Prog. Theo. Phys.*, **92**, 745–772.
- [60] Tagoshi, H., Shibata, M., Tanaka, T., Sasaki, M. 1996. *Phys. Rev. D*, **54**, 1439–1459.

- [61] Abramovici, A., Althouse, W. E., Drever, R. W., Gursel, Y., Kawamura, S., et al. 1992. *Science*, **256**, 325–333.
- [62] Tagoshi, H., et al. 2001. *Phys. Rev. D*, **63**, 062001.
- [63] Abbott, B., et al. 2004. *Phys. Rev. D*, **69**, 122001.
- [64] Nicholson, D., Dickson, C., Watkins, W., Schutz, B. F., Shuttleworth, J., et al. 1996. *Phys.Lett.*, **A218**, 175–180.
- [65] Buonanno, A., Damour, T. 1999. *Phys. Rev. D*, **59**, 084006.
- [66] Buonanno, A., Damour, T. 2000. *Phys. Rev. D*, **62**, 064015.
- [67] Baker, J. G., Campanelli, M., Lousto, C., Takahashi, R. 2002. *Phys. Rev. D*, **65**, 124012.
- [68] Baker, J. G., Bruegmann, B., Campanelli, M., Lousto, C., Takahashi, R. 2001. *Phys. Rev. Lett.*, **87**, 121103.
- [69] Pretorius, F. 2005. *Phys. Rev. Lett.*, **95**, 121101.
- [70] Campanelli, M., Lousto, C. O., Marronetti, P., Zlochower, Y. 2006. *Phys. Rev. Lett.*, **96**, 111101.
- [71] Baker, J. G., Centrella, J., Choi, D.-I., Koppitz, M., van Meter, J. 2006. *Phys. Rev. Lett.*, **96**, 111102.
- [72] Sasaki, M., Tagoshi, H. 2003. *Living Rev.Rel.*, **6**, 6.
- [73] Blanchet, L. 2006. *Living Rev.Rel.*, **9**, 4.
- [74] Futamase, T., Itoh, Y. 2007. *Living Rev.Rel.*, **10**, 2.
- [75] Barack, L. 2009. *Class. Quant. Grav.*, **26**, 213001.
- [76] Poisson, E., Pound, A., Vega, I. 2011. *Living Rev.Rel.*, **14**, 7.
- [77] Damour, T. 2013. *The general relativistic two body problem*. arXiv:1312.3505.
- [78] Landau, L. D., Lifshitz, E. M. 1962. *Classical Theory of Fields*. Second edn. Reading, MA: Addison Wesley.
- [79] Schutz, B. 2009. *A First Course in General Relativity*. Cambridge University Press, UK.
- [80] Maggiore, M. 2008. *Gravitational Waves - Volume 1*. First edn. New York, NY: Oxford University Press.
- [81] Blanchet, L., Spallicci, A., Whiting, B. (eds). 2011. *Post-Newtonian Methods: Analytic Results on the Binary Problem*. Springer Netherlands.
- [82] Epstein, R., Wagoner, R. V. 1975. *Astrophys. J.*, **197**(May), 717–723.
- [83] Bonnor, W. B., Rotenberg, M. A. 1961. *Royal Society of London Proceedings Series A*, **265**, 109–116.
- [84] Bonnor, W. B., Rotenberg, M. A. 1966. *Royal Society of London Proceedings Series A*, **289**, 247–274.
- [85] Blanchet, L. 1987. *Proc. R. Soc. Lond. A*, **409**, 383.
- [86] Blanchet, L. 1995. *Phys. Rev. D*, **51**, 2559–2583.
- [87] Blanchet, L. 1998. *Class. Quat. Grav.*, **15**, 1971–1999.
- [88] Poujade, O., Blanchet, L. 2002. *Phys. Rev. D*, **65**, 124020.
- [89] Blanchet, L., Faye, G., Nissanke, S. 2005. *Phys. Rev. D*, **72**, 044024.
- [90] Blanchet, L. 1996. *Phys. Rev. D*, **54**, 1417–1438.
- [91] Blanchet, L. 1993. *Phys. Rev. D*, **47**, 4392–4420.
- [92] Pati, M., Will, C. 2000. *Phys. Rev. D*, **62**, 124015.
- [93] Pati, M. E., Will, C. M. 2002. *Phys. Rev. D*, **65**, 104008.
- [94] Wiseman, A. 1993. *Phys. Rev. D*, **48**, 4757–4770.
- [95] Blanchet, L. 1998. *Class. Quant. Grav.*, **15**, 113–141.
- [96] Lorentz, H., Droste, J. 1917. *The Collected Papers of H.A. Lorentz*. Vol. 5. (Nijhoff, The Hague, 1937) Versl. K. Akad. Wet. Amsterdam.
- [97] Einstein, A., Infeld, L., Hoffmann, B. 1938. *Annals Math.*, **39**, 65–100.

- [98] Petrova, N. 1949. *JETP*, **19**, 989–999.
- [99] Fock, V. 1939. *J. Phys.*, **1**, 81–116.
- [100] Papapetrou, A. 1951. *Proceedings of the Physical Society A*, **64**, 57–75.
- [101] Kimura, T. 1961. *Prog. Theo. Phys.*, **26**.
- [102] Ohta, T., Okamura, H., Kimura, T., Hiida, K. 1974. *Prog. Theo. Phys.*, **51**, 1598–1612.
- [103] Ohta, T., Okamura, H., Kimura, T., Hiida, K. 1973. *Prog. Theo. Phys.*, **50**, 492–514.
- [104] Ohta, T., Okamura, H., Kimura, T., Hiida, K. 1974. *Prog. Theo. Phys.*, **51**, 1220–1238.
- [105] Bel, L., Deruelle, N., Damour, T., Ibanez, J., Martin, J. 1981. *General Relativity and Gravitation*, **13**, 963–1004.
- [106] Damour, T., Taylor, J. H. 1992. *Phys. Rev. D*, **45**, 1840–1868.
- [107] Damour, T. 1987. The problem of motion in Newtonian and Einsteinian Gravity. Chap. 6, pages 128–198 of: Hawking, S. W., Israel, W. (eds), *Three hundred years of gravitation*. Cambridge: Cambridge University Press.
- [108] Kopeikin, S. M. 1985. *Soviet Astronomy*, **29**, 516–524.
- [109] Itoh, Y., Futamase, T., Asada, H. 2001. *Phys. Rev. D*, **63**, 064038.
- [110] Blanchet, L., Faye, G. 2000. *J.Math.Phys.*, **41**, 7675–7714.
- [111] Damour, T., Jaradowski, P., Schaefer, G. 2001. *Phys.Lett.*, **B513**, 147–155.
- [112] Dirac, P. A. M. 1958. *Roy. Soc. of London Proc. Series A*, **246**, 333–343.
- [113] Dirac, P. A. 1959. *Phys. Rev.*, **114**, 924–930.
- [114] Dirac, P. A. 1959. *Phys. Rev. Lett.*, **2**, 368–371.
- [115] Arnowitt, R., Deser, S., Misner, C. W. 1960. *Phys. Rev.*, **117**, 1595–1602.
- [116] Arnowitt, R., Deser, S., Misner, C. W. 1960. *J. of Math. Physics*, **1**, 434–439.
- [117] Schwinger, J. 1963. *Phys. Rev.*, **130**, 1253–1258.
- [118] Dewitt, B. S. 1967. *Phys. Rev.*, **160**, 1113–1148.
- [119] Regge, T., Teitelboim, C. 1974. *Annals of Physics*, **88**, 286–318.
- [120] Schäfer, G. 1985. *Annals of Physics*, **161**, 81–100.
- [121] Jaradowski, P., Schaefer, G. 1999. *Phys. Rev. D*, **60**, 124003.
- [122] Damour, T., Jaradowski, P., Schaefer, G. 2000. *Phys. Rev. D*, **62**, 021501.
- [123] Damour, T., Jaradowski, P., Schaefer, G. 2001. *Phys. Rev. D*, **63**, 044021.
- [124] Ledvinka, T., Schäfer, G., Bičák, J. 2008. *prl*, **100**, 251101.
- [125] Jaradowski, P., Schaefer, G. 2012. *Phys. Rev. D*, **86**, 061503.
- [126] Jaradowski, P., Schaefer, G. 2013. *Phys. Rev. D*, **87**, 081503.
- [127] Bertotti, B., Plebanski, J. 1960. *Annals of Physics*, **11**, 169–200.
- [128] Hari Dass, N., Soni, V. 1982. *J.Phys.*, **A15**, 473.
- [129] Damour, T., Esposito-Farese, G. 1996. *Phys. Rev. D*, **53**, 5541–5578.
- [130] Goldberger, W. D., Rothstein, I. Z. 2006. *Phys. Rev. D*, **73**, 104029.
- [131] Goldberger, W. D., Rothstein, I. Z. 2006. *Gen.Rel.Grav.*, **38**, 1537–1546.
- [132] Gilmore, J. B., Ross, A. 2008. *Phys. Rev. D*, **78**, 124021.
- [133] Foffa, S., Sturani, R. 2011. *Phys. Rev. D*, **84**, 044031.
- [134] Porto, R. A. 2006. *Phys. Rev. D*, **73**, 104031.
- [135] Porto, R. A., Rothstein, I. Z. 2006. *Phys. Rev. Lett.*, **97**, 021101.
- [136] Kol, B., Smolkin, M. 2008. *Class. Quant. Grav.*, **25**, 145011.
- [137] Porto, R. A., Rothstein, I. Z. 2008. *Phys. Rev. D*, **78**, 044013.
- [138] Porto, R. A., Rothstein, I. Z. 2008. *Phys. Rev. D*, **78**, 044012.
- [139] Porto, R. A., Ross, A., Rothstein, I. Z. 2011. *JCAP*, **1103**, 009.
- [140] Porto, R. A. 2010. *Class. Quant. Grav.*, **27**, 205001.
- [141] Levi, M. 2010. *Phys. Rev. D*, **82**, 104004.

- [142] Levi, M. 2012. *Phys. Rev. D*, **85**, 064043.
- [143] Hergt, S., Steinhoff, J., Schaefer, G. 2012. *Annals Phys.*, **327**, 1494–1537.
- [144] Hergt, S., Steinhoff, J., Schaefer, G. 2014. *J.Phys.Conf.Ser.*, **484**, 012018.
- [145] Porto, R. A., Ross, A., Rothstein, I. Z. 2012. *JCAP*, **1209**, 028.
- [146] Blanchet, L., Detweiler, S. L., Le Tiec, A., Whiting, B. F. 2010. *Phys. Rev. D*, **81**, 084033.
- [147] Blanchet, L., Buonanno, A., Le Tiec, A. 2013. *Phys. Rev. D*, **87**, 024030.
- [148] Le Tiec, A., Barausse, E., Buonanno, A. 2012. *Phys. Rev. Lett.*, **108**, 131103.
- [149] Shah, A. G., Friedman, J. L., Whiting, B. F. 2014. *Phys. Rev.*, **D89**, 064042.
- [150] Blanchet, L., Faye, G., Whiting, B. F. 2014. *Phys. Rev.*, **D89**, 064026.
- [151] Bini, D., Damour, T. 2013. *High-order post-Newtonian contributions to the two-body gravitational interaction potential from analytical gravitational self-force calculations*. arXiv:1312.2503.
- [152] Mano, S., Suzuki, H., Takasugi, E. 1996. *Prog. Theo. Phys.*, **95**, 1079–1096.
- [153] Mano, S., Takasugi, E. 1997. *Prog. Theo. Phys.*, **97**, 213–232.
- [154] Mano, S., Suzuki, H., Takasugi, E. 1996. *Prog. Theo. Phys.*, **96**, 549–566.
- [155] Vines, J. E., Flanagan, E. E. 2013. *Phys. Rev. D*, **88**, 024046.
- [156] Damour, T., Nagar, A. 2010. *Phys. Rev. D*, **81**, 084016.
- [157] Bini, D., Damour, T., Faye, G. 2012. *Phys. Rev. D*, **85**, 124034.
- [158] Blanchet, L., Faye, G. 2001. *Phys. Rev. D*, **63**, 062005.
- [159] de Andrade, V. C., Blanchet, L., Faye, G. 2001. *Class. Quant. Grav.*, **18**, 753–778.
- [160] Blanchet, L., Damour, T., Esposito-Farese, G. 2004. *Phys. Rev. D*, **69**, 124007.
- [161] Itoh, Y., Futamase, T. 2003. *Phys. Rev. D*, **68**, 121501.
- [162] Foffa, S., Sturani, R. 2013. *Phys. Rev. D*, **87**, 064011.
- [163] Bini, D., Damour, T. 2013. *Phys. Rev.*, **D87**(12), 121501.
- [164] Damour, T., Jaradowski, P., Schaefer, G. 2014. *Phys. Rev.*, **D89**, 064058.
- [165] Tagoshi, H., Ohashi, A., Owen, B. J. 2001. *Phys. Rev. D*, **63**, 044006.
- [166] Faye, G., Blanchet, L., Buonanno, A. 2006. *Phys. Rev. D*, **74**, 104033.
- [167] Damour, T., Jaradowski, P., Schaefer, G. 2008. *Phys. Rev. D*, **77**, 064032.
- [168] Hartung, J., Steinhoff, J. 2011. *Annalen Phys.*, **523**, 783–790.
- [169] Marsat, S., Bohé, A., Faye, G., Blanchet, L. 2013. *Class. Quant. Grav.*, **30**, 055007.
- [170] Levi, M. 2010. *Phys. Rev. D*, **82**, 064029.
- [171] Steinhoff, J., Hergt, S., Schaefer, G. 2008. *Phys. Rev. D*, **77**, 081501.
- [172] Steinhoff, J., Hergt, S., Schaefer, G. 2008. *Phys. Rev. D*, **78**, 101503.
- [173] Blanchet, L., Damour, T., Esposito-Farese, G., Iyer, B. R. 2004. *Phys. Rev. Lett.*, **93**, 091101.
- [174] Blanchet, L., Damour, T., Esposito-Farese, G., Iyer, B. R. 2005. *Phys. Rev. D*, **71**, 124004.
- [175] Blanchet, L., Buonanno, A., Faye, G. 2006. *Phys. Rev. D*, **74**, 104034.
- [176] Blanchet, L., Buonanno, A., Faye, G. 2011. *Phys. Rev. D*, **84**, 064041.
- [177] Bohé, A., Marsat, S., Blanchet, L. 2013. *Class. Quant. Grav.*, **30**, 135009.
- [178] Marsat, S., Bohé, A., Blanchet, L., Buonanno, A. 2014. *Class. Quant. Grav.*, **31**, 025023.
- [179] Gergely, L. A. 2000. *Phys. Rev. D*, **61**, 024035.
- [180] Gergely, L. A. 2000. *Phys. Rev. D*, **62**, 024007.
- [181] Mikoczi, B., Vasuth, M., Gergely, L. A. 2005. *Phys. Rev. D*, **71**, 124043.
- [182] Vines, J., Flanagan, E. E., Hinderer, T. 2011. *Phys. Rev. D*, **83**, 084051.
- [183] Konigsdorffer, C., Faye, G., Schaefer, G. 2003. *Phys. Rev. D*, **68**, 044004.

- [184] Nissanke, S., Blanchet, L. 2005. *Class. Quant. Grav.*, **22**, 1007–1032.
- [185] Gopakumar, A., Iyer, B. R. 1997. *Phys. Rev. D*, **56**(Dec), 7708–7731.
- [186] Will, C. M. 2005. *Phys. Rev. D*, **71**, 084027.
- [187] Zeng, J., Will, C. M. 2007. *Gen.Rel.Grav.*, **39**, 1661–1673.
- [188] Wang, H., Steinhoff, J., Zeng, J., Schafer, G. 2011. *Phys. Rev. D*, **84**, 124005.
- [189] Wang, H., Will, C. M. 2007. *Phys. Rev. D*, **75**, 064017.
- [190] Blanchet, L., Faye, G., Iyer, B. R., Joguet, B. 2002. *Phys. Rev. D*, **65**, 061501.
- [191] Arun, K. G., Buonanno, A., Faye, G., Ochsner, E. 2009. *Phys. Rev. D*, **79**, 104023.
- [192] Flanagan, E. E., Hinderer, T. 2008. *Phys. Rev. D*, **77**, 021502.
- [193] Faye, G., Marsat, S., Blanchet, L., Iyer, B. R. 2012. *Class. Quant. Grav.*, **29**, 175004.
- [194] Blanchet, L., Iyer, B. R., Will, C. M., Wiseman, A. G. 1996. *Class. Quant. Grav.*, **13**, 575–584.
- [195] Arun, K., Blanchet, L., Iyer, B. R., Qusailah, M. S. 2004. *Class. Quant. Grav.*, **21**, 3771–3802.
- [196] Kidder, L. E. 2008. *Phys. Rev. D*, **77**, 044016.
- [197] Blanchet, L., Faye, G., Iyer, B. R., Sinha, S. 2008. *Class. Quant. Grav.*, **25**, 165003.
- [198] Buonanno, A., Faye, G., Hinderer, T. 2013. *Phys. Rev. D*, **87**, 044009.
- [199] Taylor, S., Poisson, E. 2008. *Phys. Rev. D*, **78**, 084016.
- [200] Alvi, K. 2001. *Phys. Rev. D*, **64**, 104020.
- [201] Chatzioannou, K., Poisson, E., Yunes, N. 2013. *Phys. Rev. D*, **87**, 044022.
- [202] Regge, T., Wheeler, J. A. 1957. *Phys. Rev.*, **108**, 1063–1069.
- [203] Zerilli, F. 1970. *Phys. Rev. D*, **2**, 2141–2160.
- [204] Teukolsky, S. A. 1973. *Astrophys.J.*, **185**, 635–647.
- [205] Sasaki, M., Nakamura, T. 1982. *Prog. Theo. Phys.*, **67**, 1788.
- [206] Cutler, C., Poisson, E., Sussman, G., Finn, L. 1993. *Phys. Rev. D*, **47**, 1511.
- [207] Apostolatos, T., Kennefick, D., Poisson, E., Ori, A. 1993. *Phys. Rev. D*, **47**, 5376–5388.
- [208] Cutler, C., Kennefick, D., Poisson, E. 1994. *Phys. Rev. D*, **50**, 3816.
- [209] Hughes, S. A. 2000. *Phys. Rev. D*, **61**, 084004.
- [210] Hughes, S. A. 2001. *Phys. Rev. D*, **64**, 064004.
- [211] Fujita, R., Tagoshi, H. 2004. *Prog. Theo. Phys.*, **112**, 415–450.
- [212] Sundararajan, P., Khanna, G., Hughes, S. A. 2007. *Phys. Rev. D*, **76**, 104005.
- [213] Sundararajan, P., Khanna, G., Hughes, S. A., Drasco, S. 2008. *Phys. Rev. D*, **78**, 024022.
- [214] Fujita, R., Tagoshi, H. 2005. *Prog. Theo. Phys.*, **113**, 1165–1182.
- [215] Zenginoglu, A., Khanna, G. 2011. *Phys. Rev. X*, **1**, 021017.
- [216] Bernuzzi, S., Nagar, A., Zenginoglu, A. 2011. *Phys. Rev. D*, **84**, 084026.
- [217] Damour, T., Nagar, A. 2007. *Phys. Rev. D*, **76**, 064028.
- [218] Sundararajan, P., Khanna, G., Hughes, S. A. 2010. *Phys. Rev. D*, **81**, 104009.
- [219] Bernuzzi, S., Nagar, A. 2010. *Phys. Rev. D*, **81**, 084056.
- [220] Bernuzzi, S., Nagar, A., Zenginoglu, A. 2011. *Phys. Rev. D*, **83**, 064010.
- [221] Barausse, E., Buonanno, A., Hughes, S. A., Khanna, G., O’Sullivan, S., et al. 2012. *Phys. Rev. D*, **85**, 024046.
- [222] Sasaki, M. 1994. *Prog. Theo. Phys.*, **92**, 17–36.
- [223] Tanaka, T., Tagoshi, H., Sasaki, M. 1996. *Prog. Theo. Phys.*, **96**, 1087–1101.
- [224] Fujita, R., Iyer, B. 2010. *Phys. Rev. D*, **82**, 044051.
- [225] Fujita, R. 2012. *Prog. Theo. Phys.*, **127**, 583–590.

- [226] Fujita, R. 2012. *Prog. Theo. Phys.*, **128**, 971–992.
- [227] Tanaka, T., Mino, Y., Sasaki, M., Shibata, M. 1996. *Phys. Rev. D*, **54**, 3762.
- [228] Poisson, E., Sasaki, M. 1995. *Phys. Rev. D*, **51**, 5753–5767.
- [229] Tagoshi, H., Mano, S., Takasugi, E. 1997. *Prog. Theo. Phys.*, **98**, 829–850.
- [230] Mino, Y., Sasaki, M., Shibata, M., Tagoshi, H., Tanaka, T. 1997. *Prog. Theor. Phys. Suppl.*, **128**, 1–121.
- [231] Dirac, P. A. M. 1938. *Roy. Soc. of London Proc. Series A*, **167**, 148–169.
- [232] DeWitt, B. S., Brehme, R. W. 1960. *Annals Phys.*, **9**, 220–259.
- [233] Mino, Y., Sasaki, M., Tanaka, T. 1997. *Phys. Rev. D*, **55**, 3457–3476.
- [234] Quinn, T. C., Wald, R. M. 1997. *Phys. Rev. D*, **56**, 3381–3394.
- [235] Detweiler, S. L., Whiting, B. F. 2003. *Phys. Rev. D*, **67**, 024025.
- [236] Gralla, S. E., Wald, R. M. 2008. *Class. Quant. Grav.*, **25**, 205009.
- [237] Pound, A. 2010. *Phys. Rev. D*, **81**, 024023.
- [238] Barack, L., Ori, A. 2001. *Phys. Rev. D*, **64**, 124003.
- [239] Detweiler, S., Messoritaki, E., Whiting, B. 2003. *Phys. Rev. D*, **67**, 104016.
- [240] Keidl, T. S., Friedman, J. L., Wiseman, A. G. 2007. *Phys. Rev. D*, **75**, 124009.
- [241] Barack, L., Lousto, C. O. 2002. *Phys. Rev. D*, **66**, 061502.
- [242] Barack, L., Sago, N. 2007. *Phys. Rev. D*, **75**, 064021.
- [243] Detweiler, S. L. 2008. *Phys. Rev. D*, **77**, 124026.
- [244] Barack, L., Sago, N. 2009. *Phys. Rev. Lett.*, **102**, 191101.
- [245] Barack, L., Sago, N. 2010. *Phys. Rev. D*, **81**, 084021.
- [246] Barack, L., Ori, A. 2003. *Phys. Rev. Lett.*, **90**, 111101.
- [247] Warburton, N., Akcay, S., Barack, L., Gair, J. R., Sago, N. 2012. *Phys. Rev. D*, **85**, 061501.
- [248] Mino, Y. 2003. *Phys. Rev. D*, **67**, 084027.
- [249] Sago, N., Tanaka, T., Hikida, W., Ganz, K., Nakano, H. 2006. *Prog. Theo. Phys.*, **115**, 873–907.
- [250] Sago, N., Tanaka, T., Hikida, W., Nakano, H. 2005. *Prog. Theo. Phys.*, **114**, 509–514.
- [251] Hughes, S. A., Drasco, S., Flanagan, E. E., Franklin, J. 2005. *Phys. Rev. Lett.*, **94**, 221101.
- [252] Drasco, S., Hughes, S. A. 2006. *Phys. Rev. D*, **73**, 024027.
- [253] Hinderer, T., Flanagan, E. E. 2008. *Phys. Rev. D*, **78**, 064028.
- [254] Rosenthal, E. 2006. *Phys. Rev. D*, **74**, 084018.
- [255] Gralla, S. E. 2012. *Phys. Rev. D*, **85**, 124011.
- [256] Pound, A. 2012. *Phys. Rev. Lett.*, **109**, 051101.
- [257] Isoyama, S., Barack, L., Dolan, S. R., Tiec, A. L., Nakano, H., et al. 2014. *Gravitational Self-Force Correction to the Innermost Stable Circular Equatorial Orbit of a Kerr Black Hole*. arXiv:1404.6133.
- [258] Barack, L., Damour, T., Sago, N. 2010. *Phys. Rev. D*, **82**, 084036.
- [259] Blanchet, L., Detweiler, S. L., Le Tiec, A., Whiting, B. F. 2010. *Phys. Rev. D*, **81**, 064004.
- [260] Le Tiec, A., Blanchet, L., Whiting, B. F. 2012. *Phys. Rev.*, **D85**, 064039.
- [261] Friedman, J. L., Uryu, K., Shibata, M. 2002. *Phys. Rev. D*, **65**, 064035.
- [262] Barausse, E., Buonanno, A., Le Tiec, A. 2012. *Phys. Rev. D*, **85**, 064010.
- [263] Akcay, S., Barack, L., Damour, T., Sago, N. 2012. *Phys. Rev. D*, **86**, 104041.
- [264] Barack, L., Sago, N. 2011. *Phys. Rev. D*, **83**, 084023.
- [265] Shah, A. G., Friedman, J. L., Keidl, T. S. 2012. *Phys. Rev. D*, **86**, 084059.
- [266] Dolan, S. R., Warburton, N., Harte, A. I., Tiec, A. L., Wardell, B., et al. 2014. *Phys. Rev. D*, 064011.

- [267] Le Tiec, A., Mroué, A. H., Barack, L., Buonanno, A., Pfeiffer, H. P., et al. 2011. *Phys. Rev. Lett.*, **107**, 141101.
- [268] Le Tiec, A., Buonanno, A., Mroué, A. H., Pfeiffer, H. P., Hemberger, D. A., et al. 2013. *Phys. Rev. D*, **88**, 124027.
- [269] Nagar, A. 2013. *Phys. Rev. D*, **88**, 121501.
- [270] Buonanno, A., Chen, Y., Damour, T. 2006. *Phys. Rev. D*, **74**, 104005.
- [271] Damour, T. 2001. *Phys. Rev. D*, **64**, 124013.
- [272] Damour, T., Jaranowski, P., Schaefer, G. 2000. *Phys. Rev. D*, **62**, 084011.
- [273] Brezin, E., Itzykson, C., Zinn-Justin, J. 1970. *Phys. Rev. D*, **1**, 2349–2355.
- [274] Damour, T., Iyer, B. R., Sathyaprakash, B. 1998. *Phys. Rev. D*, **57**, 885–907.
- [275] Davis, M., Ruffini, R., Tiomno, J. 1972. *Phys. Rev. D*, **5**, 2932–2935.
- [276] Price, R. H., Pullin, J. 1994. *Phys. Rev. Lett.*, **72**, 3297–3300.
- [277] Damour, T., Iyer, B. R., Nagar, A. 2009. *Phys. Rev. D*, **79**, 064004.
- [278] Nagar, A., Akcay, S. 2012. *Phys. Rev. D*, **85**, 044025.
- [279] Taracchini, A., Buonanno, A., Hughes, S. A., Khanna, G. 2013. *Phys. Rev. D*, **88**, 044001.
- [280] Damour, T., Iyer, B. R., Jaranowski, P., Sathyaprakash, B. 2003. *Phys. Rev. D*, **67**, 064028.
- [281] Buonanno, A., Cook, G. B., Pretorius, F. 2007. *Phys. Rev. D*, **75**, 124018.
- [282] Berti, E., Cardoso, V., Will, C. M. 2006. *Phys. Rev. D*, **73**, 064030.
- [283] Berti, E., Cardoso, V., Starinets, A. 2009. *Class. Quant. Grav.*, **26**, 163001.
- [284] Hinderer, T., Buonanno, A., Mroué, A. H., Hemberger, D. A., Lovelace, G., et al. 2013. *Phys. Rev. D*, **88**, 084005.
- [285] Damour, T., Nagar, A., Pollney, D., Reisswig, C. 2012. *Phys. Rev. Lett.*, **108**, 131101.
- [286] Damour, T., Jaranowski, P., Schaefer, G. 2008. *Phys. Rev. D*, **78**, 024009.
- [287] Barausse, E., Racine, E., Buonanno, A. 2009. *Phys. Rev. D*, **80**, 104025.
- [288] Barausse, E., Buonanno, A. 2010. *Phys. Rev. D*, **81**, 084024.
- [289] Nagar, A. 2011. *Phys. Rev. D*, **84**, 084028.
- [290] Barausse, E., Buonanno, A. 2011. *Phys. Rev. D*, **84**, 104027.
- [291] Balmelli, S., Jetzer, P. 2013. *Phys. Rev.*, **D87**, 124036.
- [292] Pan, Y., Buonanno, A., Fujita, R., Racine, E., Tagoshi, H. 2011. *Phys. Rev. D*, **83**, 064003.
- [293] Yunes, N., Buonanno, A., Hughes, S. A., Coleman Miller, M., Pan, Y. 2010. *Phys. Rev. Lett.*, **104**, 091102.
- [294] Yunes, N., et al. 2011. *Phys. Rev. D*, **83**, 044044.
- [295] Damour, T. 2010. *Phys. Rev. D*, **81**, 024017.
- [296] Israel, G., Hummel, W., Covino, S., Campana, S., Appenzeller, I., et al. 2002. *Astron. Astrophys.*, **386**, L13–L17.
- [297] Strohmayer, T. E. 2005. *Astrophys.J.*, **627**, 920–925.
- [298] Roelofs, G., Rau, A., Marsh, T., Steeghs, D., Groot, P., et al. 2010. *Astrophys. J. Lett.*, **711**, L138–L142.
- [299] Buonanno, A., Iyer, B., Ochsner, E., Pan, Y., Sathyaprakash, B. 2009. *Phys. Rev. D*, **80**, 084043.
- [300] Burgay, M., D’Amico, N., Possenti, A., Manchester, R., Lyne, A., Joshi, B., McLaughlin, M., Kramer, M., Sarkissian, J., Camilo, F., Kalogera, V., Kim, C., Lorimer, D. 2003. *Nature*, **426**, 531–533.
- [301] Berti, E., Cardoso, V., Starinets, A. O. 2009. *Class. Quant. Grav.*, **26**, 163001.
- [302] Pan, Y., Buonanno, A., Boyle, M., Buchman, L. T., Kidder, L. E., et al. 2011. *Phys. Rev. D*, **84**, 124052.

- [303] Shibata, M., Taniguchi, K. 2006. *Phys. Rev. D*, **73**, 064027.
- [304] Baiotti, L., Giacomazzo, B., Rezzolla, L. 2008. *Phys. Rev. D*, **78**, 084033.
- [305] Duez, M. D. 2010. *Class. Quant. Grav.*, **27**, 114002.
- [306] Shibata, M., Taniguchi, K., Uryu, K. 2005. *Phys. Rev. D*, **71**, 084021.
- [307] Bartos, I., Brady, P., Marka, S. 2013. *Class. Quant. Grav.*, **30**, 123001.
- [308] Shibata, M., Karino, S., Eriguchi, Y. 2003. *Mon.Not.Roy.Astron.Soc.*, **343**, 619.
- [309] Baiotti, L., De Pietri, R., Manca, G. M., Rezzolla, L. 2007. *Phys. Rev. D*, **75**, 044023.
- [310] Shibata, M., Taniguchi, K., Uryu, K. 2003. *Phys. Rev. D*, **68**, 084020.
- [311] Rosswog, S. 2010. *PoS*, **NICXI**, 032.
- [312] Shibata, M., Taniguchi, K. 2011. *Living Rev.Rel.*, **14**, 6.
- [313] Foucart, F. 2012. *Phys. Rev.*, **D86**, 124007.
- [314] Foucart, F., Deaton, M. B., Duez, M. D., Kidder, L. E., MacDonald, I., et al. 2013. *Phys. Rev.*, **D87**, 084006.
- [315] Abadie, J., et al. 2010. *Class. Quant. Grav.*, **27**, 173001.
- [316] Finn, L. S., Chernoff, D. F. 1993. *Phys. Rev. D*, **47**, 2198–2219.
- [317] Belczynski, K., Dominik, M., Bulik, T., O’Shaughnessy, R., Fryer, C., Holz, D. E. 2010. *Astrophys. J. Lett.*, **715**, L138–L141.
- [318] Bulik, T., Belczynski, K., Prestwich, A. 2011. *Astrophys.J.*, **730**, 140.
- [319] Komossa, S. 2003. *AIP Conf.Proc.*, **686**, 161–174.
- [320] Dotti, M., Sesana, A., Decarli, R. 2012. *Adv.Astron.*, **2012**, 940568.
- [321] Sesana, A., Gair, J., Berti, E., Volonteri, M. 2011. *Phys. Rev. D*, **83**, 044036.
- [322] Seoane, P. A., et al. 2013. *The Gravitational Universe*. arXiv:1305.5720.
- [323] Siemens, X., Ellis, J., Jenet, F., Romano, J. D. 2013. *Class. Quant. Grav.*, **30**, 224015.
- [324] Sesana, A. 2013. *Braz.J.Phys.*, **43**, 314–319.
- [325] Farrell, S. A., Webb, N. A., Barret, D., Godet, O., Rodrigues, J. M. 2009. *Nature*, **460**, 73–75.
- [326] Gair, J., Mandel, I., Miller, M., Volonteri, M. 2011. *Gen.Rel.Grav.*, **43**, 485–518.
- [327] Amaro-Seoane, P., Santamaria, L. 2010. *Astrophys.J.*, **722**, 1197–1206.
- [328] Sesana, A., Gair, J., Mandel, I., Vecchio, A. 2009. *Astrophys. J. Lett.*, **698**, L129–L132.
- [329] Gair, J. R. 2009. *Class. Quant. Grav.*, **26**, 094034.
- [330] Flanagan, E. E., Hughes, S. A. 1998. *Phys. Rev. D*, **57**, 4535.
- [331] Damour, T., Iyer, B. R., Sathyaprakash, B. S. 2001. *Phys. Rev. D*, **63**, 044023.
- [332] Orosz, J. A., McClintock, J. E., Narayan, R., Bailyn, C. D., Hartman, J. D., et al. 2007. *Nature*, **449**, 872–875.
- [333] Prestwich, A., Kilgard, R., Crowther, P., Carpano, S., Pollock, A., et al. 2007. *Astrophys.J.*, **669**, L21–L24.
- [334] Amaro-Seoane, P., Aoudia, S., Babak, S., Binetruy, P., Berti, E., et al. 2012. *eLISA: Astrophysics and cosmology in the millihertz regime*. arXiv:1201.3621.
- [335] Buonanno, A., Chen, Y., Vallisneri, M. 2003. *Phys. Rev. D*, **67**, 024016.
- [336] Buonanno, A., Chen, Y., Vallisneri, M. 2003. *Phys. Rev. D*, **67**, 104025.
- [337] Buonanno, A., Chen, Y., Pan, Y., Tagoshi, H., Vallisneri, M. 2005. *Phys. Rev. D*, **72**, 084027.
- [338] Abbott, B., et al. 2006. *Phys. Rev. D*, **73**, 062001.
- [339] Abbott, B., et al. 2008. *Phys. Rev. D*, **78**, 042002.

- [340] Boyle, M., Brown, D. A., Kidder, L. E., Mroue, A. H., Pfeiffer, H. P., et al. 2007. *Phys. Rev. D*, **76**, 124038.
- [341] Lovelace, G., Boyle, M., Scheel, M. A., Szilágyi, B. 2012. *Class. Quant. Grav.*, **29**, 045003.
- [342] Damour, T., Nagar, A., Trias, M. 2011. *Phys. Rev. D*, **83**, 024006.
- [343] MacDonald, I., Mroue, A. H., Pfeiffer, H. P., Boyle, M., Kidder, L. E., et al. 2013. *Phys. Rev. D*, **87**, 024009.
- [344] Pan, Y., Buonanno, A., Taracchini, A., Boyle, M., Kidder, L. E., et al. 2014. *Phys. Rev. D*, **89**, 06150 (R).
- [345] Pan, Y., Buonanno, A., Baker, J. G., Centrella, J., Kelly, B. J., et al. 2008. *Phys. Rev. D*, **77**, 024014.
- [346] Taracchini, A., Buonanno, A., Barausse, E., Boyle, M., Chu, T., Lovelace, G., Pfeiffer, H. P., Scheel, M. A. 2012. *Phys. Rev. D*, **83**, 104034.
- [347] Buonanno, A., Pan, Y., Baker, J. G., Centrella, J., Kelly, B. J., et al. 2007. *Phys. Rev. D*, **76**, 104049.
- [348] Damour, T., Nagar, A., Dorband, E. N., Pollney, D., Rezzolla, L. 2008. *Phys. Rev. D*, **77**, 084017.
- [349] Damour, T., Nagar, A., Hannam, M., Husa, S., Brugmann, B. 2008. *Phys. Rev. D*, **78**, 044039.
- [350] Buonanno, A., Pan, Y., Pfeiffer, H. P., Scheel, M. A., Buchman, L. T., et al. 2009. *Phys. Rev. D*, **79**, 124028.
- [351] Damour, T., Nagar, A. 2009. *Phys. Rev. D*, **79**, 081503.
- [352] Pan, Y., Buonanno, A., Buchman, L. T., Chu, T., Kidder, L. E., et al. 2010. *Phys. Rev. D*, **81**, 084041.
- [353] Damour, T., Nagar, A., Bernuzzi, S. 2013. *Phys. Rev. D*, **87**, 084035.
- [354] Taracchini, A., Buonanno, A., Pan, Y., Hinderer, T., Boyle, M., et al. 2014. *Phys. Rev. D*, **89**, 061502(R).
- [355] Littenberg, T. B., Baker, J. G., Buonanno, A., Kelly, B. J. 2013. *Phys. Rev. D*, **87**, 104003.
- [356] Pan, Y., Buonanno, A., Taracchini, A., Kidder, L. E., Mroué, A. H., et al. 2014. *Phys. Rev. D*, **89**, 084006.
- [357] Ajith, P., et al. 2007. *Class. Quat. Grav.*, **24**, S689–S699.
- [358] Santamaría, L., et al. 2010. *Phys. Rev. D*, **82**, 064016.
- [359] Ajith, P., Hannam, M., Husa, S., Chen, Y., Bruegmann, B., et al. 2011. *Phys. Rev. Lett.*, **106**, 241101.
- [360] Hannam, M., Schmidt, P., Bohé, A., Haegel, L., Husa, S., et al. 2013. *Twist and shout: A simple model of complete precessing black-hole-binary gravitational waveforms*. arXiv:1308.3271.
- [361] Mroue, A. H., Scheel, M. A., Szilagyi, B., Pfeiffer, H. P., Boyle, M., et al. 2013. *Phys. Rev. Lett.*, **111**, 241104.
- [362] Pekowsky, L., O’Shaughnessy, R., Healy, J., Shoemaker, D. 2013. *Phys. Rev. D*, **88**, 024040.
- [363] Abadie, J., et al. 2012. *Phys. Rev. D*, **85**, 082002.
- [364] Aasi, J., et al. 2013. *Phys. Rev. D*, **87**, 022002.
- [365] Abadie, J., et al. 2012. *Phys. Rev. D*, **85**, 102004.
- [366] Aasi, J., et al. 2013. *Prospects for Localization of Gravitational Wave Transients by the Advanced LIGO and Advanced Virgo Observatories*. arXiv:1304.0670.
- [367] Iyer, B., Unnikrishnan, C., Dhurandhar, S., Raja, S., Sengupta, A. 2012. <https://dcc.ligo.org/LIGO-M1100296>.

- [368] Aylott, B., Baker, J. G., Boggs, W. D., Boyle, M., Brady, P. R., et al. 2009. *Class. Quant. Grav.*, **26**, 165008.
- [369] Ajith, P., Boyle, M., Brown, D. A., Brugmann, B., Buchman, L. T., et al. 2012. *The NINJA-2 catalog of hybrid post-Newtonian/numerical-relativity waveforms for non-precessing black-hole binaries*. arXiv:1201.5319.
- [370] Hinder, I., Buonanno, A., Boyle, M., Etienne, Z. B., Healy, J., et al. 2014. *Class. Quant. Grav.*, **31**, 025012.
- [371] Aasi, J., et al. 2014. *The NINJA-2 project: Detecting and characterizing gravitational waveforms modelled using numerical binary black hole simulations*. arXiv:1401.0939.
- [372] Postnov, K., Yungelson, L. 2005. *Living Rev. Rel.*, **9**, 6.
- [373] O’Shaughnessy, R., Kim, C., Kalogera, V., Belczynski, K. 2008. *Astrophys. J.*, **672**, 479–488.
- [374] Hannam, M., Brown, D. A., Fairhurst, S., Fryer, C. L., Harry, I. W. 2013. *Astrophys.J.*, **766**, L14.
- [375] Fong, W., Berger, E. 2013. *Astrophys. J.*, **776**, 18.
- [376] Schutz, B. F. 1986. *Nature*, **323**, 310.
- [377] Del Pozzo, W. 2012. *Phys. Rev. D*, **86**, 043011.
- [378] Dalal, N., Holz, D. E., Hughes, S. A., Jain, B. 2006. *Phys. Rev. D*, **74**, 063006.
- [379] Sathyaprakash, B., Schutz, B., Van Den Broeck, C. 2010. *Class. Quant. Grav.*, **27**, 215006.
- [380] Nissanke, S., Holz, D. E., Hughes, S. A., Dalal, N., Sievers, J. L. 2010. *Astrophys.J.*, **725**, 496–514.
- [381] Berger, E., Fong, W., Chornock, R. 2013. *Astrophys. J. Lett.*, **774**, L23.
- [382] Tanvir, N. R., Levan, A. J., Fruchter, A. S., Hjorth, J., Hounsell, R. A., Wiersema, K., Tunnicliffe, R. L. 2013. *Nature*, **500**, 547–549.
- [383] Holz, D. E., Hughes, S. A. 2005. *Astrophys.J.*, **629**, 15–22.
- [384] Messenger, C., Read, J. 2012. *Phys. Rev. Lett.*, **108**, 091101.
- [385] Ghez, A., Salim, S., Hornstein, S. D., Tanner, A., Morris, M., et al. 2005. *Astrophys.J.*, **620**, 744–757.
- [386] Shternin, P. S., Yakovlev, D. G., Heinke, C. O., Ho, W. C., Patnaude, D. J. 2011. *Mon.Not.Roy.Astron.Soc.*, **412**, L108–L112.
- [387] Page, D., Prakash, M., Lattimer, J. M., Steiner, A. W. 2011. *Phys. Rev. Lett.*, **106**, 081101.
- [388] Del Pozzo, W., Li, T. G. F., Agathos, M., Van Den Broeck, C., Vitale, S. 2013. *Phys. Rev. Lett.*, **111**, 071101.
- [389] Markakis, C., Read, J. S., Shibata, M., Uryu, K., Creighton, J. D., et al. 2009. *J.Phys.Conf.Ser.*, **189**, 012024.
- [390] Mishra, C. K., Arun, K., Iyer, B. R., Sathyaprakash, B. 2010. *Phys. Rev. D*, **82**, 064010.
- [391] Li, T. G. F., et al. 2012. *Phys. Rev. D*, **85**, 082003.
- [392] Will, C. M. 2006. *Living Rev.Rel.*, **9**, 3.
- [393] Yunes, N., Siemens, X. 2013. *Living Rev.Rel.*, **16**, 9.
- [394] Ryan, F. D. 1997. *Phys. Rev. D*, **56**, 1845.
- [395] Barack, L., Cutler, C. 2007. *Phys. Rev. D*, **75**, 042003.
- [396] Gair, J., Vallisneri, M., Larson, S., Baker, J. 2013. *Living Rev.Rel.*, **16**, 7.
- [397] Gossan, S., Veitch, J., Sathyaprakash, B. 2012. *Phys. Rev. D*, **85**, 124056.
- [398] Nitz, A. H., Lundgren, A., Brown, D. A., Ochsner, E., Keppel, D., et al. 2013. *Phys. Rev.*, **D88**, 124039.
- [399] Peters, P. C., Mathews, J. 1963. *Phys. Rev.*, **131**(Jul), 435–440.

- [400] Kowalska, I., Bulik, T., Belczynski, K., Dominik, M., Gondek-Rosinska, D. 2011. *Astron. Astrophys.*, **527**, A70.
- [401] Miller, M., Hamilton, D. 2002. *Astrophys. J.*, **576**, 894–898.
- [402] Wen, L. 2003. *Astrophys. J.*, **598**, 419–430.
- [403] Kocsis, B., Levin, J. 2012. *Phys. Rev. D*, **85**, 123005.
- [404] Naoz, S., Kocsis, B., Loeb, A., Yunes, N. 2013. *Astrophys.J.*, **773**, 187.
- [405] Pan, Y., Buonanno, A., Chen, Y., Vallisneri, M. 2004. *Phys. Rev. D*, **69**, 104017.
- [406] Buonanno, A., Chen, Y., Pan, Y., Vallisneri, M. 2004. *Phys. Rev. D*, **70**, 104003.
- [407] Ajith, P. 2011. *Phys. Rev. D*, **84**, 084037.
- [408] Schmidt, P., Hannam, M., Husa, S. 2012. *Phys. Rev. D*, **86**, 104063.
- [409] Harry, I., Fairhurst, S. 2011. *Class. Quant. Grav.*, **28**, 134008.
- [410] Privitera, S., Mohapatra, S. R. P., Ajith, P., Cannon, K., Fotopoulos, N., et al. 2014. *Phys. Rev. D*, **89**, 024003.
- [411] Cannon, K., Chapman, A., Hanna, C., Keppel, D., Searle, A. C., et al. 2010. *Phys. Rev. D*, **82**, 044025.
- [412] Cannon, K., Hanna, C., Keppel, D. 2011. *Phys. Rev. D*, **84**, 084003.
- [413] Field, S. E., Galley, C. R., Herrmann, F., Hesthaven, J. S., Ochsner, E., et al. 2011. *Phys. Rev. Lett.*, **106**, 221102.
- [414] Field, S. E., Galley, C. R., Hesthaven, J. S., Kaye, J., Tiglio, M. 2013. *Fast prediction and evaluation of gravitational waveforms using surrogate models*. arXiv:1308.3565.
- [415] Pürller, M. 2014. *Frequency domain reduced order models for gravitational waves from aligned-spin black-hole binaries*. arXiv:1402.4146.
- [416] Bernuzzi, S., Nagar, A., Thierfelder, M., Brugmann, B. 2012. *Phys. Rev. D*, **86**, 044030.
- [417] Damour, T., Nagar, A., Villain, L. 2012. *Phys. Rev. D*, **85**, 123007.
- [418] Favata, M. 2014. *Phys. Rev. Lett.*, **112**, 101101.
- [419] Yagi, K., Yunes, N. 2013. *Phys. Rev.*, **D89**, 021303.
- [420] Djorgovski, S., et al. 2011. *Towards an Automated Classification of Transient Events in Synoptic Sky Surveys*. arXiv:1110.4655.
- [421] Fairhurst, S. 2011. *Class. Quant. Grav.*, **28**, 105021.
- [422] Van Den Broeck, C., Sengupta, A. 2007. *Class. Quat. Grav.*, **24**, 1089–1113.
- [423] Capano, C., Pan, Y., Buonanno, A. 2014. *Phys. Rev. D*, **89**, 102003.
- [424] Raymond, V., van der Sluys, M., Mandel, I., Kalogera, V., Rover, C., et al. 2009. *Class. Quant. Grav.*, **26**, 114007.
- [425] Hanna, C., Mandel, I., Vossen, W. 2014. *Astrophys.J.*, **784**, 8.
- [426] Arzoumanian, Z., et al. 2014. *NANOGrav Limits on Gravitational Waves from Individual Supermassive Black Hole Binaries in Circular Orbits*. arXiv:1404.1267.
- [427] Burke-Spolaor, S. 2013. *Class. Quant. Grav.*, **30**, 224013.
- [428] Ando, S., Beacom, F., Yüksel, H. 2005. *Phys. Rev. Lett.*, **95**, 171101.
- [429] Dimmelmeier, H., Ott, C. D., Marek, A., Janka, H.-T. 2008. *Phys. Rev. D*, **78**, 064056.
- [430] Ott, C. D. 2009. *Class. Quant. Grav.*, **26**, 204015.
- [431] Owen, B. J. 2005. *Phys. Rev. Lett.*, **95**, 211101.
- [432] Andersson, N., Ferrari, V., Jones, D., Kokkotas, K., Krishnan, B., et al. 2011. *Gen.Rel.Grav.*, **43**, 409–436.
- [433] Knispel, B., Allen, B. 2008. *Phys. Rev. D*, **78**, 044031.

- [434] Chamel, N., Haensel, P. 2008. *Living Rev. Rel.*, **11**.
- [435] Espinoza, C. M., Lyne, A. G., Stappers, B. W., Kramer, M. 2011. *Mon. Not. Roy. Astr. Soc.*, **414**, 1679–1704.
- [436] Kaspi, V. M. 2010. *Proc. Nat. Acad. Sci.*, **107**, 7147–7152.
- [437] Andersson, N., Kokkotas, K. 1998. *Mon. Not. Roy. Astron. Soc.*, **299**, 1059–1068.
- [438] Chakrabarty, D. 2005. Millisecond Pulsars in X-Ray Binaries. Page 279 of: Rasio, F. A., Stairs, I. H. (eds), *Binary Radio Pulsars*. Astronomical Society of the Pacific Conference Series, vol. 328.
- [439] Wagoner, R. V. 1984. *Astrophys. J.*, **278**, 345–348.
- [440] Bildsten, L. 1998. *Astrophys. J. Lett.*, **501**, L89.
- [441] Chakrabarty, D., Morgan, E. H., Munro, M. P., Galloway, D. K., Wijnands, R., et al. 2003. *Nature*, **424**, 42–44.
- [442] Watts, A. L., Krishnan, B., Bildsten, L., Schutz, B. F. 2008. *Mon. Not. Roy. Astr. Soc.*, **389**, 839–868.
- [443] Klimenko, S., Yakushin, I., Mercer, A., Mitselmakher, G. 2008. *Class. Quant. Grav.*, **25**, 114029.
- [444] Abadie, J., et al. 2012. *Phys. Rev. D*, **85**, 122007.
- [445] Abadie, J., et al. 2011. *Astrophys.J.*, **737**, 93.
- [446] Abadie, J., et al. 2011. *Astrophys. J. Lett.*, **734**, L35.
- [447] Abadie, J., et al. 2012. *Astrophys. J.*, **760**, 12.
- [448] Abbott, B., et al. 2008. *Astrophys. J.*, **681**, 1419–1430.
- [449] Metzger, B. D., Berger, E. 2012. *Astrophys. J.*, **746**, 48.
- [450] Aasi, J., et al. 2014. *Astrophys.J.*, **785**, 119.
- [451] Abadie, J., et al. 2010. *Astrophys. J.*, **722**, 1504–1513.
- [452] Abbott, B., et al. 2009. *Phys. Rev. D*, **79**, 022001.
- [453] Knispel, B., Eatough, R., Kim, H., Keane, E., Allen, B., et al. 2013. *Astrophys.J.*, **774**, 93.
- [454] Allen, B., Knispel, B., Cordes, J., Deneva, J., Hessels, J., et al. 2013. *Astrophys.J.*, **773**, 91.
- [455] Aasi, J., et al. 2013. *Phys. Rev. D*, **87**, 042001.
- [456] Aasi, J., et al. 2013. *Phys. Rev. D*, **88**, 102002.
- [457] Benacquista, M. J., Downing, J. M. 2013. *Living Rev.Rel.*, **16**, 4.
- [458] Andersson, N., Kokkotas, K. D., Stergioulas, N. 1999. *Astrophys. J.*, **516**, 307–314.
- [459] Cutler, C. 2002. *Phys. Rev. D*, **66**, 084025.
- [460] Muller, B., Janka, H.-T., Dimmelmeier, H. 2010. *Astrophys.J.Suppl.*, **189**, 104–133.
- [461] Ott, C. D., Abdikamalov, E., Msta, P., Haas, R., Drasco, S., et al. 2013. *Astrophys.J.*, **768**, 115.
- [462] Logue, J., Ott, C., Heng, I., Kalmus, P., Scargill, J. 2012. *Phys. Rev. D*, **86**, 044023.
- [463] Mueller, E., Rampp, M., Buras, R., Janka, H.-T., Shoemaker, D. H. 2004. *Astrophys.J.*, **603**, 221–230.
- [464] Ushomirsky, G., Cutler, C., Bildsten, L. 2000. *Mon. Not. R. Astron. Soc.*, **319**, 902.
- [465] Cutler, C. 2002. *Phys. Rev. D*, **66**, 084025.

- [466] Payne, D., Melatos, A., Phinney, E. 2003. Gravitational waves from an accreting neutron star with a magnetic mountain. Pages 92–95 of: Centrella, J. (ed), *Astrophysics of Gravitational Wave Sources*. AIP Conference Proceedings, vol. 686. Melville, NY: American Institute of Physics.
- [467] Schutz, B. F. 1989. Data Analysis Requirements of Networks of Detectors. Page 315 of: Schutz, B. F. (ed), *NATO ASIC Proc. 253: Gravitational Wave Data Analysis*.
- [468] Brady, P. R., Creighton, T., Cutler, C., Schutz, B. F. 1998. *Phys. Rev. D*, **57**, 2101–2116.
- [469] Jaranowski, P., Krolak, A., Schutz, B. F. 1998. *Phys. Rev. D*, **58**, 063001.
- [470] Creighton, J., Anderson, W. 2011. *Gravitational-Wave Physics and Astronomy*. Wiley-VCH Verlag GmbH & Co.
- [471] Starobinsky, A. A. 1979. *JETP Lett.*, **30**, 682–685.
- [472] Grishchuk, L. P. 1975. *Sov. Phys. JETP*, **40**, 409–415.
- [473] Allen, B. 1988. *Phys. Rev. D*, **37**, 2078–2085.
- [474] Maggiore, M. 2000. *Phys. Rep.*, **331**, 283.
- [475] Allen, B., Romano, J. D. 1999. *Phys. Rev. D*, **59**, 102001.
- [476] Ade, P., et al. 2013. *Planck 2013 results. XVI. Cosmological parameters*. arXiv:1303.5076.
- [477] Kamionkowski, M., Kosowsky, A., Stebbins, A. 1997. *Phys. Rev. D*, **55**, 7368–7388.
- [478] Seljak, U., Zaldarriaga, M. 1997. *Phys. Rev. Lett.*, **78**, 2054–2057.
- [479] Weinberg, S. 2004. *Phys. Rev. D*, **69**, 023503.
- [480] Pritchard, J. R., Kamionkowski, M. 2005. *Annals Phys.*, **318**, 2–36.
- [481] Smith, T. L., Kamionkowski, M., Cooray, A. 2006. *Phys. Rev. D*, **73**, 023504.
- [482] Boyle, L. A., Steinhardt, P. J. 2008. *Phys. Rev. D*, **77**, 063504.
- [483] Khlebnikov, S. Y., Tkachev, I. I. 1997. *Phys. Rev. D*, **56**, 653–660.
- [484] Kibble, T. 1976. *J.Phys.*, **A9**, 1387–1398.
- [485] Vilenkin, A. 1985. *Phys.Rept.*, **121**, 263.
- [486] Sarangi, S., Tye, S. H. 2002. *Phys.Lett.*, **B536**, 185–192.
- [487] Berezinsky, V., Hnatyk, B., Vilenkin, A. 2000. *Superconducting cosmic strings as gamma-ray burst engines*. astro-ph/0001213.
- [488] Damour, T., Vilenkin, A. 2000. *Phys. Rev. Lett.*, **85**, 3761–3764.
- [489] Copeland, E. J., Myers, R. C., Polchinski, J. 2004. *JHEP*, **06**, 013.
- [490] Damour, T., Vilenkin, A. 2005. *Phys. Rev. D*, **71**, 063510.
- [491] Olmez, S., Mandic, V., Siemens, X. 2010. *Phys. Rev. D*, **81**, 104028.
- [492] Turner, M. S., Wilczek, F. 1990. *Phys. Rev. Lett.*, **65**, 3080–3083.
- [493] Kamionkowski, M., Kosowsky, A., Turner, M. 1994. *Phys. Rev. D*, **49**, 2837–2851.
- [494] Buonanno, A. 2003. *TASI Lectures on Gravitational Waves from the Early Universe*. arXiv:0303085.
- [495] Binetruy, P., Bohé, A., Caprini, C., Dufaux, J.-F. 2012. *JCAP*, **1206**, 027.
- [496] Thorne, K. 1987. Gravitational Radiation. Chap. 9, pages 330–458 of: Hawking, S. W., Israel, W. (eds), *Three Hundred Years of Gravitation*. Cambridge: Cambridge University Press.
- [497] Flanagan, E. E. 1993. *Phys. Rev. D*, **48**, 2389–2407.
- [498] Sesana, A., Vecchio, A., Colacino, C. N. 2008. *Mon. Not. Roy. Astr. Soc.*, **390**, 192–209.
- [499] Sesana, A. 2013. *Mon. Not. Roy. Astr. Soc.*, **433**, L1–L5.

- [500] Kramer, M. 2004. *Fundamental physics with the SKA: Strong-field tests of gravity using pulsars and black holes.* astro-ph/0409020.
- [501] Copi, C. J., Schramm, D. N., Turner, M. S. 1997. *Phys. Rev. D*, **55**, 3389–3393.
- [502] Abbott, B. P., et al. 2009. *Nature*, **460**, 990.
- [503] Smith, T., Pierpaoli, E., Kamiokowski, M. 2006. *Phys. Rev. Lett.*, **97**, 021301.
- [504] Abbott, B. P., et al. 2009. *Phys. Rev. D*, **80**, 062002.
- [505] Aasi, J., et al. 2014. *Phys. Rev. Lett.*, **112**, 131101.
- [506] Boyle, L. A., Buonanno, A. 2008. *Phys. Rev. D*, **78**, 043531.
- [507] Shannon, R., Ravi, V., Coles, W., Hobbs, G., Keith, M., et al. 2013. *Science*, **342**, 334–337.
- [508] Jenet, F. A., Hobbs, G., van Straten, W., Manchester, R., Bailes, M., et al. 2006. *Astrophys.J.*, **653**, 1571–1576.
- [509] Peebles, P., Vilenkin, A. 1999. *Phys. Rev. D*, **59**, 063505.
- [510] Giovannini, M. 1998. *Phys. Rev.*, **D58**, 083504.
- [511] Giovannini, M. 1999. *Phys. Rev.*, **D60**, 123511.
- [512] Riazuelo, A., Uzan, J.-P. 2000. *Phys. Rev. D*, **62**, 083506.
- [513] Tashiro, H., Chiba, T., Sasaki, M. 2004. *Class. Quant. Grav.*, **21**, 1761–1772.